University of St Andrews

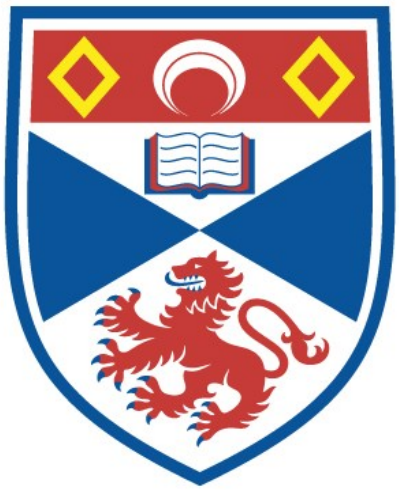

Full metadata for this thesis is available in
St Andrews Research Repository
at:
http://research-repository.st-andrews.ac.uk/

This thesis is protected by original copyright

Behaviour of Small Biomolecules on the Cu(110) Surface

Daniel J. Frankel

March 2002

BIBLIOTHECA UNIVERSITATIS ARBOREANAE

Behaviour of Small Biomolecules on the Cu(110) Surface

By Daniel Frankel

University of St-Andrews

A dissertation submitted to the University of St-Andrews for the degree of Doctor of Philosophy

March 2002

Behaviour of Small Biomolecules on the Cu(110) Surface

ABSTRACT

The adsorption behaviour of small biomolecules on the Cu(110) surface have been investigated in order to elucidate the formation of nanostructures, two dimensional crystals and hydrogen bonding systems.

It was found that the chiral amino acid phenylglycine formed well ordered chiral structures with a chiral unit cell which allows the low energy electron diffraction patterns of the two enantiomers to be readily differentiated. Thus it has been possible to create a well characterised chiral surface.

A study of the modified amino acid, amino benzoic acid, revealed the formation of a number of well ordered periodic structures, the transitions depending on the successive removal of hydrogen from the adsorbed species. Flat lying molecules exist at room temperature in a overlayer structure represented by the (4×3)g unit cell. Increasing surface coverage results in the appearance of upright molecules bonded through the carboxylic acid moiety to the Cu surface. These upright molecules form "nanowires" at

domain boundaries. Upon annealing to 464K partial desorption of H_2 occurs and the formation of a $\begin{pmatrix} 2 & 4 \\ 5 & -2 \end{pmatrix}$ periodicity. STM images suggest the formation of dimers. On annealing to 510K, further dehydrogenation occurs and a $\begin{pmatrix} 1 & 2 \\ 6 & -5 \end{pmatrix}$ overlayer forms. Finally at 540K a $\begin{pmatrix} 1 & 2 \\ 4 & -3 \end{pmatrix}$ periodicity is revealed in which all species correspond to dehydrogenated dimers

An analogue to the pyrimidine nucleic acid bases, α-pyridone, was investigated. Upon annealing to 560K, an (8×2)gg LEED pattern with glide planes along both <110> and <001> directions was observed, which indicates the formation of a well ordered monolayer. Following low temperature adsorption, temperature programmed desorption revealed the existence of a multilayer with a desorption temperature of 310K, followed by the formation of (8×2)gg at 590K. High resolution electron energy loss spectroscopy shows that initially in the monolayer at room temperature, the molecule has both flat lying and up-right geometry. However, annealing leaves only the out-of-plane CH bending mode at about 875cm^{-1} which suggests that the molecule exclusively lies flat on the surface when the (8×2)gg periodicity is formed. Scanning tunnelling microscopy reveals molecular resolution images of well ordered monolayers. The experimental

results are consistent with a model in which molecular dimers, held together by H-bonding, are the basic unit of the two dimensional array.

The pyrimidine bases cytosine and thymine both formed well ordered two dimensional crystals on the Cu(110) surface. Cytosine initially forms islands, at low coverage, of (6×6) structure. At higher coverage the same structure remains and both STM measurements and the presence of predominantly in-plane modes in HREELS spectra suggest that the molecules are in an upright orientation with respect to the surface. The twelve molecules per unit cell are thought to be π stacked along the zig-zags in the [001] direction. Upon further annealing a phase transition occurs in which a (6×2)gg structure is formed. A model is proposed in which adjacent cytosine molecules dimerise in adjacent zig-zags with the loss of a proton. This leads to a charge delocalisation in which it is possible for the dimer to bond to the copper via the oxygen groups in the dimer.

Thymine also forms a (6×2)gg overlayer but STM reveals that the arrangement of molecules within the unit cell is different to that of cytosine. Here is is proposed that there are four molecules per unit cell forming two rows. Upright thymine molecules are π stacked along the [001] direction

The final molecule investigated was the purine nucleic acid base adenine. STM shows that at low coverage, ordered one-dimensional molecular chain grow along (±1, 2) directions. At higher coverages, on annealing to 430K, the chains order into chiral domains of $\begin{pmatrix} 1 & 2 \\ 6 & 0 \end{pmatrix}$ periodicity. High resolution STM images reveal the details of molecular structure within the unit cell. EELS shows that the molecular plane is parallel to the substrate with a tilted C-NH_2 bond. *Ab initio* calculations confirm the molecular orientation and shows an sp^3 hybridisation on the N (amino) atom, which is directly bonded to the substrate. The origin of the chains lies in homochiral rows of molecules, linked by two types of H-bonding interactions, commensurate with the substrate.

Acknowledgements

There are so many people to thank. Let me start with my supervisor Neville Richardson who gave me the chance to work on an exciting project using very big instruments to study very tiny things. Without doubt, my postdoctoral supervisor, Dr. Q. Chen taught me everything I know about UHV systems, mechanics, electronics, physics, chemistry, computing and chinese proverbs. Chen, I am eternally grateful. Both Neville and Chen will always be my scientific role models. The rest of the surface chemistry research group including Steve Francis, who made my years in the lab, seem so short. My close friends… in no particular order;

Angela..Your cauliflower soup, and spilling wine over the carpet made Howard Place, our flat, a true home. We had some great times. It was a pleasure to listen to your divine tin whistle playing.

Cyrus.Thanks for putting up with my early morning singing and making Deans Court so much fun. It was a pleasure to unwind watching the ducks bob up and down near the pier.

Marek..We planned how to kill all noisy seagulls, destroy the useless video shop and the massive celebrations we would throw when we finished the phd. Prague now feels like my second home.

Nadja .Taught me to cook, to garden, to be afraid of a rolling pin, very afraid. The race to finish the phd was close but in the end I won as was the case with the arm wrestling, drinking vodka and being spontaneous. I am already missing the style and sophistication that you brought to breakfast.

Stefanie. Introduced me to the fact that not all philosophers sleep all day and that St-Andrews is exciting enough to write stories about.

Ian. Sunday lunch in the Radcliffe arms cannot be recreated anywhere in the world. Thankyou for bringing some life to Oxford.

Dave.. For teaching me about the importance of working hard…and introducing me to The Smiths as an aid to scientific research

Most of all I would like to thank my family for their love and support without which none of this would have been possible.

This thesis is dedicated to my mum, dad, brother Jonathan and aunty Pauline

CONTENTS

CHAPTER 1 . Introduction

1.1 Biomolecules on surfaces

Several reasons exist for the study of biological molecules and their relationship in terms of bonding, orientation and reactivity to surfaces. Many naturally occurring reactions take place at interfaces including biomineralisation[1-5] and cell membrane interactions [6-14]. Applications led research concentrates on the exploitation of molecular recognition, especially relevant to the development of biosensors [15-20] and biocompatibility [2-5,21-31] for medical implants.

A fusion of independent sciences is required to investigate the phenomena that occur at interfaces whereby either the gas phase or solution state of a biological molecule is in contact with a surface. Physics is the language of the instrumentation and techniques used to probe bond breaking and making. Chemistry describes the bonding in terms of physical and electronic structure, biology lends itself to the larger scale of how the molecules organise themselves and react in their local environment.

The tools available in surface science to study organic thin films have been advanced by the advent of non-ultra high vacuum (UHV) methods such as reflection absorption infrared spectroscopy (RAIRS) and ambient scanning tunnelling (STM) microscopy. However, these are used exclusively to determine structural/molecular information as opposed to functionality and reactivity of the surface, parameters that are

particularly important in biological systems.

At the other extreme, interfaces can be considered only in terms of their functionality. Here, the experimental repetoir encompasses circular dichroism, ellipsometry and the use of ultra sensitive mass sensors. [20,32-38]

Ideally, for the most complete picture, the two approaches should be married together in order to understand the organic film as both a structural entity and as a reactive interface.

1.2 Formation of ultra-thin organic thin films

Three methodologies are commonly employed to deposit monolayers/multilayers of organic compounds on surfaces. Each has its own merits under different circumstances and these along with the disadvantages are listed in table 1.1.

The Langmuir Blodgett [39-45] method involves assembling the monolayers at the gas/water interface and then transferring the film onto a substrate. Care has to be taken in order for the film not to lose its structure on transferral. Requiring UHV conditions, organic vapour deposition is the most expensive technique but allows mono-layer by mono-layer growth of ultra-thin films with more control of coverage, structure and orientation which is harder to achieve using the other methods [46-49].Self-assembly relies on immersion of the substrate in a solution of the organic solvent or aqueous solution[1,50-57]. The solute molecules attach to the substrate leading to

thermodynamically stable monolayers. The most widely used technique is self-assembly, as it requires inexpensive equipment and is quick to produce monolayers of high quality.

Table 1.1 Monolayer formation techniques

Self Assembly	Langmuir - Blodgett	Organic Vapour
Adsorbate doesn't have to be water compatible	Adsorbate has to be water compatible and ampiphillic to form a single monolayer at the gas water interface	Adsorbate required to vaporise before decomposition
No special equipment necessary	LB trough necessary	UHV system essential
Control of orientation by formation using mixed monolayers of adsorbate with small polymers	Often sample has to be maintained constantly in aqueous solution to avoid changes in structure of film	Control of orientation by varying surface coverage and growth process. Greater control of deposition temperature
Structure of adsorbate has to be characterised in solution and on film only	Film characterised in solution/on film and at gas/water interface	Characterise in UHV
Adsorbate covalently linked to substrate, therefore film less subject to desorption	Compressing film can permit control of the orientation of the adsorbate at the surface	Strong bond between adsorbate and substrate. Less chance of contamination in UHV

The goal of these production routes is to construct a surface with interesting and useful chemical properties either in a biological, chemical or electrical sense. Control of molecular orientation can influence the functional group availability for further

reaction. This could be beneficial to biosensors for example whereby the size of the signal measured is proportional to the amount of reaction at the surface.

1.3 Biomolecules

Amino acids, peptides and proteins

Twenty different amino acids are coded for by DNA sequences in the genes. All of these naturally occurring monomers combine in a large number of permutations to form proteins. It is this rich diversity that leads to the myriad of different enzymes and reactants in biological systems. α-amino acids have the form represented in Fig. 1.1

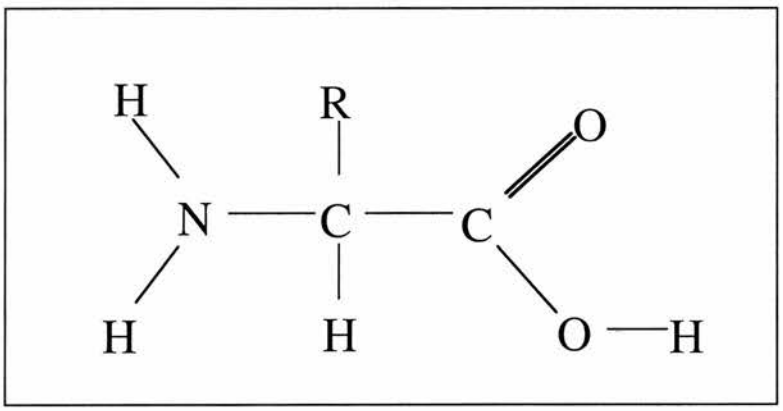

Fig. 1.1 Generalised structure of an α-amino acid

The monomer consists of a carboxyl group, an amino group, and the R group which is responsible for giving the amino acid its' individual properties. Most commonly the molecule exists in the solid or neutral pH solutions as a zwitterion in which the carboxyl group is deficient of one proton and the amino group has gained

one $^{+}NH_3.CHR.CO_2^{-}$. Table 1.2 summarises how the R group effects the properties of the amino acids.

Table 1.2 R group classification of amino acids [58]

R Group	Examples	Properties	Comments
Aliphatic	Glycine, alanine, valine, leucine, isoleucine	From left to right of list become increasingly hydrophobic	
Containing Hydroxyl /Sulphur	Serine, cysteine, threonine, methionine	Weakly polar side chain. More hydrophilic	Oxidation can occur between pairs of cysteine chains to form a disulphide bond
Aromatic	Phenylalanine, tyrosine, tryptophan	With valine and leucine, isoleucine most hydrophobic	Aromatic AA's strong absorption of UV light. Used for detection of proteins
Basic	Histidine, lysine, arginine	Strongly polar ∴ found on exterior surface of proteins for hydration with aqueous solution	
Acidic	Aspartic acid, glutamic acid	Only AA's with –ve Charges at pH 7	

As the carbon atom has four different units attached to it (except glycine where R=H), the asymmetric molecule is said to be chiral, with the central carbon being the stereocenter. Two stereoisomers can exist, each being a mirror image of the other. D

and L enantiomers can be distinguished from each other experimentally as their solutions rotate the plane of polarised light in opposite directions. Hence they are sometimes known as optical isomers. Chirality is an important feature in many biochemical pathways and molecular recognition is usually a key element. Enzymes demonstrate this phenomenon with the lock and key mechanism of catalysis/substrate interactions being stereospecific. One unsolved mystery is why only the L form of amino acids are incorporated into proteins by humans and only the D configuration of the carbohydrate residue in nucleic acids

So far only the amino acids coded for by DNA have been considered. Certain amino acids may become chemically modified after they are assembled into proteins. An example of such a case is O–phosphoserine which consists of a conventional serine molecule to which is attached a negatively charged phosphate group to a terminal oxygen. Amino acids join together via peptide bonds, fig. 1.2.

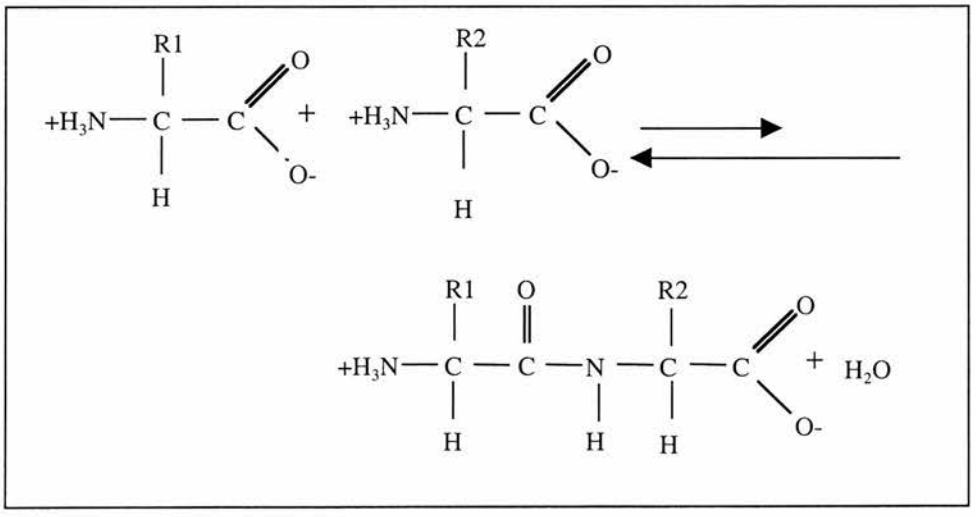

Fig. 1.2 Formation of peptides [59]

A sequence of more than more than ten amino acids are called a polypeptide and all proteins are polypeptides but can also contain other residues, for example lipids or carbohydrates. Proteins can have complex three dimensional forms characterised by the sequence of amino acids (primary structure), regular repeat units or random order i.e. α helix, pleated sheet (secondary structure). The overall three-dimensional conformation of the protein is the tertiary structure.

1.4 Nucleic acid bases and DNA

It is not an understatement to say that genes control cell function and are thus the key to biochemistry. Each gene is made of DNA (Deoxy Ribose Nucleic Acid) which through various processes are responsible for the syntheses of both structural (cell organelles, membranes etc) and enzyme proteins. A flow chart of the stages in this pathway is shown in fig. 1.3.

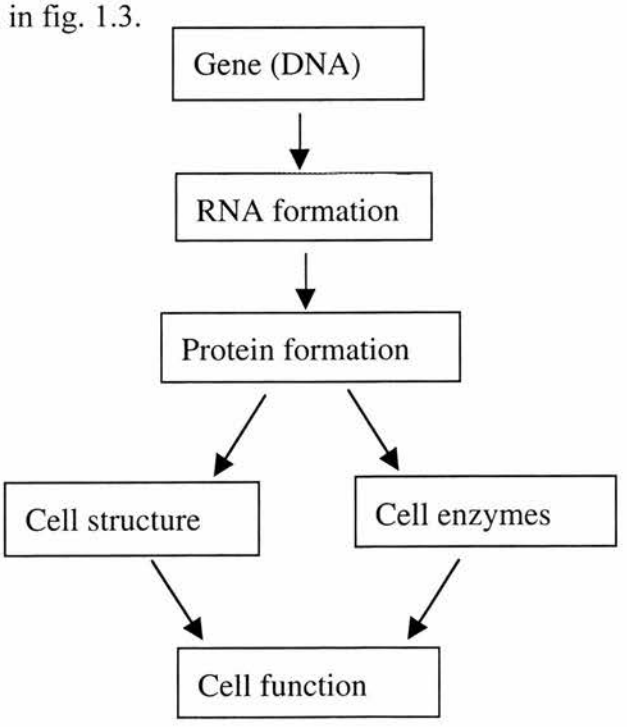

Fig. 1.3 Protein synthesis from DNA [60]

Vital to the formation of the famous double helix and the processes of transcription and translation are the pairings of the nucleic acid bases, fig. 1.4.

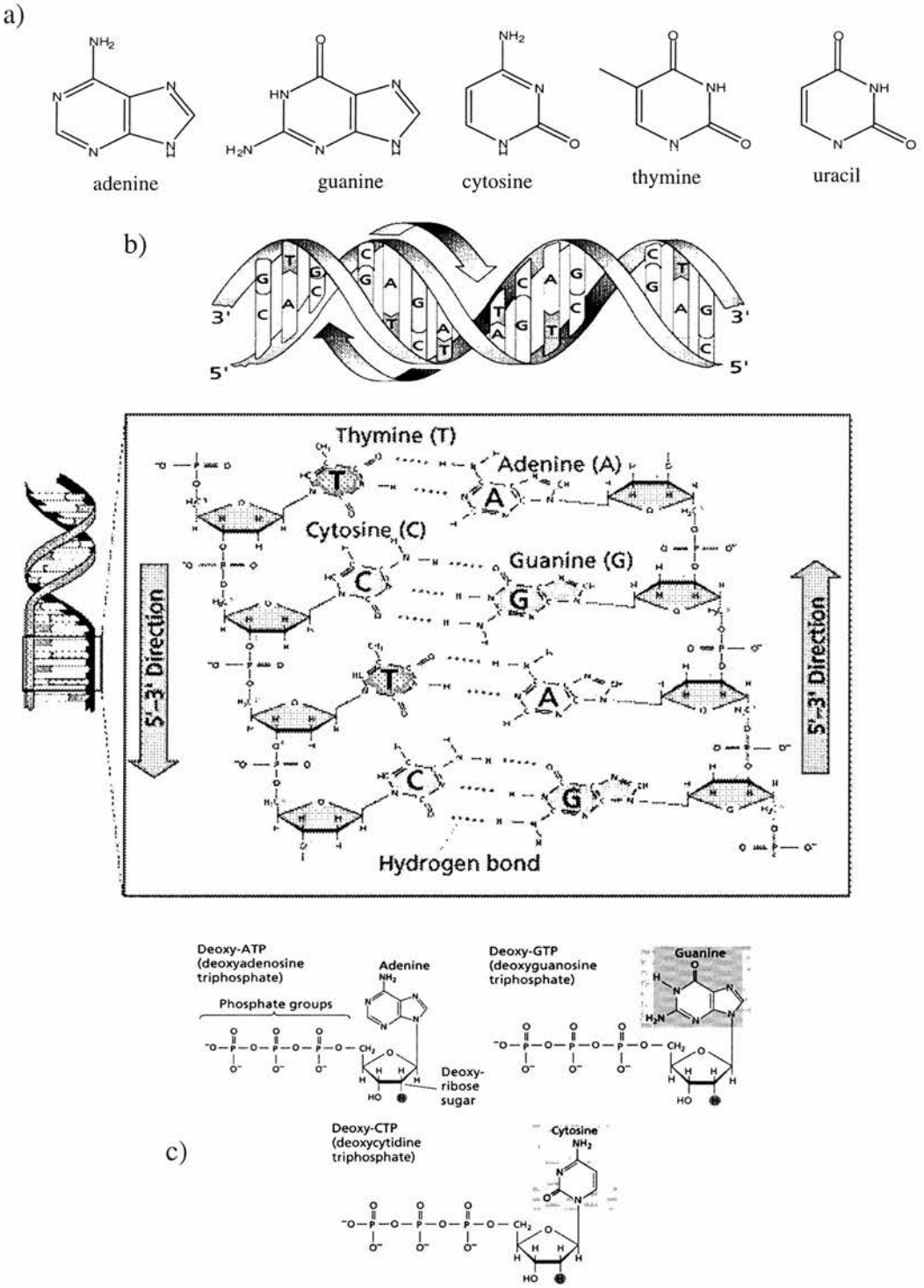

Fig. 1.4 [61] Structure of DNA and hydrogen bonding involved in the base pair formation (a) nucleic acid bases, (b) base pairing /double helix (c) sub unit of DNA

Fig 1.4 a presents the nucleic acid bases which can be seperated into one of two heterocyclic compounds, purine and pyrimidine. The purines being adenine(A) and guanine (G), the pyrimidines thymine(T) and cytosine(C). Uracil(U) replaces cytosine in RNA. As a consequence of base pair hydrogen bonding the DNA structure forms the well known double helix, fig 1.4b. The specificity being that A can only pair with T and C only with G. It is sequences of nucleic acid bases or Genes, held together by the sugar phosphate backbone which code for a particular function for example hair colour or the synthesis of a particular protein. RNA unlike DNA is single stranded and as previously mentioned contains the base uracil instead of thymine. The RNA's function is to copy the genetic code from the DNA which is restricted to the cells nucleus and transfer it out to the protein synthesising organelles, ribosomes . Another type of RNA then plays an integral part in protein synthesis.

1.5 Biomolecules on surfaces

Origins of life

It has been postulated that terrestrial life on earth began with the primordial soup consisting of small biomolecules on mineral surfaces [62]. More specifically, the nucleic acid bases and amino acids on platforms such as molybdenite [63]. One of the most fundamental questions presenting itself from the origins of life, is why human beings incorporate exclusively left handed amino acids and not the right handed

counterparts. That is, why the left -handed chirality was chosen and at what stage this occurred. There is also an intimate relationship between the chirality of nucleic acid bases and that of the amino acids in this respect.

Self assembled monolayers

Within the last decade a growing importance has been attached to self–assembled monolayers both as models for biological membranes, and as thin film coatings. It has been hypothesised that self-assembly of nucleic acid bases on inorganic surfaces had a role in the emergence of terrestrial life[62]. Thiols on gold have been extensively studied, with modification of the head groups being essential for the realisation of further surface reactions. This strategy has been successfully employed to immobilise amines onto gold using aldehyde-terminated SAMs[64].

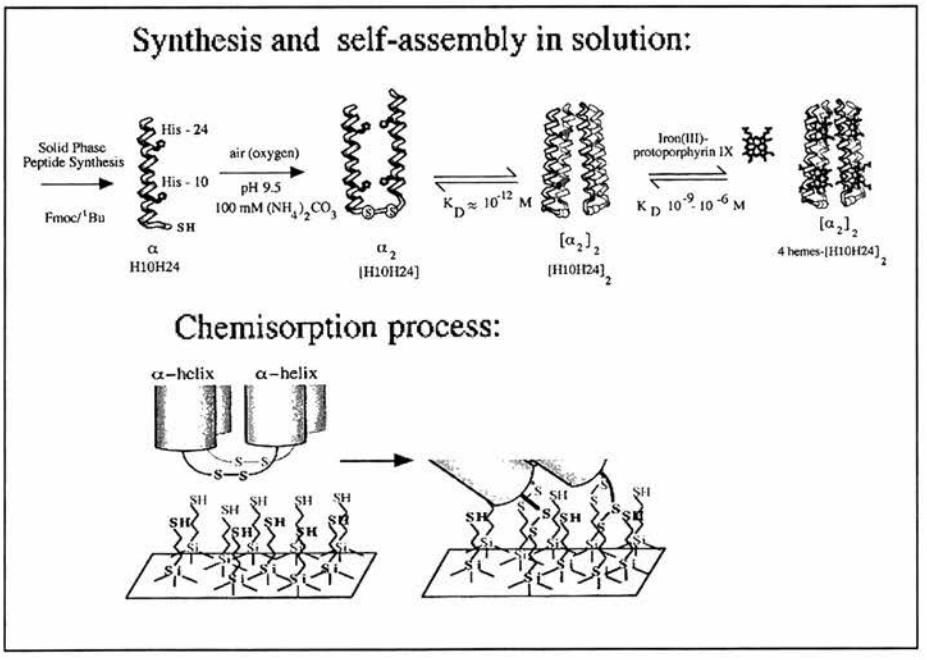

Fig. 1.5 Self organized monolayers of heme protein maquettes onto silanized quartz[67]

As organic chemists have had more success in tailoring the head groups, biological surface chemistry is playing a more prominent role. For example the immobilisation of DNA has been achieved using self-assembled monolayers on gold[65]. Another such example of the tailoring of surface chemistry has been in the development of selective functional thin films with, for example, the attachment of antigenic peptide to SAMs[66]. Pilloud et al have formed organised monolayers of peptide sections of heme proteins onto silanized quartz[67], fig. 1.5, and demonstrated the more complex, in terms of reaction pathways, aspect of SAMs research, which in this case does not just involve dipping a substrate into a solution, a common misconception.

Formation of chiral self-assembled monolayers has been reported by Nissink et al[68]. However in this paper, no evidence for creation of a chiral surface has been presented and there is an absence of techniques such as circular dichroism, which can detect chirality. Characterisation of SAM's is usually carried out using techniques such as ellipsometry, contact angle goniometry and infrared spectroscopy as demonstrated by Leidberg et al on the self-assembly of α-functionalized terthiophenes on gold[69]. UHV is not routinely used for the characterisation of complex SAMs, because they are produced in the realms of solution chemistry and are thus best characterised as they are formed, in solution.

Solution deposition

Unfortunately, the use of UHV to detect water interactions is limited to simple molecules. Inevitably, solution chemistry is required for the more complex systems Relying on a similar principle to the formation of self-assembled monolayers from solution, Leidberg and Ihs attempted to bond aqueous cysteine to evaporated gold and copper surfaces [70]. They inferred from the infrared spectra that the L- cysteine bonded to the gold and copper via the sulphur moiety, fig. 1.6.

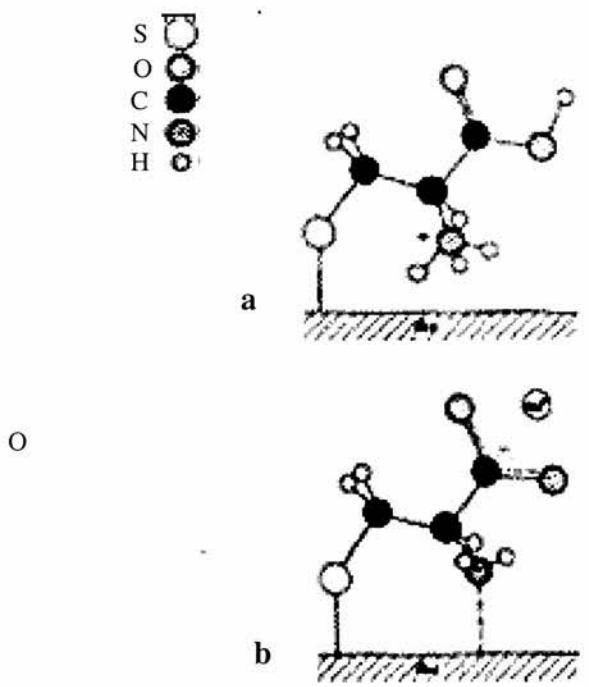

Fig. 1.6 Proposed structure of L-cysteine a) on gold , b) on copper [70]

Chiral Surfaces

It is the aim of pharmaceutical companies to synthesise drugs of one pure enantiomeric form as these are more effective and have less risk of undesirable side effects than the more easily produced racemic mixtures. Currently, homogeneous catalysts are of prime importance. Investigations into the manufacture of optically pure compounds have been spearheaded by the design of enantioselective catalysis. One approach is to attach chiral modifier molecules to a reactive metal surface. Raval and coworkers [71] studied the surface behaviour of R, R-tartaric acid and its enantiomer on the Cu(110) single crystal, fig 1.7. In these cases, the chiral molecules act as nanoscopic molecular guidance systems, which enforce the reactant to produce only one optical product. An important distinction should be made between chirality of the molecule in its free state and the chirality of the absorbed molecule on the substrate. When considering the chirality of the surface the symmetry of the unit cell of adsorbate on the crystal is the determining condition for chirality. It has been reported that molecular chirality has been directly observed using the STM[72]. Walba et al studied liquid crystals adsorbed on graphite, which were imaged under constant current mode.

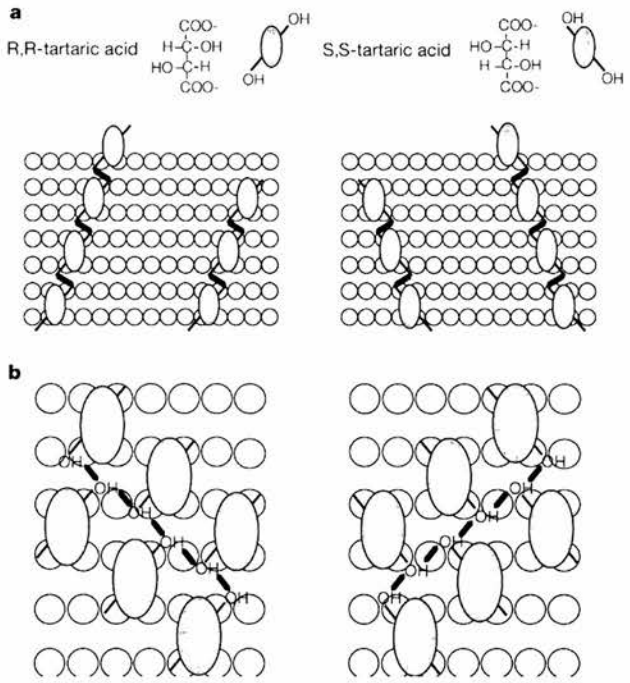

Fig 1.7 Intermolecular hydrogen bonding interactions of the α-hydroxy groups on the two enantiomers of tartaric acid. Left column shows the (R,R)-TA and the right column (S,S)-TA. The short thick lines indicate hydrogen bond interactions. In **a** the interactions dictate the direction of the chain growth, in **b** they link the molecular chains[71]

Interactions with water

When amino acids are adsorbed onto a surface, there is always a competition between inter-molecular forces and molecule-surface forces. As expected, this effect is surface coverage dependent. Complications are likely to occur when water is co-adsorbed. Hydrogen bonding interactions can affect the configuration of the surface

species. Little is understood in terms of molecular detail at the current time but research in this area is important, as an aqueous solution is a natural environment for biomolecules. UHV deposition is an ideal experimental method to investigate these problems as, unlike solution techniques, water surface coverage can be controlled, albeit at low temperatures, and effects of surface coverage can be measured on adsorbate orientation. It is possible that conformational changes in peptides could be measured as a consequence of interactions with the water. Within a protein, the hydrophobic amino acids arrange to be on the inside of the structure, with the hydrophilic ones being in contact with the water thus causing contortions and folding. It might be possible to observe the conformational changes in the peptides by inserting these interactive amino acids in different places within the sequence, then reacting with water molecules in a UHV environment.

Enquist and Liedberg studied the interaction of water with self-assembled monolayers using UHV system[73]. Changes in the IRAS spectrum after dosing the monolayer with D_2O indicated that the water did interact with the methylmervaptohexadecanoate.

In order to condense water (D_2O) on an organic surface in UHV, the environment has to be cooled down to less than 150K. The best way to analyse whether the water molecules interact with an organic thin film is by a combination of TPD and

surface spectroscopy which has also been employed by Enquist et al to examine how the organic monolayers characteristics (wettability) affects interactions with D_2O.[74]

1.6 Adsorption of larger molecules

Barlow et al used a combination of RAIRS and LEED to describe the adsorption of glycine on Cu (110) [75]. Using vibrational spectroscopy, which gave information on the orientation of the adsorbed species relative to the surface, and the electron diffraction, which yields information on the 2D crystal structure, a model could be developed for the system, fig 1.8.

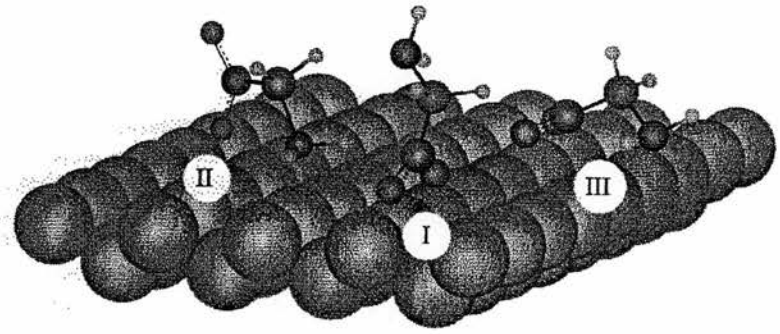

Fig 1.8 Proposed conformational models for the glycinate species adsorbed on the Cu (110) surface [75] at low coverage (1), room temperature saturation coverage (11) and after annealing to 420K (111)

Surface enhanced Raman spectroscopy (SERS) has been applied to the adsorption of glycine, alanine and aminobenzoic acid on silver colloid particles [76]. Chemisorption was detected, however SERS is only employable to very specialised systems.

Fundamental studies on amino acids and nucleic acid bases are useful in terms of understanding molecular interactions but, for practical purposes, for example construction of a biosensor, the larger polyunit molecules must be considered. The natural progression from amino acids would be peptides and Weib et al have bonded cyclopeptides onto gold surfaces [77], being electrodes for a quartz crystal micro-balance. Enantiomeric discrimination of the ultrathin film was measured in solution. Cysteine within the cyclopeptides, fig.1.9, was responsible for the anchoring of the molecules to the gold coated quartz.

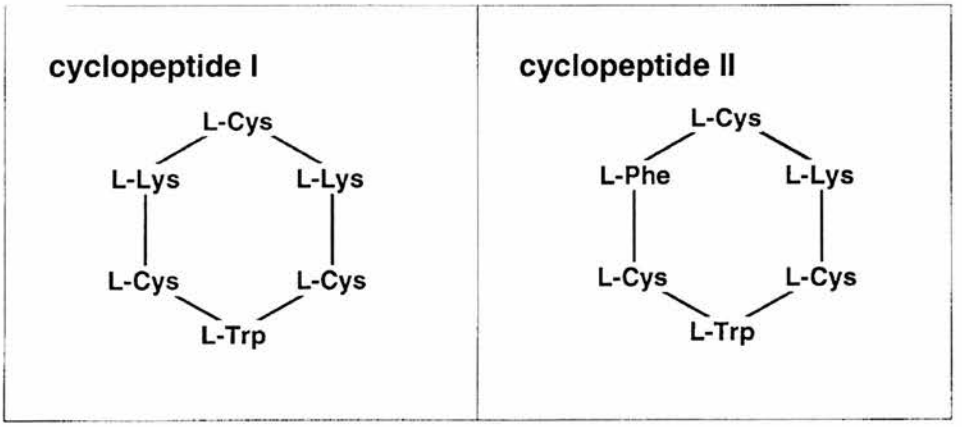

Fig 1.9 Chemical structure of the two synthetic cyclohexapeptides used for the preparation of chiral monolayers on quartz micro-balance sensors [77]

This approach seems quite exciting as maybe two levels of periodicity could be created, the first due to the amino acid sequence and the second a consequence of the constriction of the cyclic structure (similar to tiling).

It is the specificity of the molecular recognition between base pairs that has inspired investigations into the potential tethering of DNA and its analogue PNA (peptide nucleic acid) to surfaces for biosensors to detect genetic defects[78]. Additionally the DNA base molecules are both stiff and planar thus leading to a potentially fascinating observation of hydrogen bonding systems using surface science techniques. Edelwirth et al used molecular mechanics calculations to study the hydrogen bonding of adenine monolayers on graphite[79]. Uracil and thymine have been adsorbed onto Au (111) electrodes and investigated using STM and IR[80]. The *in situ* study performed in electrolytes of water and D_20 showed that both of the bases chemisorbed, with uracil in particular forming highly ordered regions. The infrared data was used to determine the surface co-ordination with the ordering, i.e. uracil forming a $c(3\times\sqrt{3})$, being realised from STM data.

In terms of complexity, the two dimensional crystallisation of proteins represents the ultimate achievement of ordering at a surfaces which has mostly been achieved on lipid layers [81]. Recent work by Whitesides [82] has pioneered the attachment and selectivity of proteins onto self assembled monolayers on gold. By controlling the head group of the alkyl thiol chains, which are tethered to gold, SAMs have been

produced which can selectively bind to proteins and in some cases resist protein adsorption altogether.

1.7 Cell attachment

Tethering of cells to surfaces has been a priority in biomaterials research with the ultimate objective being micro-patterning in order to obtain selective cell and therefore metabolic activity. If, for example, osteoblasts were to be attached to synthetic bone, the role of the implant could be to promote healing and thus bypass the difficulty associated with trying to design a structure for load bearing.

Certain peptides have been found to be important for cell binding. These include the Arg-Gly-Asp and Tyr-Lle-Gly-Ser-Arg containing peptides used by Massia et al [83]. Self-assembled monolayers have been synthesised that contain cell binding peptide domains as the functional groups [84]. One method for studying the adhesion of cells to thin films is the quartz crystal balance, which has been used to measure the attachment of living cells to. surfaces[85].

1.8 STM of Biomolecules

Before describing the current state of research in this area of characterisation, attention should be drawn to the sometimes subtle difference between attaching a molecule to a surface in order to study the system as a whole as in the case for example

of cysteine on gold and the use of surface attachment as a means of sample preparation (For structural integrity and fulfilling the conductivity requirement).

A major problem that scientists are actively tackling is the means of depositing the biomolecules on the conducting substrates in their whole form without fragmentation, which can be induced by heating. One such procedure is the pulse injection method, which was used by Tanaka et al to deposit single stranded and double stranded plasmid DNA on the Cu(111) single crystal[86]. The observed height of 0.2nm for STM image features, is the typical value for the height of nucleic acid base molecules on Cu(111) , fig 1.10.

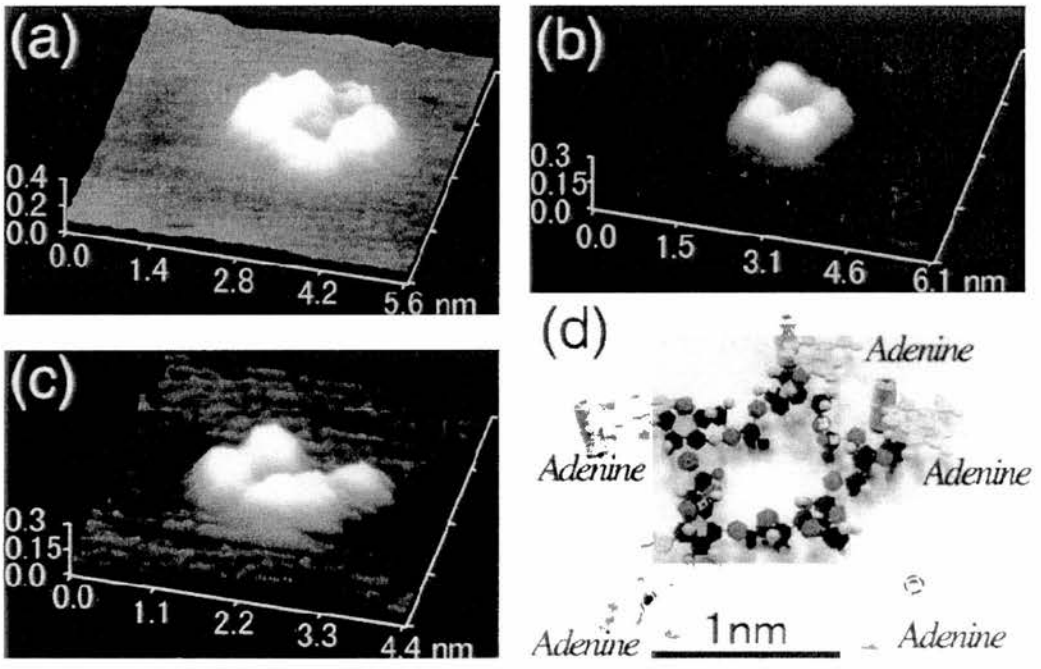

Fig 1.10 A series of high magnification STM Images of DNA molecules on Cu(111) [86]

When interpreting STM images of larger biological molecules, special care is needed, as many contrast features can be contributions from uncontrollable factors. Biologists became very excited when they first saw the first clear images of DNA in its double helix arrangement[87] but it was later shown that the image was actually an artefact produced by the graphite substrate.

As the sample, tip and substrate need to be conducting for a tunnelling current to be detected, the electrical properties of the biological molecule must be known. An important case, is the role of water as a contrast mechanism in the imaging of proteins by STM[88]. Theories for the reason why proteins can be observed at all by STM have concluded that deformation of the adsorbate by the tip alters the samples electronic state, thus allowing resonant tunnelling to occur. Leggett et al found that under normal (hydrated) conditions the protein islands are observed to be higher than the gold substrate whereas, under dehydrated conditions, the reverse is true.

Chemisorption of organic molecules on electrodes has been routinely used to modify electrochemical properties. Cysteine has been absorbed on Au(111) electrodes and cyclic voltamograms were used to measure the change in electrochemical response[89]. Bearing this in mind and how the organic molecules effect electron transfer, it is not difficult to see how it could be hypothesised that similarly modified tips could affect imaging in the STM. Ambient STM studies with chemically modified tips have

been relatively successful in distinguishing between molecular species[90] and using polypyrrole tips for functional group recognition.

1.9 Thesis scope and aim

It is the objective of this study to find out whether the adsorbtion of small bio-molecules can be controlled in such a way that ordered two-dimensional crystals could be formed. It is of particular importance to examine the hydrogen bonding systems and see how the functional groups and complexity of the molecule affects the nanostructures.

Chapter two described the experimental methods and some theory of surface physics. In chapter three the adsorption of the chiral amino acid, phenylglycine, is shown to form a chiral surface to which a model is proposed to explain this phenomenon. The focus of chapter 4 is the amino acid, amino benzoic acid. It is demonstrated to be to orientate in both a flat lying and upright configuration, depending on surface coverage. The molecular wires so formed are explained as being formed by the upright molecules at domain boundaries. Chapter 5 deals with α-pyridone and how this nucleic acid base analogue forms hydrogen bonded two-dimensional crystals. Pyrimidine bases thymine and cytosine are examined in chapter 6, both being able to form highly ordered crystal structures, and models have been proposed. The purine

base adenine self assembly and chiral surface behaviour is described in chapter 7. Finally a general conclusion brings the thesis findings together in chapter 8.

References:

1 J. Kuther, M. Bartz, R. Seshadri, G. B. M. Vaughan, and W. Tremel, *J. Mater. Chem.* **11,** 503-506 (2001).

2 C. Robinson, J. Zhang, R. C. Shore, S. Brookes, S. Wood, D. A. Smith, M. Wallwork, and J. Kirkham, *J. Dent. Res.* **79,** 72 (2000).

3 N. L. Huq, K. J. Cross, and E. C. Reynolds, *J. Mol. Model.* **6,** 35-47 (2000).

4 K. K. W. Wong and S. Mann, *Curr. Opin. Colloid Interface Sci.* **3,** 63-68 (1998).

5 W. Stumm, in *Aquatic Chemistry*, Vol. 244 (1995), pp. 1-32.

6 A. Boulbitch, Z. Guttenberg, and E. Sackmann, *Biophys. J.* **81,** 2743-2751 (2001).

7 R. Gessner and R. Tauber, in *Epithelial Transport nd Barrier Function*, Vol. 915 (2000), pp. 136-143.

8 E. Granot, D. Shouval, and Y. Ashur, *Mediat. Inflamm.* **10,** 253-258 (2001).

9 M. Ohgaki, T. Kizuki, M. Katsura, and K. Yamashita, *J. Biomed. Mater. Res.* **57,** 366-373 (2001).

10 S. S. Schaus and E. R. Henderson, *Biophys. J.* **73,** 1205-1214 (1997).

11 K. Smetana, J. Lukas, V. Paleckova, J. Bartunkova, F. T. Liu, J. Vacik, and H. J. Gabius, *Biomaterials* **18,** 1009-1014 (1997).

12 V. N. Sytnyk, A. E. Dityatev, and S. M. Korogod, *Neurophysiology* **33,** 11-14 (2001).

13 K. Tsuchiya, G. P. Chen, T. Ushida, T. Matsuno, and T. Tateishi, *Mater. Sci. Eng. C-Biomimetic Supramol. Syst.* **17,** 79-82 (2001).

14 J. D. Whittard and S. K. Akiyama, *J. Cell Sci.* **114,** 3265-3272 (2001).

15 H. Cai, C. Xu, P. G. He, and Y. Z. Fang, *J. Electroanal. Chem.* **510,** 78-85 (2001).

16 K. D. Fowers and J. Kopecek, *Colloid Surf. B-Biointerfaces* **9,** 315-330 (1997).

17 T. Hianik, V. Gajdos, R. Krivanek, T. Oretskaya, V. Metelev, E. Volkov, and P. Vadgama, *Bioelectrochemistry* **53,** 199-204 (2001).

18 B. Piro, L. A. Dang, M. C. Pham, S. Fabiano, and C. Tran-Minh, *J. Electroanal. Chem.* **512,** 101-109 (2001).

19 M. Thompson, *Abstr. Pap. Am. Chem. Soc.* **222,** 301-COLL (2001).

20 H. Wang, Z. Y. Wu, G. L. Shen, and R. Q. Yu, *Chem. J. Chin. Univ.-Chin.* **22,** 1305-1309 (2001).

21 W. G. Brodbeck, M. S. Shive, E. Colton, Y. Nakayama, T. Matsuda, and J. M. Anderson, *J. Biomed. Mater. Res.* **55,** 661-668 (2001).

22 R. J. Friedman, Y. H. H. An, J. Ming, R. A. Draughn, and T. W. Bauer, *J. Orthop. Res.* **14,** 455-464 (1996).

23 J. A. Hunt, B. F. Flanagan, P. J. McLaughlin, I. Strickland, and D. F. Williams, *J. Biomed. Mater. Res.* **31,** 139-144 (1996).

24 G. L. Kenausis, J. Voros, D. L. Elbert, N. P. Huang, R. Hofer, L. Ruiz-Taylor, M. Textor, J. A. Hubbell, and N. D. Spencer, *J. Phys. Chem. B* **104,** 3298-3309 (2000).

25 G. F. Khan and W. Wernet, *Thin Solid Films* **300,** 265-271 (1997).

26 J. G. McGovern, C. P. Garvin, D. S. Jones, A. D. Woolfson, and S. P. Gorman, *Int. J. Pharm.* **149,** 251-254 (1997).

27 M. D. Phaneuf, S. A. Berceli, M. J. Bide, W. C. Quist, and F. W. LoGerfo, *Biomaterials* **18,** 755-765 (1997).

28 M. Qhobosheane, S. Santra, P. Zhang, and W. H. Tan, *Analyst* **126,** 1274-1278 (2001).

29 S. E. Sakiyama-Elbert and J. A. Hubbell, *Ann. Rev. Mater. Res.* **31,** 183-201 (2001).

30 M. C. Shen and T. A. Horbett, *J. Biomed. Mater. Res.* **57,** 336-345 (2001).

31 J. G. Steele, C. McFarland, B. A. Dalton, G. Johnson, M. D. M. Evans, C. R. Howlett, and P. A. Underwood, *J. Biomater. Sci.-Polym. Ed.* **5,** 245-257 (1993).

32 S. Babacan, P. Pivarnik, S. Letcher, and A. G. Rand, *Biosens. Bioelectron.* **15,** 615-621 (2000).

33 T. H. Ha and K. Kim, *Langmuir* **17,** 1999-2007 (2001).

34 M. Liebau, A. Hildebrand, and R. H. H. Neubert, *Eur. Biophys. J. Biophys. Lett.* **30,** 42-52 (2001).

35 H. Matsuno, K. Niikura, and Y. Okahata, *Chem.-Eur. J.* **7,** 3305-3312 (2001).

36 V. S. Muralidharan, *Bull. Electrochem.* **17,** 183-192 (2001).

37 C. Pickering, *Surf. Interface Anal.* **31,** 927-937 (2001).

38 T. P. Vikinge, K. M. Hansson, P. Sandstrom, B. Liedberg, T. L. Lindahl, I. Lundstrom, P. Tengvall, and F. Hook, *Biosens. Bioelectron.* **15,** 605-613 (2000).

39 M. Bardosova, P. Hodge, A. Korenova, F. Nakanishi, and R. H. Tredgold, *Thin Solid Films* **397,** 8-11 (2001).

40 T. S. Berzina, V. I. Troitsky, and M. P. Fontana, *Mater. Sci. Eng. C-Biomimetic Supramol. Syst.* **15,** 315-317 (2001).

41 S. W. Jeong and H. S. Lim, *Synth. Met.* **123,** 183-187 (2001).

42 K. Muramatsu, M. Takahashi, K. Tajima, and K. Kobayashi, *J. Colloid Interface Sci.* **242,** 127-132 (2001).

43 J. F. Nierengarten, J. F. Eckert, Y. Rio, M. D. Carreon, J. L. Gallani, and D. Guillon, *J. Am. Chem. Soc.* **123,** 9743-9748 (2001).

44 M. Sano, A. Kamino, J. Okamura, and S. Shinkai, *Langmuir* **17,** 5125-5128 (2001).

45 T. Yamaki, R. Shinohara, and K. Asai, *Thin Solid Films* **393,** 154-160 (2001).

46 T. Bitzer, N. V. Richardson, and D. J. Schiffrin, *Surf. Sci.* **382,** L686-L689 (1997).

47 T. Bitzer and N. V. Richardson, *Appl. Surf. Sci.* **145,** 339-343 (1999).

48 Q. Chen, C. C. Perry, B. G. Frederick, P. W. Murray, S. Haq, and N. V. Richardson, *Surf. Sci.* **446,** 63-75 (2000).

49 Q. Chen, S. Haq, B. G. Frederick, and N. V. Richardson, *Surf. Sci.* **368,** 310-317 (1996).

50 J. Benesch, S. Svedhem, S. C. T. Svensson, R. Valiokas, B. Liedberg, and P. Tengvall, *J. Biomater. Sci.-Polym. Ed.* **12,** 581-597 (2001).

51 Z. Dai and H. X. Ju, *Phys. Chem. Chem. Phys.* **3,** 3769-3773 (2001).

52 C. B. Gorman, Y. F. He, and R. L. Carroll, *Langmuir* **17,** 5324-5328 (2001).

53 X. P. Jiang, C. Ortiz, and P. T. Hammond, *Abstr. Pap. Am. Chem. Soc.* **222,** 115-COLL (2001).

54 T. Ohgi, D. Fujita, W. Deng, Z. C. Dong, and H. Nejoh, *Surf. Sci.* **493,** 453-459 (2001).

55 Z. Q. Peng and S. J. Dong, *Langmuir* **17,** 4904-4909 (2001).

56 D. Z. Shen, M. H. Huang, L. M. Chow, and M. S. Yang, *Sens. Actuator B-Chem.* **77,** 664-670 (2001).

57 M. Tanahashi and T. Matsuda, *J. Biomed. Mater. Res.* **34,** 305-315 (1997).

58 V. H. Matthews, (1996).*Biochemistry*

59 L. Stryer, (Fourth Edition). *Biochemistry*

60 Guyton, (eighth edition). *Textbook of Medical Physiology*

61 Purves, (4th Edition). *Life the science of Biology*

62 S. J. Sowerby, M. Edelwirth, and W. M. Heckl, *J. Phys. Chem. B* **102,** 5914-5922 (1998).

63 S. J. Sowerby, W. M. Heckl, and G. B. Peterson, **43,** 419 (1996).

64 R. C. Horton, T. M. Herne, and D. C. Myles, *J. Am. Chem. Soc.* **119,** 12980-12981 (1997).

65 N. Higashi, T. Minoru, and M. Niwa, **15,** *Langmuir* 111 (1999).

66 L. Scheibler, P. Dumy, M. Boncheva, K. Leufgen, H. J. Mathieu, M. Mutter, and H. Vogel, *Angew. Chem.-Int. Edit.* **38,** 696-699 (1999).

67 D. L. Pilloud, F. Rabanal, B. R. Gibney, R. S. Farid, P. L. Dutton, and C. C. Moser, *J. Phys. Chem. B* **102,** 1926-1937 (1998).

68 J. W. M. Nissink and J. H. van der Maas, *Appl. Spectrosc.* **53,** 33-39 (1999).

69 B. Liedberg, Z. Yang, I. Engquist, M. Wirde, U. Gelius, G. Gotz, P. Bauerle, R. M. Rummel, C. Ziegler, and W. Gopel, *J. Phys. Chem. B* **101,** 5951-5962 (1997).

70 A. Ihs and B. Liedberg, *J. Colloid Interface Sci.* **144,** 282-292 (1991).

71 M. Ortega Lorenzo, C. J. Baddeley, C. Muryn, and R. Raval, *Nature* **404** (2000) 376-379.

72 M. Walba, S. Forrest, N. Clark, and D. Parks, *Accounts of Chemical Research* **29** (1996).

73 I. Engquist and B. Liedberg, *J. Phys. Chem.* **100,** 20089-20096 (1996).

74 I. Engquist, I. Lundstrom, and B. Liedberg, *J. Phys. Chem.* **99,** 12257-12267 (1995).

75 S. M. Barlow, K. J. Kitching, S. Haq, and N. V. Richardson, *Surf. Sci.* **401,** 322-335 (1998).

76 J. S. Suh and M. Moskovits, *J. Am. Chem. Soc.* **108,** 4711-4718 (1986).

77 T. Weiss, D. Leipert, M. Kaspar, G. Jung, and W. Gopel, *Advanced Materials* **11,** 331 (1999).

78 J. Wang, P. E. Nielsen, M. Jiang, X. H. Cai, J. R. Fernandes, D. H. Grant, M. Ozsoz, A. Beglieter, and M. Mowat, *Anal. Chem.* **69,** 5200-5202 (1997).

79 M. Edelwirth, J. Freund, S. J. Sowerby, and W. M. Heckl, *Surf. Sci.* **417,** 201-209 (1998).

80 W. H. Li, W. Haiss, S. Floate, and R. J. Nichols, *Langmuir* **15,** 4875-4883 (1999).

81 S. Koppenol and P. S. Stayton, *J. Pharm. Sci.* **86,** 1204-1209 (1997).

82 G. M. Whitesides, J. P. Mathias, and C. T. Seto, Science **254,** 1312 (1991).

83 S. P. Massia and J. A. Hubbell, *Anal. Biochem.* **187,** 292-301 (1990).

84 C. Roberts, C. S. Chen, M. Mrksich, V. Martichonok, D. E. Ingber, and G. M. Whitesides, *J. Am. Chem. Soc.* **120,** 6548-6555 (1998).

85 C. Fredriksson, S. Kihlman, M. Rodahl, and B. Kasemo, *Langmuir* **14,** 248-251 (1998).

86 H. Tanaka, C. Hamai, T. Kanno, and T. Kawai, *Surf. Sci.* **432,** L611-L616 (1999).

87 C. R. Clemmer and T. P. Beebe, *Science* **251,** 640 (1991).

88 G. J. Leggett, M. C. Davies, D. E. Jackson, C. J. Roberts, S. J. B. Tendler, and P. M. Williams, *J. Phys. Chem.* **97,** 8852-8854 (1993).

89 W. R. Fawcett, M. Fedurco, Z. Kovacova, and Z. Borkowska, *Langmuir* **10,** 912-919 (1994).

90 T. Ito, P. Buhlmann, and Y. Umezawa, *Anal. Chem.* **70,** 255-259 (1998).

912-919 (1994).

.

CHAPTER 2 . Experimental Methods

In the proceeding discussion the various experimental methods used will be described. For a more rigorous treatment, standard textbooks can be recommended[1-11] Ultra high vacuum conditions are required for several reasons:

1) Techniques that utilise electrons require low pressure otherwise the mean free path would be too low.

2) Simplification of systems with minimum contamination.

3) Low pressure allows realistic times for gas/surface reactions to be accurately measured and hence repeated.

2.1 Low energy electron diffraction (LEED)

Unlike transmission electron microscopy, whereby electrons require high energies to pass through the bulk sample, LEED utilises electrons in the range 10 – 300eV so as to penetrate and be reflected by only the top few surface layers of the crystal. As the wavelength of the electrons is similar in magnitude to the inter atomic spacing, diffraction occurs and the electrons are scattered at angles which satisfy the Bragg equation.

$$n\lambda = d\sin\theta \quad (2.1)$$

Where n is the order of diffraction θ is the diffraction angle measured from the surface normal, d is the interatomic spacing.

A grid system, fig. 2.1, filters out inelastically scattered electrons and an image of the diffraction pattern is displayed on a phosphor screen. The pattern is in reciprocal space, which can be simply related to real space crystal structure, equations 2.1-2.3.

$G = n\mathbf{a}^* + m\mathbf{b}^*$ (where n and m are integers) (2.2)

$\mathbf{a}^* = 2\pi/\mathbf{a}$ $\mathbf{b}^* = 2\pi/\mathbf{b}$ $\mathbf{a}.\mathbf{b}^* = \mathbf{a}^*.\mathbf{b} = 0$ (2.3)

a and **b** are real lattice vectors, **a*** and **b*** the corresponding reciprocal lattice vectors The principle of conservation of parallel momentum of the electrons allows the use of the Ewald sphere construction, which is a graphical representation of the conditions that will satisfy the diffraction conditions, fig. 2.2. From LEED, the size and shape of the two dimensional unit cell of adsorbate and substrate can be determined.

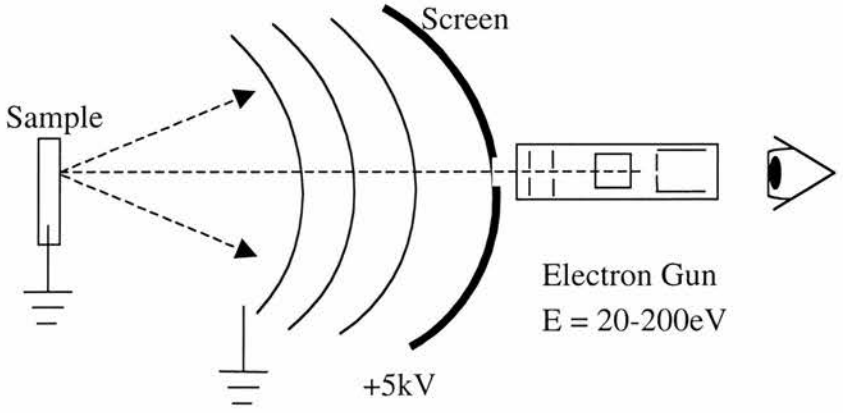

Fig. 2.1 A typical LEED system and its optics.

2.2 Description of over-layer structures

At this point, it is appropriate to describe the methodology and notation to describe the system and notation for describing adsorbate structures in relation to the crystal substrate.

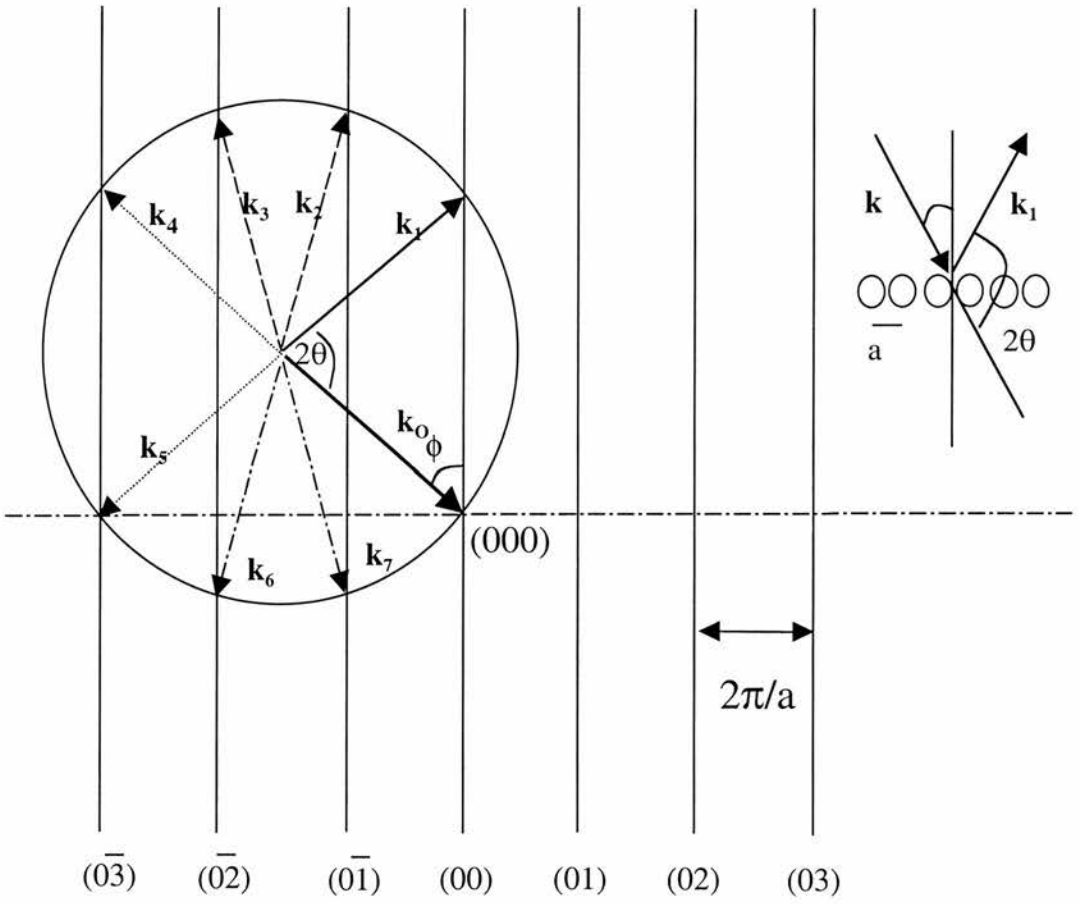

Fig. 2.2 Ewald sphere construction applied to diffraction from a square net of atoms side a. Incident wavevector k_0 arriving at angle of incidence to the surface normal. Four beams are shown back scattered from the surface. Three beams are shown transmitted into the solid. Real space diagram of the specular beam K_1'[5]

Firstly the diffraction pattern is expressed in terms of four reciprocal space vectors, two defining the substrate spots ($\mathbf{a_S}$*,$\mathbf{b_S}$*) and two defining the over-layer spots ($\mathbf{a_0}$*, $\mathbf{b_0}$*). Figure 2.3 presents these vectors for a (4×3) pattern. Only some of the over-layer spots are shown.

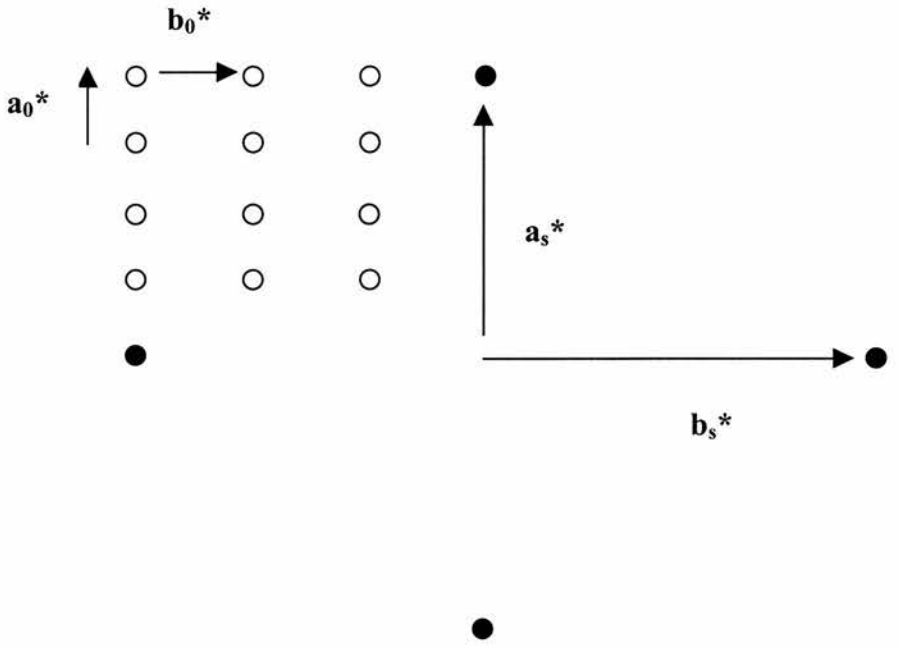

Fig.2.3 Obtaining real space structure from diffraction pattern, the open circles represent diffraction spots due to the absorbate, the black spots are the contributions from the Cu(110) substrate

Relationship between substrate reciprocal lattice vectors $\mathbf{a_S}^*$, $\mathbf{b_S}^*$ and adsorbate reciprocal lattice vectors $\mathbf{a_0}^*$, $\mathbf{b_0}^*$.

$$\mathbf{a_0}^* = 1/4\ \mathbf{a_S}^* + 0\ \mathbf{b_S}^*$$

$$\mathbf{b_0}^* = 0\ \mathbf{a_S}^* + 1/3\ \mathbf{b_S}^*$$

Forming a matrix G* of the coefficients gives:

$$G^* = \begin{pmatrix} 1/4 & 0 \\ 0 & 1/3 \end{pmatrix}$$

Transforming G* to real space by taking the inverse transpose:

$$G = ([G^*]^{-1})^t = 1/12 = \begin{pmatrix} 1/4 & 0 \\ 0 & 1/3 \end{pmatrix} = \begin{pmatrix} 3 & 0 \\ 0 & 4 \end{pmatrix}$$

Hence the relationship between the real space adsorbate and substrate vectors can now be expressed as:

$$\mathbf{a_0} = 3\mathbf{a_S} + 0\mathbf{b_S}$$

$$\mathbf{b_0} = 0\mathbf{a_S} + 4\mathbf{b_S}$$

$\therefore$ (3×4)

Some LEED patterns exhibit "missing" spots due to glide plane symmetry [12]. This can aid in interpreting the structure of the over-layer by limiting the possible positions of features in a unit cell. The operation of a glide plane is described by a translation half the distance of the unit cell followed by a reflection in the glide line. Several examples of these patterns are examined in this thesis. Glide planes are donated by the symbol **g**.

2.3 Scanning tunnelling microscopy (STM)

The modus operandi of the STM, fig. 2.4, is simple with the explanation of the imaging process requiring some effort. An atomically sharp tip is bought into close proximity to the conducting surface. Application of a small voltage, typically less than 1eV, when the tip is in an appropriate position causes a tunnelling current to flow. The magnitude of the current is strongly; exponentially dependent on the tip sample separation and this can be used for high resolution imaging. Two modes of scanning may be employed. Constant height mode allows the tip to remain stationary in the z direction, while being scanned in the x y domain, producing variations in current with position. Alternatively, constant current operation relies on the value of the tunnelling current remaining constant by adjustment of movement in the z direction.

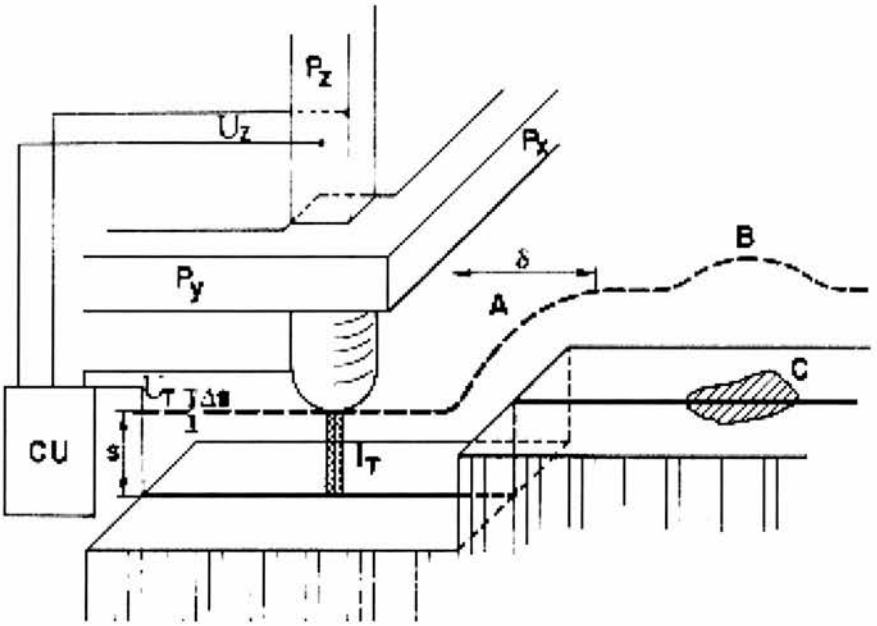

Fig. 2.4 Principle of STM[10] - piezodrives Px and Py scan the metal tip over the surface. The control unit (CU) applies the appropriate voltage Uz to the piezodrive Pz for constant tunnel current I_T at constant tunnel voltage U_T. The broken line indicates the z displacement in a scan over a surface step (A) and a chemical inhomogeneity (B).

In order to interpret images of molecules, it is crucial to gain an understanding of the mechanism by which the tunnelling current is produced and what entity, i.e. bonding molecular orbital, the electrons are tunnelling into.

Considering one dimensional tunnelling in which an electron is incident upon an infinitely thick barrier of height V, writing down the Schrodinger equation [10].

For $x < 0$ $\quad \mathbf{H} = -(\hbar^2/2m)(d^2/dx^2)$ (2.4)

$x>0$ $\quad \mathbf{H} = -(\hbar^2/2m)(d^2/dx^2) + V$ (2.5)

The solutions of the above second order differential equation are of the standard form:

$\psi = Ae^{ikx} + Be^{-ikx}$, where $k = (2mE/\hbar^2)$ inside the well (2.6)

$\psi = Ce^{ik'x} + De^{-ik'x}$, where $k = (2m(E-V)/\hbar^2)^{1/2}$ inside the barrier (2.7)

It is a worthwhile exercise to derive these equations as they show that electrons can be present in a region where classical mechanics forbids them to be. This can be seen, as in the region where E<V the wavefunction is non-zero.

Under constant height mode whereby the gap distance is maintained, the local density of states can be explored. Additionally changing the polarity of the applied voltage allows the probing of occupied and unoccupied states. A negative bias allows electrons to tunnel from occupied states in the tip to unoccupied states in the sample and for a positive bias the tunnelling is in the opposite direction. In the proceeding experimental typical tunnelling currents used were of the order of 10-1000 pA.

2.4 High resolution electron energy loss spectroscopy (HREELS)

A monochromatic electron beam can experience energy losses due to the excitation of surface vibrations. As a consequence of excitation energies being of the order of fractions of an electron volt the beam must be extremely monochromatic with a small energy spread. Excitation of vibrations can take place by three independent mechanisms. A typical EELS chamber is presented in fig. 2.5.

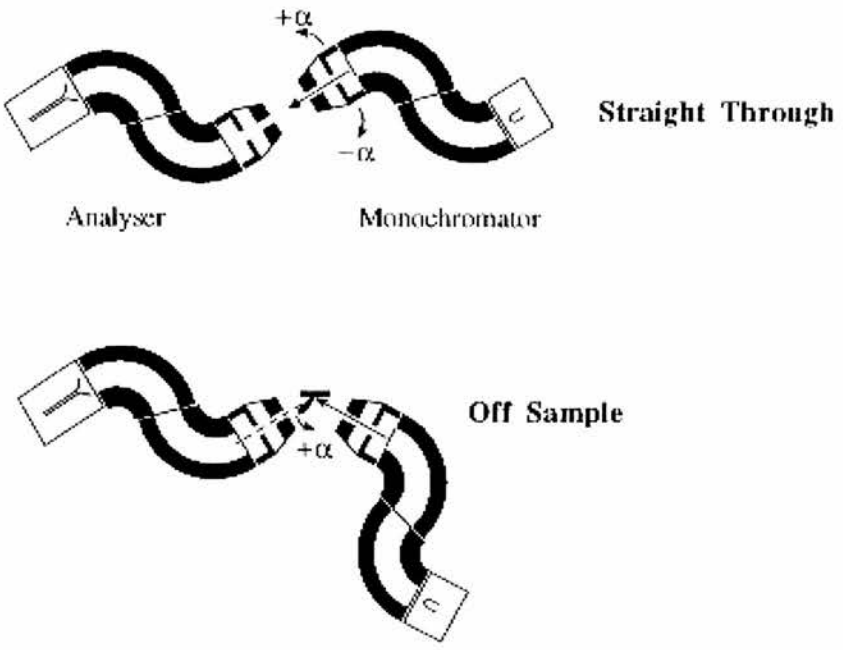

Fig. 2.5 Schematic diagram of a high-resolution electron energy loss spectrometer [12] illustrating the arrangement of monochromator and analyser and required to optimise the electron beam for high resolution.

Dipole Scattering Involves long range interaction between the electric field of the incident electron and the dynamic electric field from the molecular vibration. Only vibrations with dipole changes perpendicular to the surface will be excited. This mechanism is strongest in the specular direction or other direction which satisfies the Bragg condition, (eq 2.1) in ordered systems. When a dipole is situated in close proximity to a metal surface, an image dipole is evoked as a result of the behaviour of metal conduction electrons. This phenomenon is responsible for the surface dipole selection rule. If the dipole is aligned perpendicular to the surface, figure 2.6a, an image dipole is induced along the same direction. The effective result of the summation is a doubling of the amplitude. Alignment of the dipole parallel to the surface, figure 2.6b induced an image of opposite polarity and thus the summation is zero. The dipoles have cancelled each other out. To summarise, for these two cases, dipoles that are aligned parallel to the surface are unobservable while those aligned perpendicular to the surface are measurable. Within these two extreme orientations there are a range of angular alignment, but only the normal component is detectable.

b) Impact Scattering invokes an impact between incoming electron and adsorbed molecule, so only a short-range mechanism. Vibrations with dipole moments both parallel and perpendicular to the surface can be activated. Optimum conditions for observation of this mode is off specular. Because electrons are scattered in more

directions than in the dipole mode, intensities produced by impact scattering are considerably weaker.

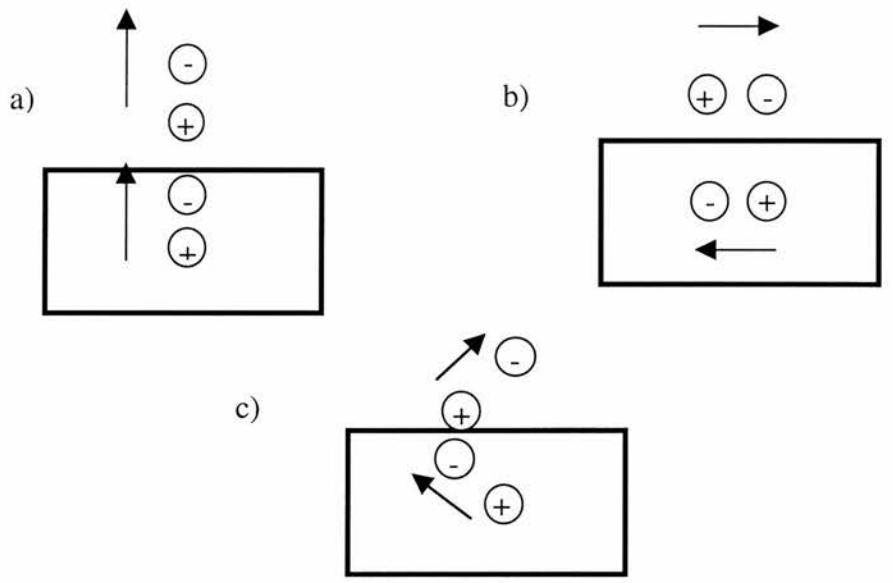

Fig. 2.6 Dipole selection rules: dipole moment aligned a) perpendicular to surface, b) parallel to the surface, c) angle to surface normal

c) Negative Ion Resonance requires an electron to be captured by an unoccupied electronic state of the absorbed molecule at the resonance energy. Thus a negative ion is formed temporarily, a lifetime of between 10^{-10} and 10^{-15} seconds. This phenomenon occurs at a particular energy, which is equivalent to the energy of an unoccupied state of the molecule and is known as the resonance energy. A model for this process is shown in figure 2.7.

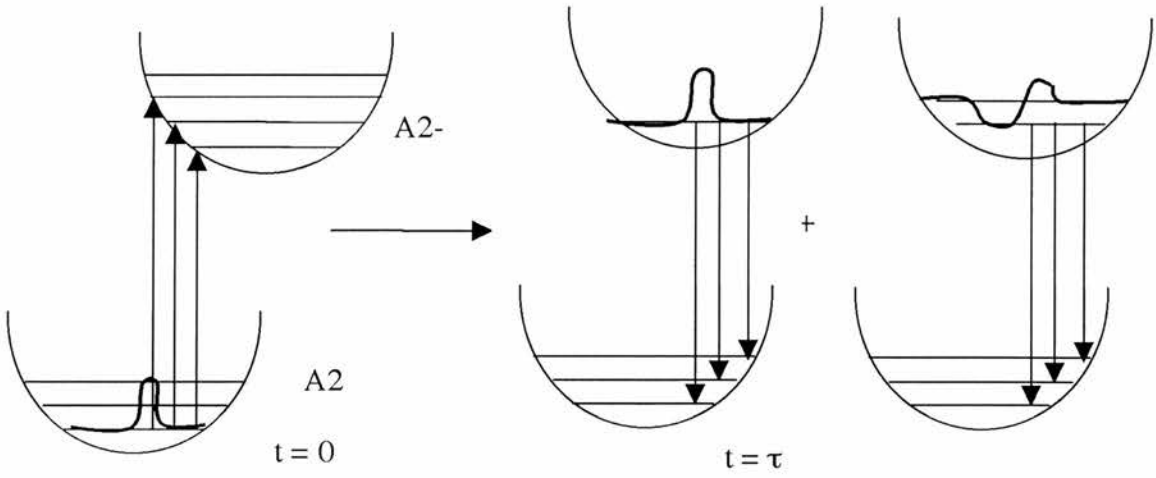

Figure 2.7 Negative Ion resonance mechanism of vibration excitation. The displacement of the oscillator potential of a neutral molecule for the duration of the lifetime of a negative ion is explained by the Frank-Condon picture[13]

2.5 Temperature programmed desorption (TPD)

TPD can yield information on the strength of interactions between adsorbed molecules and substrate. A linear temperature ramp programme increasing the sample temperature is applied to the sample and the rate of desorption of ionic species is monitored using a quadrupole mass spectrometer. Direct measurement of temperature of the sample can be achieved by spot welding a thermocouple to the crystal and tungsten wire can be positioned for direct current heating. Heating rate used in the proceeding experimental work was 1 degree/ second. TPD was carried out typically in

the range of 100 –500 Kelvin so as to try and explore the multi-layer (depending on condensation) and mono-layer desorption temperature. The rate of evolution of adsorbed material from a surface is described by the Arrhenius type equation[14]:

$$\frac{-\partial N}{\partial t} = K_n N^m \exp(-E_d / RT) \quad (2.8)$$

Given that N is the surface concentration of adsorbed particles per unit area, K_m is the frequency factor, R is the Universal gas constant, m is the order of desorption rate, E_d is the activation energy of the desorption process and T is the absolute temperature. As the temperature rises, the thermal energy becomes sufficient to break bonds, either adsorbate/adsorbate i.e. the multi-layer peak, or adsorbate/ substrate i.e. the mono-layer desorption.

2.6 The Cu (110) Crystal

Copper is a face centred cubic metal and the 110 face it has dimensions as shown in fig. 2.8.

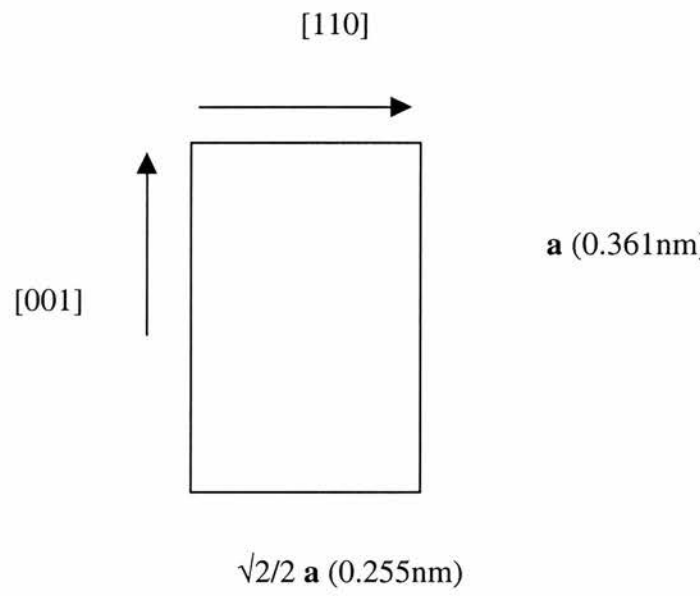

Fig. 2.8 Orientation and dimensions of the Cu (110) unit cell specified by two lattice parameters.

2.7 Experimental procedures

Evaporation of the chemicals was achieved through the use of a custom designed doser, fig 2.9. This consisted of a heating wire wrapped around a glass tube, into which was inserted a smaller ceramic tube where the chemicals to be studied were placed. A thermocouple wire for temperature measurement would be placed inside the ceramic tube for direct contact with the chemicals. Once heated,

the chemicals would be realeased into the chamber by opening a gate valve. The doser would be pumped by a rotary pump for roughing and a diffustion pump to achieve ultra high vacuum.

Three separate Ultra High Vacuum (UHV) chambers were used throughout the course of this research project, each chamber having a unique leading technique:

a) HREELS chamber – equipped with an Ibach double pass electron energy loss spectrometer; this apparatus also has a preparation chamber with LEED for the optimisation of dosing conditions prior to the HREELS measurement. A sample transfer mechanism allows movement of the crystal between the two chambers while maintaining UHV conditions, fig 2.10

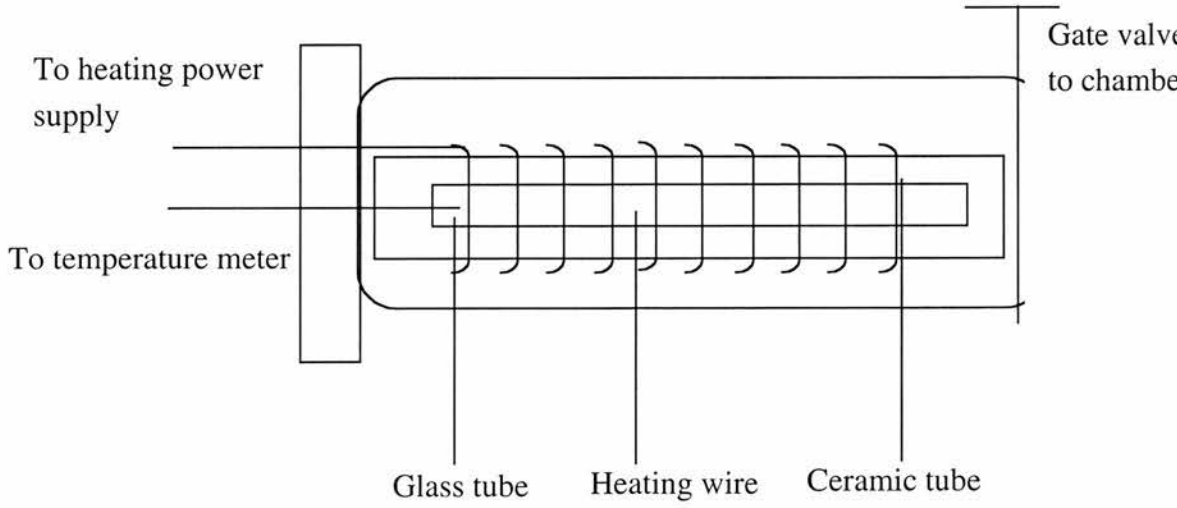

Fig. 2.9 Schematic of doser used to evaporate chemicals. The associated electronics are necessarily connected through an ultra high vacuum feed through flange.

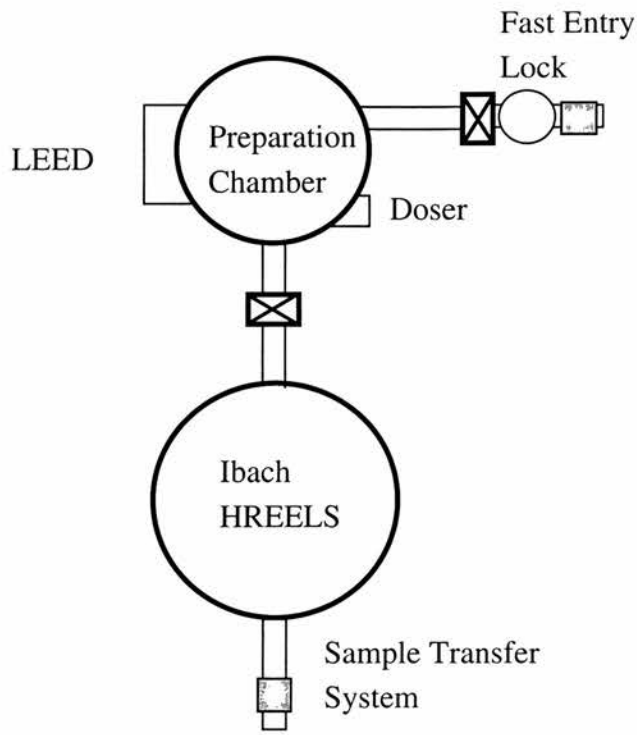

Fig. 2.10 HREELS Chamber for surface vibrational spectroscopy. Sample transfer system allows the sample to be prepared and analysed without breaking vacuum

b) TPD chamber – Via the cooling of a backplate the sample can be cooled to liquid nitrogen temperatures. Mounted via tungsten wires, the single crystal can be heated. A computer controls the ramping of the temperature and a Hiden quadruple mass spectrometer detects the desorption species.

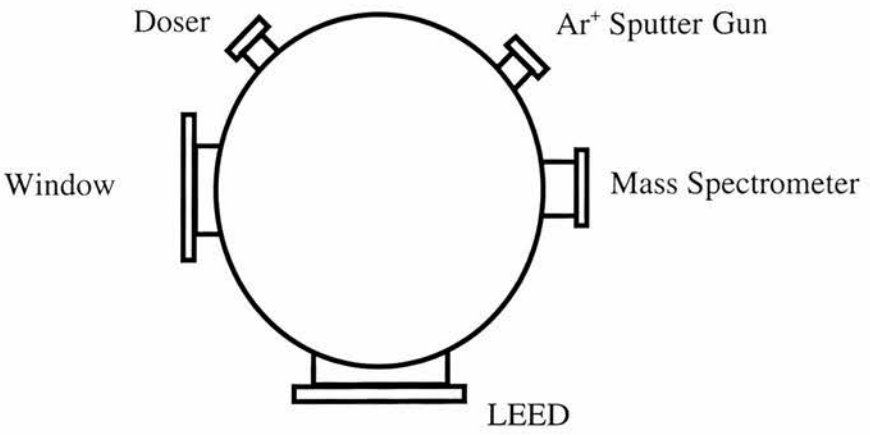

Fig. 2.11 TPD Chamber , sample cleaning is performed in situ with cycles of argon sputtering and annealing

c) STM chamber – The Omicron variable temperature STM is equipped with a fast entry lock for the changing of tips and sample, and a sample transfer system for the manipulation of the sample between the preparation and STM chamber. Tungsten tips were prepared by electrochemical etching.

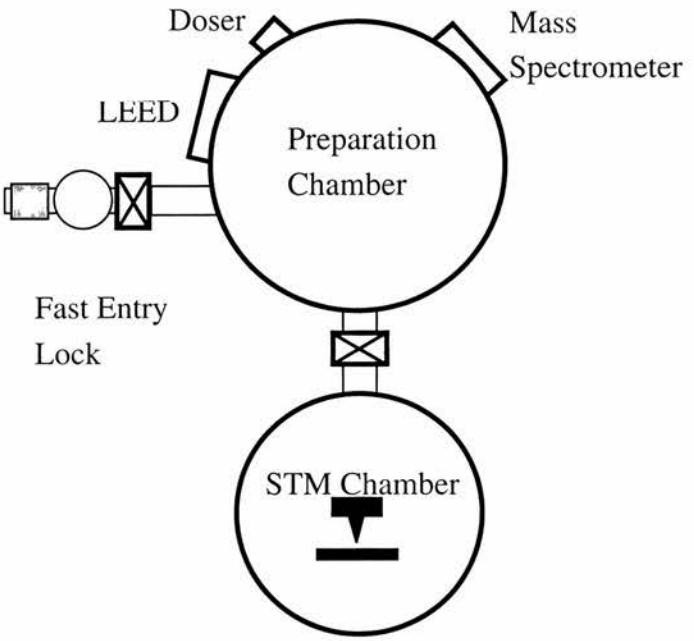

Fig 2.12 STM Chamber. The fast entry lock allows changing the STM tip and sample without breaking vacuum

References:

1 G. Attard and C. Barnes, *Surfaces,* Oxford Chemistry Primers

2 K. Christmann,*Surface Physical Chemistry* (1991).

3 T. A. Delchar and D. Woodruff,*Modern Techniques of Surface Science* , Cambridge Solid State Science Series

4 H. Luith,*Surfaces snd Interfaces of Solids,* Springer Series in Surface Science (1992).

5 M. Prutton, *Surface Physics*, Oxford Science Publications(1984).

6 G. Somorjai, *Surface Chemistry and Catalysis* , Wiley-Interscience (1994).

7 R. Vanselow and R. Howe,*Chemistry and Physics of Solid Surfaces*, Springer Series in Surface Science .

8 J. C. Vickerman,*Surface Analysis -the Principle Techniques,* Wiley .

9 J. M. Walls and R. Smith, *Surface Science Techniques,* Pergamon Press

10 R. Weisendanger,*Scanning Probe Microscopy and Spectroscopy -Methods and Applications*, Cambridge (1994).

11 A. Zangwill,*Physics at Surfaces,* Cambridge (1988).

12 H. Froitzheim, H. Ibach, and S. Lehwald, *Rev. Sci. Instr.* **46**, 1325 (1975).

13 I. W. Gadzuk and S. Holloway, *Physica Scripta*,**32**, 413 (1985).

14 B. W. Holland and D. P Woodruff, *Surface Sciencce* ,**36**, 488 (1973).

CHAPTER 3 . Creation of a Chiral Surface, the Adsorption of Phenylglycine

3.1 Introduction

A chiral surface is not simply achieved by adsorbing chiral molecules on-to a non- chiral surface. It is only chiral if the combined symmetry of the surface and overlayer is chiral, i.e the unit cell of the adsorbate is chiral. Interest in these chiral systems has its foundations both in terms of enatioselective heterogeneous catalysis as well as an examination of origins of life.

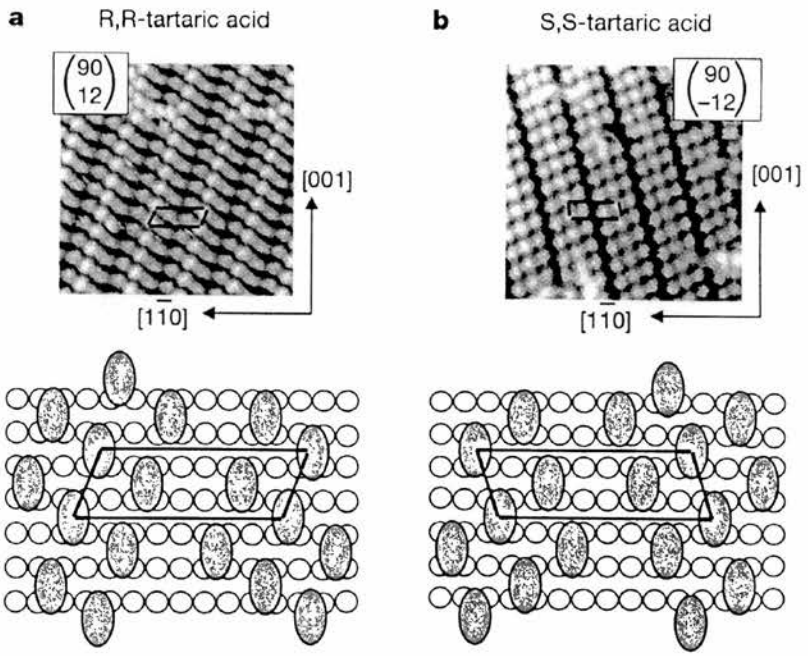

Fig. 3.1 STM Images showing mirror chiral surfaces created by R,R and S,S tartaric acid adsorbed on Cu(110) [1]

Ortega Lorenzo and co workers deposited R,R and S,S tartaric acid, onto Cu (110) single crystals[1]. They observed that single chiral domains could exist and STM images showed mirror chiral surfaces, fig. 3.1. This adsorption phenomenon was attributed to a rigid adsorption geometry.Cyclic peptides have been used as candidates for chiral surfaces by Weib et al.The molecules which were studied are shown in fig. 3.2. The stereospecificity of the surface was determined by using the ultra sensitive quartz crystal microbalance. Another related system is that of the solid liquid interface as opposed to the gas surface interface encountered in UHV studies. Two main issues arise for the creation of such a chiral surface. Is there segregation and how large are the racemic domains that form. Such phenomena have been investigated by Lahav et al[2]. In these studies the amphiphillic monolayers are created by the Langmuir Blodgett technique. Several arguments are presented for and against the formation of chiral domains. For example two dimensional crystals possess more disorder than three dimensional counterparts and thus should also have a lower chance of forming such ordered enantiomorphic zones. In contrast mono-layers at an interface do not possess centre of inversion symmetry so this should increase the chances of success in formation of chiral domains. Another such study involved segregation of 2 different amphiphilic molecules from a racemic mixture at the air / water interface[4].

Fig. 3.2 Cyclopeptides used to create a chiral surface[3] on gold coated quartz crystal balance sensors.

An alternative approach to the formation of a chiral surface is to mechanically create the desired symmetry. This can be achieved by taking surfaces with high miller indices. In these systems kinks can be either left handed or right handed. One such example was achieved by Mc Fadden et al who cut a silver single crystal so that the Ag $(643)^S$ surface was exposed on one side and the Ag $(643)^R$ on the other[5].

Once a chiral surface is formed the issue is then what are the applications and what environments do they represent. Certainly in nature there are few, if not any, chiral surfaces. It might therefore be surprising to note that Eldadi et al found cells could distinguish between R,R and S,S calcium tartrate tetrahydrate crystals[6]. Cells would grow on one enatiomorph but not the other. It was hypothesised that certain cell coating polymers were responsible for this discrimination.

A number of techniques have been used to detect the chirality of a surface but none of them are developed enough to be used routinely. Grazing incidence x-ray diffraction has been used to distinguish between two diastereomeric systems at the

air water interface[7]. Electron transmission through thin films of organised chiral thin films manifests a large asymmetry in scattering probability due to the chiral nature of the films[8]. In the following chapter LEED is used as the tool for determining surface chirality.

3.2 Experimental

The experiments were performed in a TPD chamber, equipped with a rear view LEED and quadrupole mass spectrometer. The diffraction pattern recorded from the rear view LEED optics corresponds directly to the unit cell via the standard relationship linking real and reciprocal space unit cell. The quadrupole mass spectrometer is terminated with an outlet of 5mm internal diameter that can be moved towards the sample surface to increase sensitivity and reduce the background in the TPD experiments so the dosing temperature is well controlled and the reproducibility is ensured.

3.3 Results

In order to understand enantiomeric differentiation on the (110) surface, which has a non-chiral p2mm space group, Fig 3.3, both R and S-phenylglycine and a quantitatively well defined mixture of the two enantiomers have been studied on Cu{110} surfaces. The structures of this pair of enantiomers are presented in Fig. 3.4, along with those of glycine and alanine molecules.

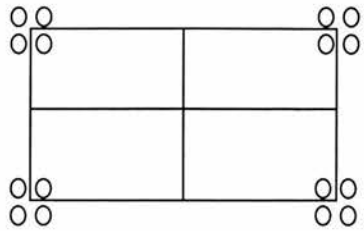

Fig. 3.3 p2mm space group

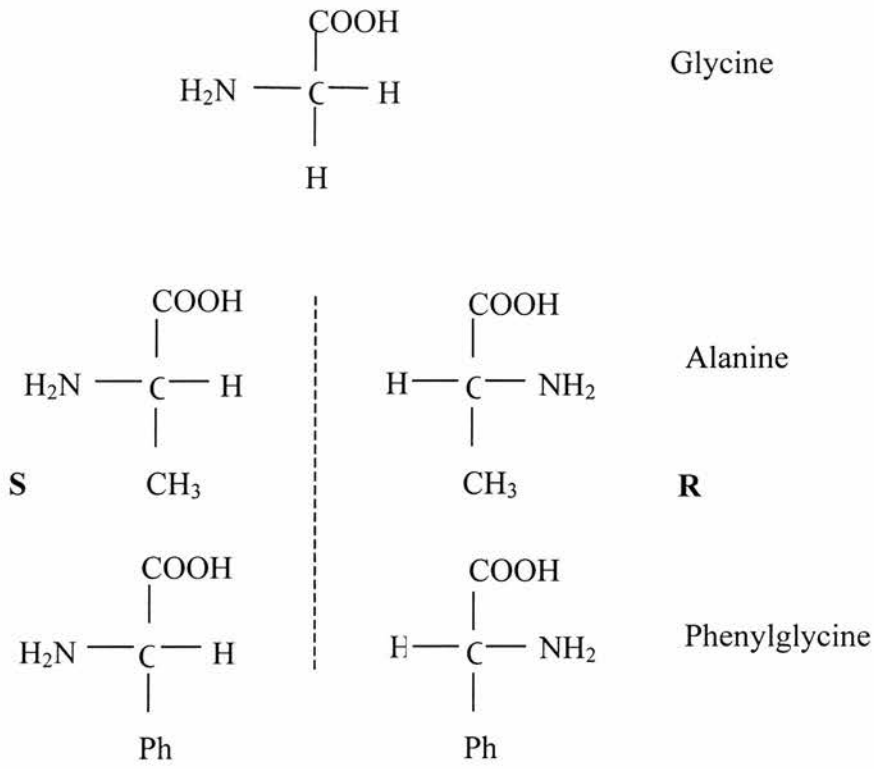

Fig 3.4 Comparative structures of amino acids

An ordered surface overlayer of R-phenylglycine is achieved by dosing to saturation at room temperature followed by annealing to 450 K. LEED shows a $\begin{pmatrix} 5 & -3 \\ 4 & 1 \end{pmatrix}$ periodicity[9], shown in Fig. 3.5, with a unit cell spanning 17 Cu atoms. The periodic structures of both R(S)-phenylglycine and R(S)-alanine have a unit cell vector along the (5,-(+)3) direction.

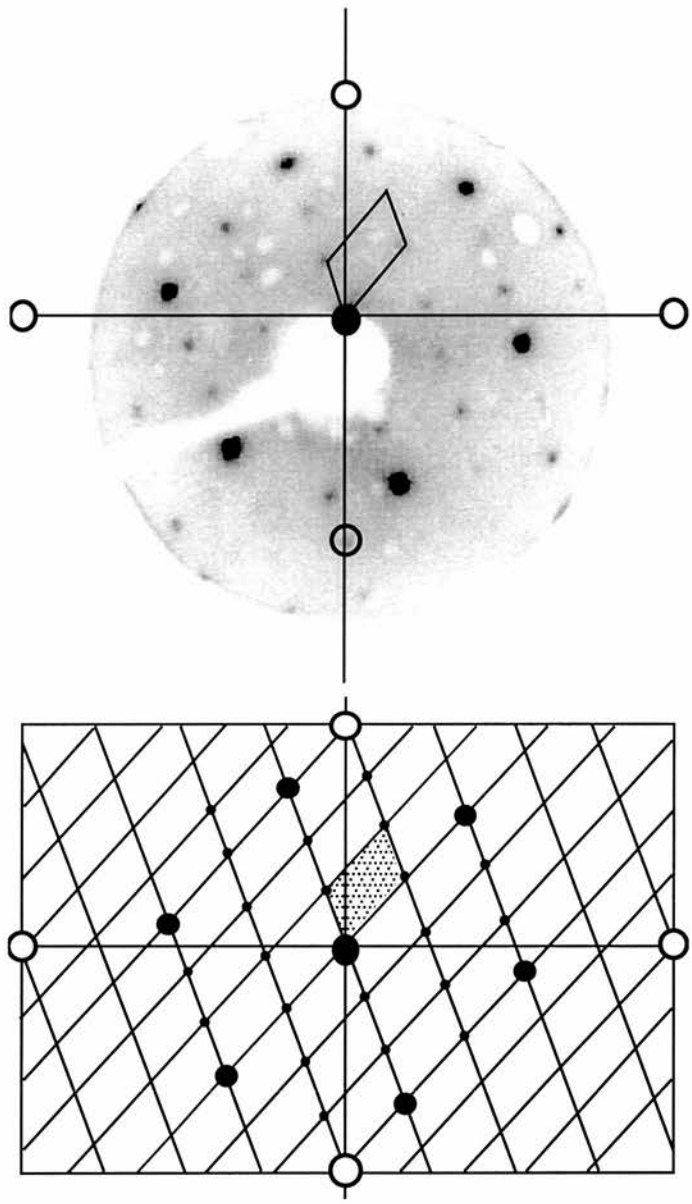

Fig. 3.5 LEED pattern of R-Phenylglycine, 26eV

Although the periodicity, in each case, is commensurate with the Cu substrate, the LEED pattern does not show mirror symmetry. The corresponding Bravais lattice is oblique and the primitive vectors are not aligned along high symmetry directions of the underlying Cu lattice. The macroscopic 2D structures and the real

space unit cells are therefore chiral. The packing arrangement of S-phenylglycine molecules in the unit cell appropriate to R-phenylglycine is anticipated to be substantially different i.e the S-modification requires the unit cell of opposite chirality. The matrix notation for the structure of S-phenylglycine on Cu{110} is therefore $\begin{pmatrix} 5 & 3 \\ 4 & -1 \end{pmatrix}$. This structure is confirmed by the LEED pattern of Fig. 3.6b which is the mirror image of that formed by R-phenylglycine shown in Fig. 3.6a.

This demonstrates that each enantiomer forms distinctive 2D crystals with inverse optical response. It can be seen that R- phenylglycine/Cu{110}, and R-alanine/Cu{110}, (Fig. 3.6c), have in common the 5, -3 primitive vector suggesting that inter-adsorbate interactions determined by the chiral, α-amino skeleton, common to the two molecules, is responsible for the ordering, at least in this direction. In contrast, glycine may exhibit chiral domains but these are necessarily matched, elsewhere on the surface, by domains of the complementary chirality. In any case, they are not distinguished in the LEED pattern since the Bravais lattice of the (3x2)-glycine/Cu{110} structure has mirror symmetry, although LEED I/V measurements can, in principle, distinguish the two domains. Two, C_2 correlated, domains will exist for each enantiomer of phenylglycine which present the same LEED patterns and a real-space technique such as STM is necessary to distinguish these two domain types.

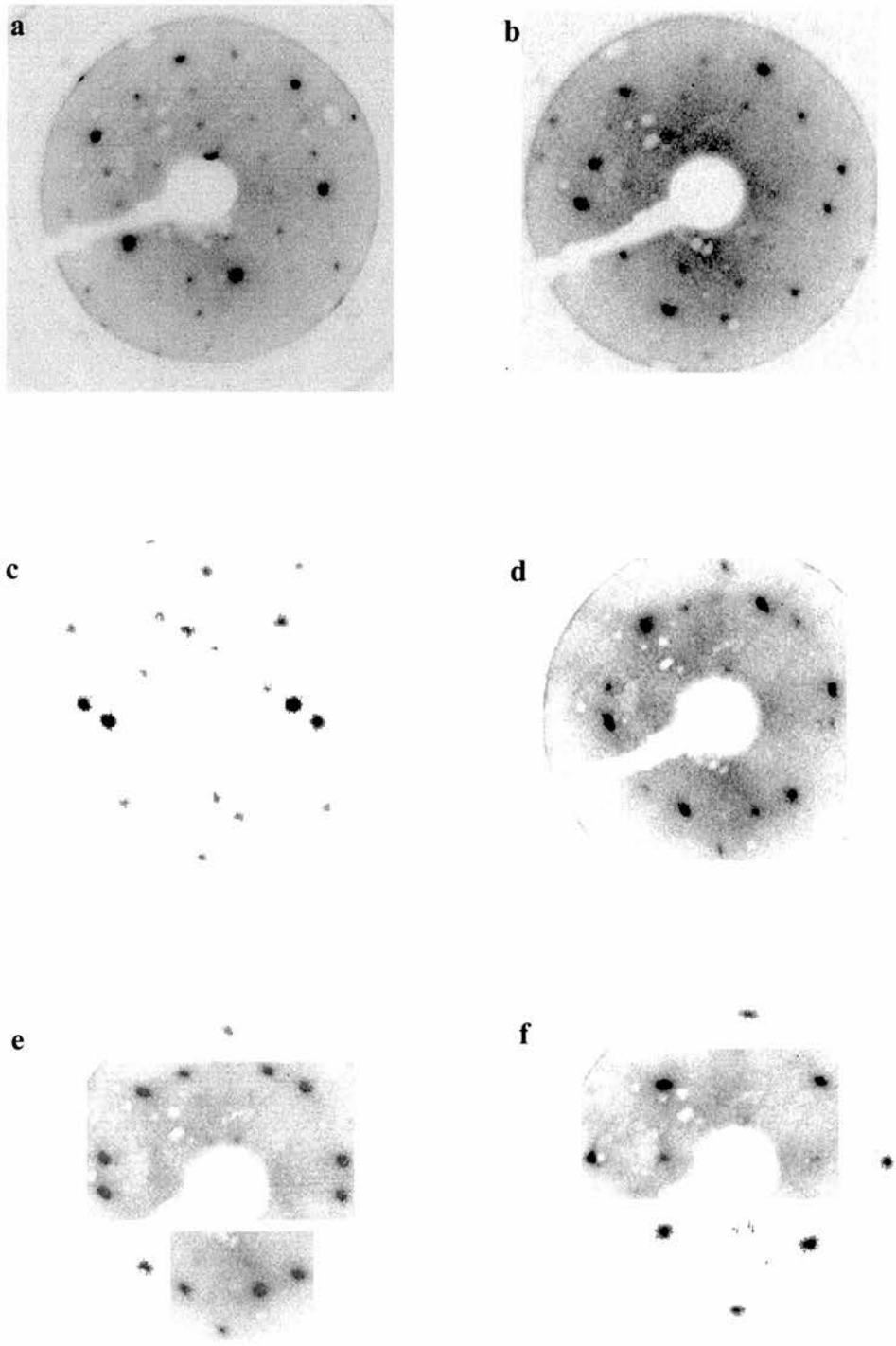

Fig. 3.6 LEED Pattern of a) R Phenylglycine 26eV b) S phenylglycine 26eV c) R-Alanine 35eV d) Mixture S and R Phenylglycine 3:1 26eV e) Mixture 1:1 26eV f) p(3×2)g after annealing to 420K

On the ordered p(3x2)g glycine/Cu{110}, the surface saturation coverage was found to be 0.33 ML (2 glycine/6 Cu in the unit cell). Based on the peak intensities of 27 amu (HCN), 44 amu (CO_2) and 28 amu (CO) mass fragments in thermal desorption experiments, glycine and phenylglycine have very similar saturation coverages, which, together with the unit cell size, suggests a surface coverage of 0.35 ML (6 molecules per 17 Cu atoms in the unit cell) for the $\begin{pmatrix} 5 & -3 \\ 4 & 1 \end{pmatrix}$ periodicity of R-phenylglycine. In the case of S-alanine, it can be suggested that the coverage is most likely six molecules in the $\begin{pmatrix} 5 & 3 \\ 2 & -2 \end{pmatrix}$ unit cell spanning 16 Cu atoms. For R-phenylglycine, in addition to the (0, 0) spot, there are six other intense spots which form a pseudo-hexagonal pattern with a periodicity of $\begin{pmatrix} 5/2 & -3/2 \\ 4/3 & 1/3 \end{pmatrix}$. This can be considered to be the unit cell of the adsorbate ignoring the substrate. Consistent with the above discussion of coverage, it contains one molecule and, hence, 2.83 (=17/6) Cu atoms. The intensity of this pattern suggests the coherent electron scattering by the molecules is strong and that all molecules are in very similar chemical environment, in terms of bonding to the substrate and molecular orientation.

Mixtures of R- and S- phenylglycine have been dosed on the clean Cu{110} surface. Fig. 3.6d shows the LEED pattern of the mixture with a ratio of S/R=3.

Similarly, the LEED pattern, following dosing with a mixture of S/R=1, is shown in Fig. 3.6e. The patterns present both the periodicities of $\begin{pmatrix} 5 & -3 \\ 4 & 1 \end{pmatrix}$ of R-phenylglycine and $\begin{pmatrix} 5 & 3 \\ 4 & -1 \end{pmatrix}$ of S-phenylglycine strongly suggesting that phase separation of the two enantiomers occurs. The spots contributed by the S-phenylglycine phase are more intense than those from the R-phenylglycine phase in Fig 3.6d, simply due to the difference in the surface coverages of the two isomers. As the surface coverage of R- and S- enantiomers are equal in the case of Fig 3.6e, the LEED intensities from the two molecular arrays are similar. Annealing this surface above 420 K causes a phase transition to the p(3x2)g periodicity; the same periodicity as glycine. At this stage, it is not possible to determine from the LEED data alone whether phase separation is maintained, although this phenomena has also been observed for the single enantiomer S-alanine on Cu{110}. Fig. 3.6f shows the LEED pattern of the p(3x2)g periodicity.

3.4. Discussion

The proposed real space structure of the $\begin{pmatrix} 5 & -3 \\ 4 & 1 \end{pmatrix}$ R-phenylglycine/Cu{110} is presented in Fig. 3.7 with a surface coverage of 0.35 ML (6 molecules per 17 Cu atoms in the unit cell). By analogy with glycine[10] and alanine[11-12], the adsorbed species is considered to be in the anionic form with the displaced proton leaving the surface as H_2 following recombination on the surface. The phenyl ring is directed

away from the normal to limit stearic interaction in the adsorbate plane. In this geometry, the molecule has a projected size on the surface plane similar to glycine consistent with the similar, saturation coverage, TPD intensities for the two species. The unit cell corresponding to the pseudo-hexagonal pattern with a periodicity of $\begin{pmatrix} 5 & -3 \\ 4 & 1 \end{pmatrix}$ is also marked on Fig. 3.7. It is presumed that this unit cell contains only one molecule. However, the presence of the substrate causes imperfection in this $\begin{pmatrix} 5 & -3 \\ 4 & 1 \end{pmatrix}$ periodicity, because different adsorption sites are implied when projected into the bulk. This gives rise to the weak spots forming a $\begin{pmatrix} 5 & -3 \\ 4 & 1 \end{pmatrix}$ pattern which is the truly periodic, commensurate structure. In this model, all the carboxylate groups are aligned along the $[1\bar{1}0]$ azimuth, which is supported by EELS impact scattering results [13].

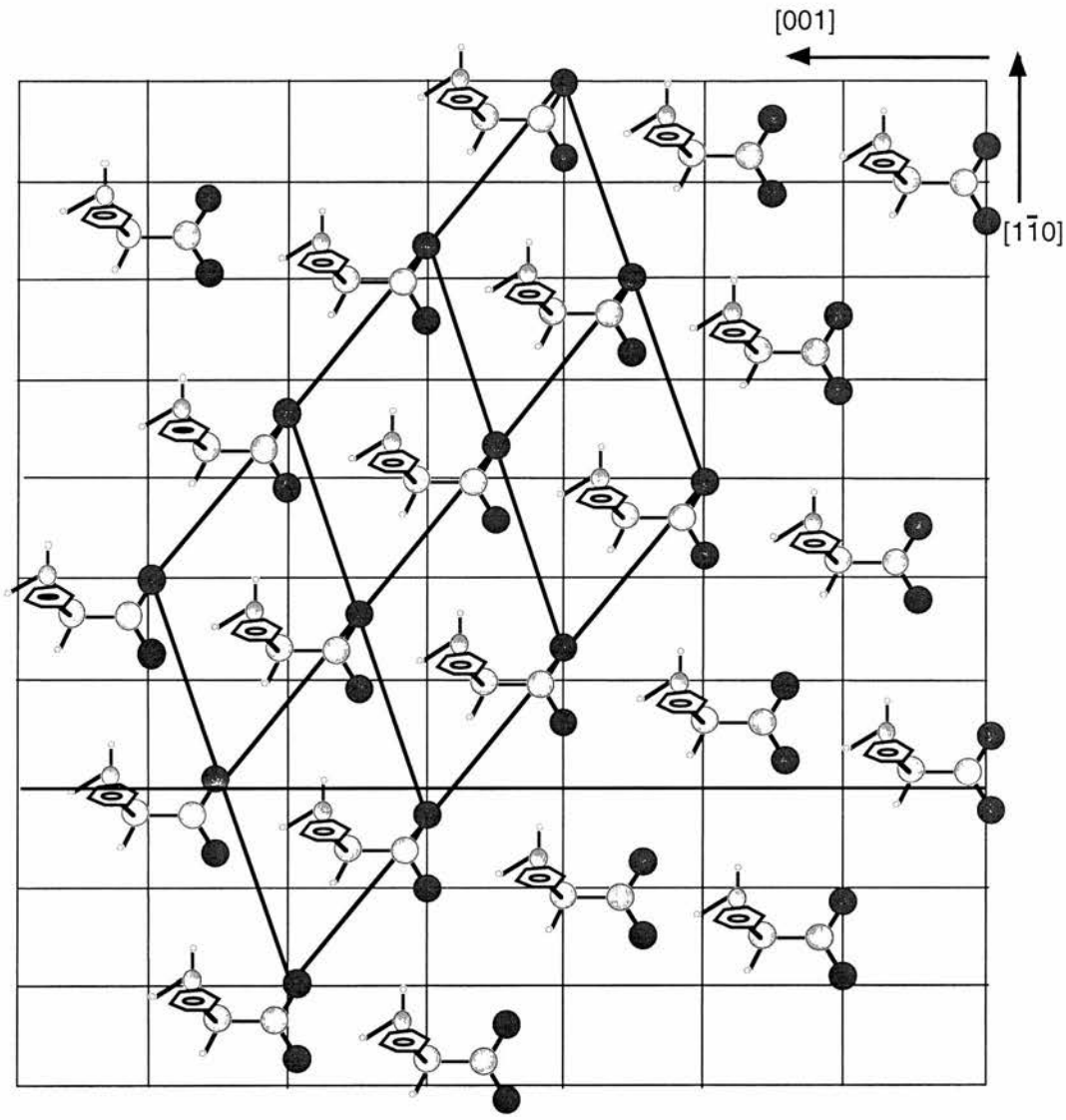

Fig. 3.7 Real space model of R-Phenylglycine with periodicity $\begin{pmatrix} 5 & -3 \\ 4 & 1 \end{pmatrix}$

The structure is a compromise between strong adsorbate substrate bonding requirements, demanded by the carboxylate group and N atoms, and interadsorbate interactions, which are probably both hydrogen bonding and Pauli exclusion in origin. The structure shown in Fig 3.7 gives rise to favourable N-H--O bonding

(linear with H--O distance of ca 1.5Å) in the adsorbate layer, whereas attempting to place the enantiomeric S-phenylglycine into the $\begin{pmatrix} 5 & -3 \\ 4 & 1 \end{pmatrix}$ structure, reserved for R-phenylglycine, produces a less favourable N-H--O interaction (nonlinear with H--O distance ca 2.0Å) and unfavourably short adsorbate-adsorbate distances along the 5,-3 direction leading to repulsive interactions. The favourable interactions for S-phenylglycine, and indeed S-alanine, are to be found on the mirror image, 5,3 direction. This is the likely origin of chirality in these unit cells and consequently the 2D ordered chiral overlayers.

There is also the possibility that Cu atom rearrangement may occur to make local bonding of molecules to the surface Cu atoms more equivalent than suggested by Fig. 3.7. It may be, for example, that the surface reconstructs to the extent that an additional Cu atom is incorporated into the unit cell to give 18 rather 17 Cu atoms. This would then allow the pair of O atoms and the N atom in each molecule to bind to a different Cu atom in the most effective manner.

A model for the p(3x2)g structure, observed after annealing the phenylglycine covered surface at 420 K, is presented at Fig. 3.8. The proposed structure is very similar to that for p(3x2)g of glycine [5-7] on Cu{110} surfaces. Two pseudo-glide planes, along the [001] direction, are indicated by the dashed lines. However, for a chiral molecule, the glide operation projects to its enantiomer, rather than itself, so a

glide line is not a perfect symmetry operation. Nevertheless, they appear to be sufficiently well defined to remove intensity from the 1/2 order beams.

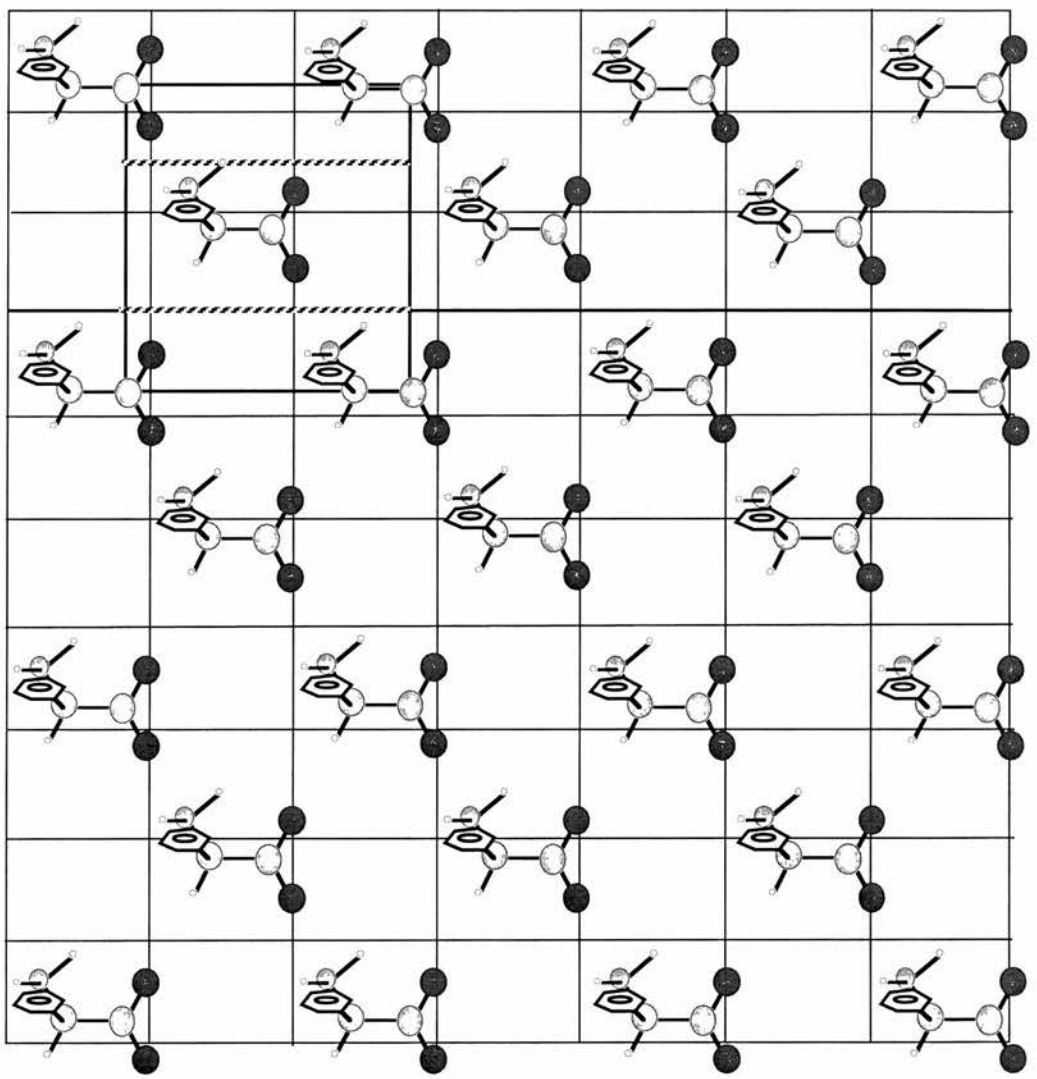

Fig. 3.8 Real space model of R-Phenylglycine with periodicity p (3×2)g with the Cu (110) substrate mesh

3.5 Conclusions

LEED measurements, with support from TPD, have been used to characterise the adsorption of R- and S-phenylglycine on a Cu{110} surface. At saturation coverage, the molecules form well ordered, chiral structures with a chiral unit cell which determines that the LEED patterns of the two enantiomers are readily differentiated. The origin of enantiomeric specificity in the structures is thought to arise from the interadsorbate H-bonding which occurs in the saturated monolayer. The commensurate $\begin{pmatrix} 5 & -3 \\ 4 & 1 \end{pmatrix}$ unit cell (R-phenylglycine) contains six adsorbate molecules most likely in anionic form by analogy with glycine and formally 17 Cu atoms, although reconstructions in the outermost Cu layer may well produce a structure with 18 Cu atoms, such that each O and N atom of the adsorbate is bonded to a separate Cu atom in equivalent local bonding geometries. Comparison is made with analogous structures observed for the non-chiral species glycine and R, S-alanine adsorbed on Cu{110}. As also observed for both these species, the stable structure on annealing the surface is a (3x2) periodicity with a glide line, although we recognise that in chiral adsorption systems a glide line is formally forbidden.

References:

[1] M. Ortega Lorenzo, C. J. Baddeley, C. Muryn, and R. Raval, *Nature* **404** (2000).

[2] I. Kuzmenko, I. Weissbuch, E. Gurovich, L. Leiserowitz, and M. Lahav, *Chirality* **10,** 415-424 (1998).

[3] T. Weib, D. Leipert, M. Kaspar, G. Jung, and W. Gopel, *Advanced Materials* **11,** 331 (1999).

[4] I. Kuzmenko, K. Kjaer, J. Als-Nielsen, M. Lahav, and L. Leiserowitz, *J. Am. Chem. Soc.* **121,** 2657-2661 (1999).

[5] C. F. McFadden, P. S. Cremmer, A. J. Gellman, Langmuir, **12** (1996) 2483.

[6] D. Hanein, B. Geiger, and L. Addadi, *Science* **263,** 1413-1416 (1994)

[7] I. Kuzmenko, R. Buller, W.G. Bouwman, K. Kjaer, J. AlsNielsen, M. Lahav, and A. M. Leiserowitz, *Science*. **274**, 2046 (1996) .

[8] K. Ray, S. P. Ananthowel, D. H. Waldeck, R. Naaman, *Science* **283**, 814 (1999)

.

[9] The matrix notation, $\left(\begin{smallmatrix} a & b \\ c & d \end{smallmatrix}\right)\left(\begin{smallmatrix} \mathbf{i} \\ \mathbf{j} \end{smallmatrix}\right)$ for the real space structures on the fcc (110) surface has been adopted. The translation vectors of the substrate unit cell, **i** and **j**, form a right-handed coordinate system directed along $[1\bar{1}0]$ and [001] respectively. For a commensurate overlayer, a, b, c and d are integers.

[10] S. M Barlow, K. J. Kitching, S. Haq, N. V. Richardson, *Surf. Sci.* **401**, 322 (1998) .

[11] J. Williams, S.Haq, R. Raval, *Surf. Sci.* 368, 303 (1996).

[12], R. Raval, C. J. Baddeley, S. Haq, S. Louafi, P. Murray, C. Muryn, M. O. Lorenzo, J. Williams, Reaction Kinetics and the Development of Catalytic Processes, Elsevier Science (1999).

[13] To be published.

CHAPTER 4 . The modified amino acid, amino benzoic acid

4.1 Introduction

Restricting this study to naturally occurring bio-molecules has its limitations, especially in a systematic approach to study the effects of different functional groups and molecular architectures on surface structures. Amino benzoic acid was selected for investigation despite being a "modified" amino acid because of the possibility of the molecule being adsorbed onto the copper in an upright geometry via one of the functional groups or in a flat lying position as a consequence of the aromatic ring. It was a natural evolution in terms of complexity of the simple amino acids previously studied.

4.2 Experimental

4-Amino benzoic acid was dosed at room temperature with a pressure on evaporation of approximately 1×10^{-9}. The Cu (110) single crystal was maintained at room temperature

4.3 Results

At room temperature, 4-amino benzoic acid forms a (3x4)g LEED pattern, Fig. 4.1, with very low background. The glide plane is found along the <001> direction, indicated by missing half order spots at (0, ±(2n+1)/2). The unit cell contains 12 Cu atoms with a size of 7.65Åx14.44Å, *i.e.* 110.5 $Å^2$. Since it has a glide plane symmetry, only an even number of molecules is possible within the unit cell. The

flat-lying molecule has a projected size of 5.25Åx8.76Å, *i.e.* 46Å^2, including 0.5 Å for the radius of an H atom. Thus the ideal surface coverage must be two molecules per 12 Cu atoms or 0.167ML.

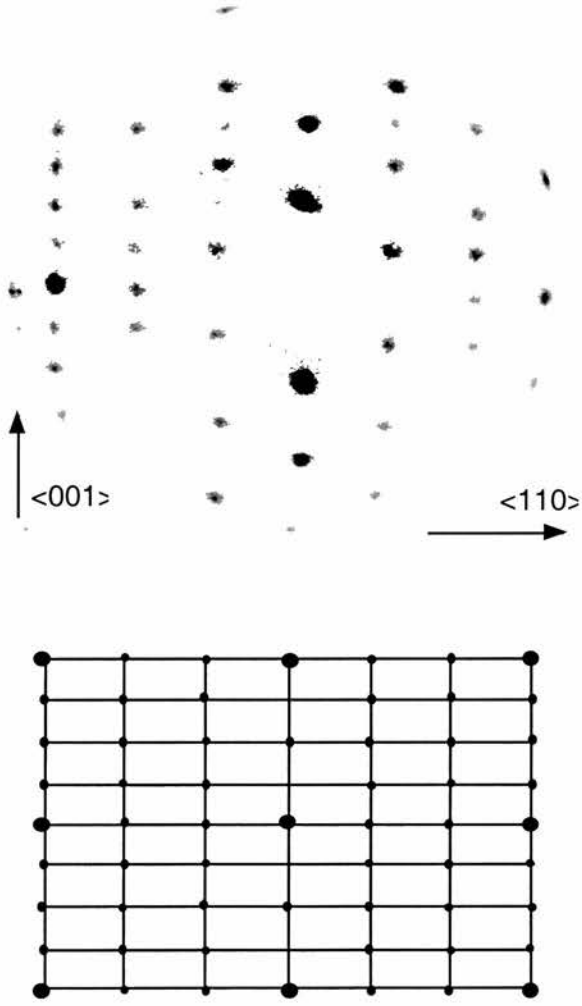

Fig 4.1 LEED pattern of (3x4)g room temperature 4-aminobenzoic acid on Cu(110), 54eV.

Fig. 4.2 shows the room temperature on-specular HREELS spectra with a resolution of 24 cm^{-1} at two different surface coverages. At the lower coverage, the

strongly dipole active, out-of-plane CH deformation mode, γ(CH) with B_2 symmetry, is observed at 780 cm^{-1}. This mode is characteristic of aromatic rings aligned parallel to the surface[1-4] and indicates that initially, exposure to 4-aminobenzoic acid results in a flat-lying species. The frequency is strongly dependent on the electron withdrawing properties of the substituent if the α-atom, the atom directly attached to the ring, does not have a lone pair electrons[5]. It was found at 820cm^{-1} in sodium benzoate[6]and at 808cm^{-1} in benzoic acid[5]. For groups which do have a lone pair electrons, the frequency in monosubstituted benzenes is rather constant at about 750~780 cm^{-1}[5], which could be rationalised as the lone pair electrons back donating to the phenyl ring through the delocalised π orbitals to counteract any positive charge distribution induced by electron affinity of the substitute through the σ bond. This flat-lying geometry is also consistent with the relatively small intensities of both A_1 and B_1 modes, for example, the OCO symmetrical stretch at 1404 cm^{-1} and OCO asymmetrical stretch at 1530 cm^{-1}. Once a monolayer of flat-lying species is formed, further dosing forms the upright species. At this stage, the HREELS spectrum, Fig. 4.2b, shows an increase in the intensity of the A_1 symmetry OCO stretch at 1404 cm^{-1}, while most of the B_2 modes have no change. This suggests there is no change in coverage and geometry of the original flat-lying. It is assumed that the upright molecule bonds to the substrate through the carboxylate group, similar to benzoate and formate species on Cu(110) surfaces[7-11]. Comparing the relative intensities at frequencies of 1404 and 780 cm^{-1} and taking account of the relative crosssection based on earlier work on benzoic acid, the ratio between the flat-lying and upright species is about 8:1 at this coverage.

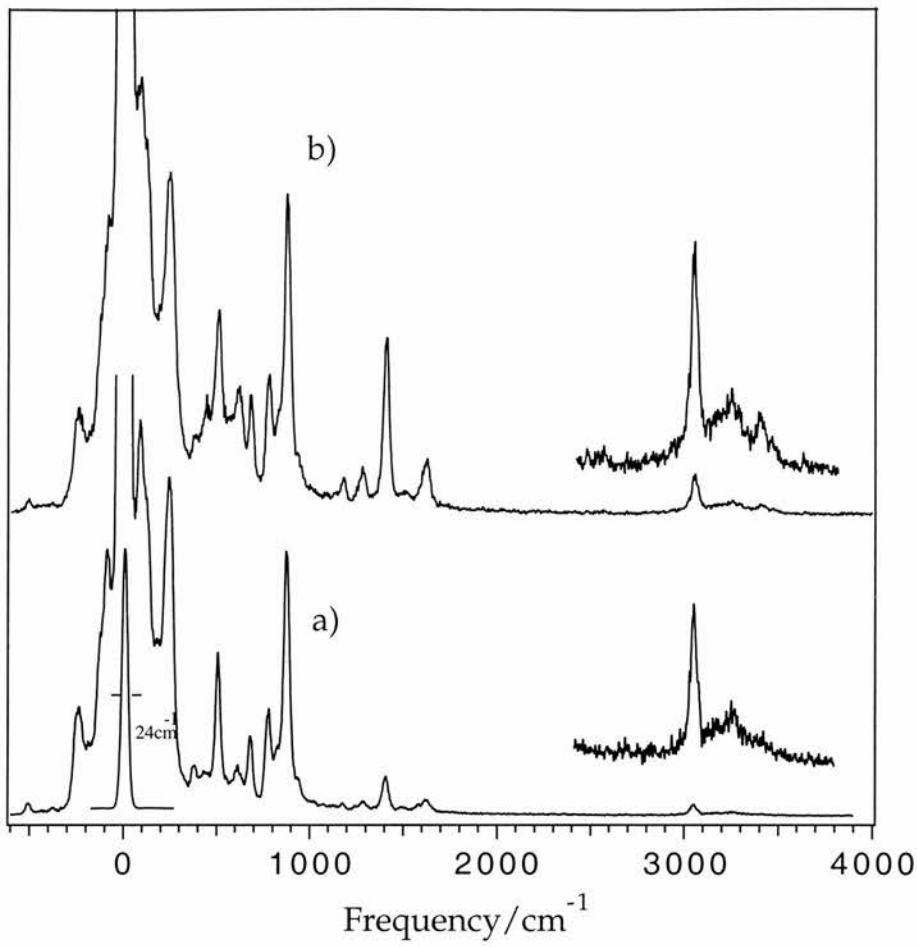

Fig 4.2 Room temperature HREELS on-specular spectra of (3×4)g 4 - aminobenzoic acid on Cu(110) at : a) low coverage; b) high coverage

It is also interesting to compare the relative intensity changes in the CH and NH stretching regions at different coverages. For the flat-lying species, the NH stretching modes at 3407 and 3487 cm^{-1} have very low intensity. With higher coverage of upright species, these modes increase in the intensities relative to the CH stretch modes at 3050, 3164 and 3259 cm^{-1}. This can be attributed to the bonding between N and Cu substrate, at the flat-lying geometry, the NH bonds are more or less parallel to the surface. However, the flat-lying molecule is not necessarily planar. The X-ray diffraction of the crystalline structure of 4-aminobenzoic acid[12] has clearly shown that the NH_2 plane is rotated about 14.5° out

of phenyl ring plane, while the carboxylic plane is slight bent (0.1Å) and rotated (4.6°) out of the phenyl ring plane. Indeed, while the molecule is in a flat lying geometry, small intensities of B_1 modes, such as the ring stretch modes at 1081, 1186, 1500 and 1630 cm^{-1} and the CH in plane deformation at 1351 cm^{-1} can be observed. On this basis, the phenyl ring would be expected to be slightly twisted along the molecular axis, while the NH_2 group is almost parallel to the surface. Increasing the coverage with upright species, the CH stretch increases its intensity somewhat, while the NH stretch now becomes clearly observable. At this stage, the upright species is interacting with the substrate through its carboxylate group. This is similar to the most common co-ordination of Cu carboxylate complexes[13], in which the carboxylic acid group is deprotonated and two (or a chain of) Cu atoms are strongly held within a similar distance as the metallic Cu crystal lattice distance, 2.55Å.

Dosing to higher coverage does not alter the (3x4)g LEED pattern, which suggests the upright species are incorporated into the same periodicity as the flat-lying molecule, or the upright species adsorb at the domain boundaries. This behaviour is initially similar to the benzoic acid on Cu(110)[8-10], which forms flat-lying species with a $\begin{pmatrix} 4 & 3 \\ -1 & 5 \end{pmatrix}$ periodicity at low coverage then incorporate upright species before it converts to upright geometry when the coverage is increased to form a c(8x2) structure. In the case of 4-amino benzoic acid, the first structure relates both orientations of the molecules. A critical difference between 4-aminobenzoic acid and benzoic acid is that the former can form hydrogen bonds linking NH_2 group of one molecule with carboxylic groups of neighbourghing molecules. Also the strong dipole of the adsorbed species favours the flat lying

geometry. These attractive interactions are strong enough to establish a high potential energy barrier for the phase transition from the flat-lying geometry to the upright geometry

In Fig 4.3 the desorption spectra for a series of selected masses with a ramping rate of 1K/sec are presented. Multilayer desorption occurs at *ca* 200 K. Thus, when the chemical is dosed at room temperature, only monolayer, chemisorbed species would be expected. There are three stages of desorption. Hydrogen has a desorption peak at low temperature, 500K, as well as at 570 and 700 K, while all other species desorb at a peak temperature of 570 K, which leaves residual N containing species.

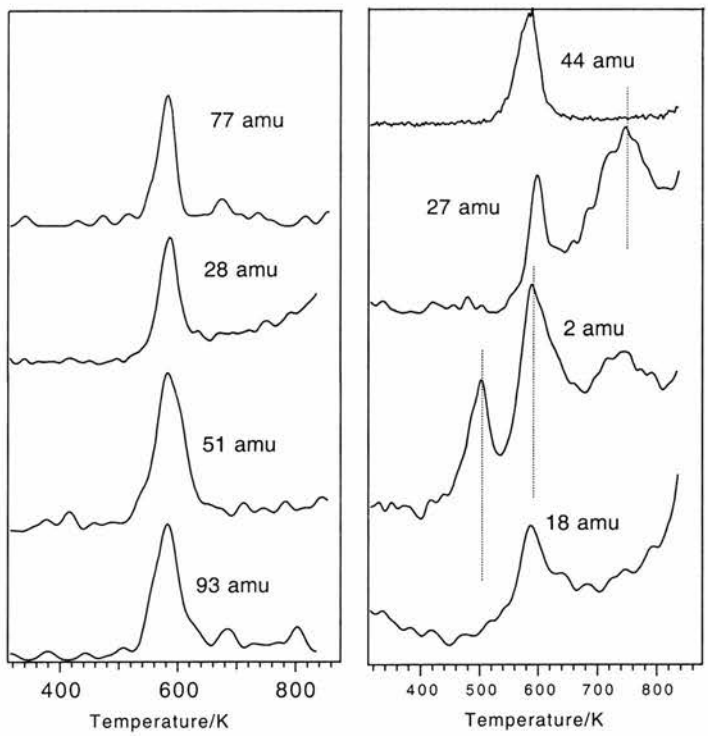

Fig 4.3 TPD spectra of 4-aminobenzoic acid on Cu(110) with a ramping rate of 1K/s. Masses 77 and 51 amu are phenyl ring related species. Mass 27 is HCN

The desorption of H_2 at 500 K is unlikely to be the result of forming amide bonds between molecules, since no H_2O desorption peak at this temperature. However, it is possible that the adsorbed species form chemical bonds between the aromatic rings, which give rise to a polymer structure, related to polyaniline, by dehydrogenation. Relatively high desorption temperature of HCN (27 amu) and H_2 suggests that the remaining species, which still contains the NH_2 group, are relative thermally stable.

Fig 4.4 shows a typical STM image of the (3x4)g periodic structure of 4-aminobenzoic acid. Clearly, there are two molecules per unit cell, as we estimated from LEED observation. The molecule species always has an elongated shape with a longer dimension of 8 Å along the <001> direction and a shorter dimension of 4Å along the <110> direction, thus, it is likely that the long axis of the molecule is aligned along the <100> azimuth. Because the glide plane symmetry is along the <001> azimuth, within a single domain, all the amino groups will point in the same direction, either [001] or $[00\bar{1}]$ direction. In this arrangement, all the amino groups are linked to the carboxylate groups (and vice versa) and the maximum exploitation of hydrogen bonding and favourable dipole interactions are achieved. Also, because of the glide plane symmetry, the molecule inside the unit cell has to be in the middle of the unit cell along the <001> direction, while along the <110> direction, there is no restriction on the molecular position. This gives the molecules the possibility to adjust their lateral distance and registration on the substrate along the <110> azimuth, although the STM image does indicate that the molecule at the centre lies along the <110> direction relative to the corner molecules.

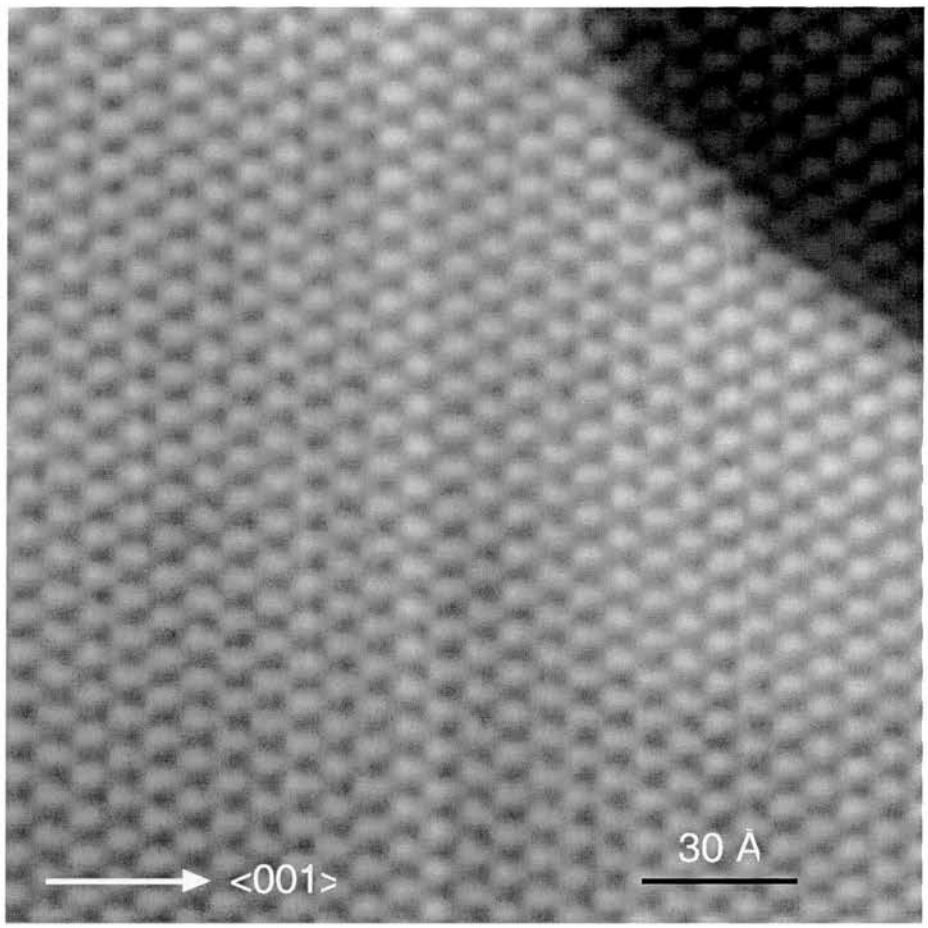

Fig 4.4 An STM image (200×200Å, sample bias 0.1V, current 0.71nÅ) of the (3×4)g periodic structure of 4-aminobenzoic acid on Cu(110). The step edge in the upper right corner is aligned along the (3, ±4) vectors.

A schematic model of the molecular arrangement is depicted in Fig 4.5a. The glide planes are indicated with dash lines along the <001> direction. In Fig 4.5b, the structure is related to the substrate mesh. Since it has 3-fold periodicity along the <110> azimuth, if one of the molecule is bonded at a short bridge site, the other molecule within the unit cell must be on the atop site. Meanwhile, if one of the phenyl rings is on a short bridge site, than the adjacent phenyl ring must be at an on atop site with a Cu atom under the centre of the ring. This may be the origin of

alternation of intensity in the STM image line profile shown in Fig. 4.6b. Fig. 4.6a shows an STM image in which the molecules appears to be a hat shaped. The image is rarely being achieved only once in about 500 images. It can be assumed that it is due to the adsorption of a molecule on the tip, with the middle of the 'hat' representing the centre of the phenyl ring. By measuring the line profile, Fig. 4.6b, it is found that the height of the feature has an oscillation along the (3, 4) direction, while the line profiles along both <001> and <110> directions do not show any oscillation in grey scale intensity (height). It is also found, that not only the bright features (maxima in grey scale) but also the dark features (minima in grey scale) are oscillating along the (3, 4) direction. This intensity oscillation certainly suggests that the phenyl ring bonding sites, as well as the unoccupied space of the substrate in between the adjacent rings, are different for the two molecules within the unit cell.

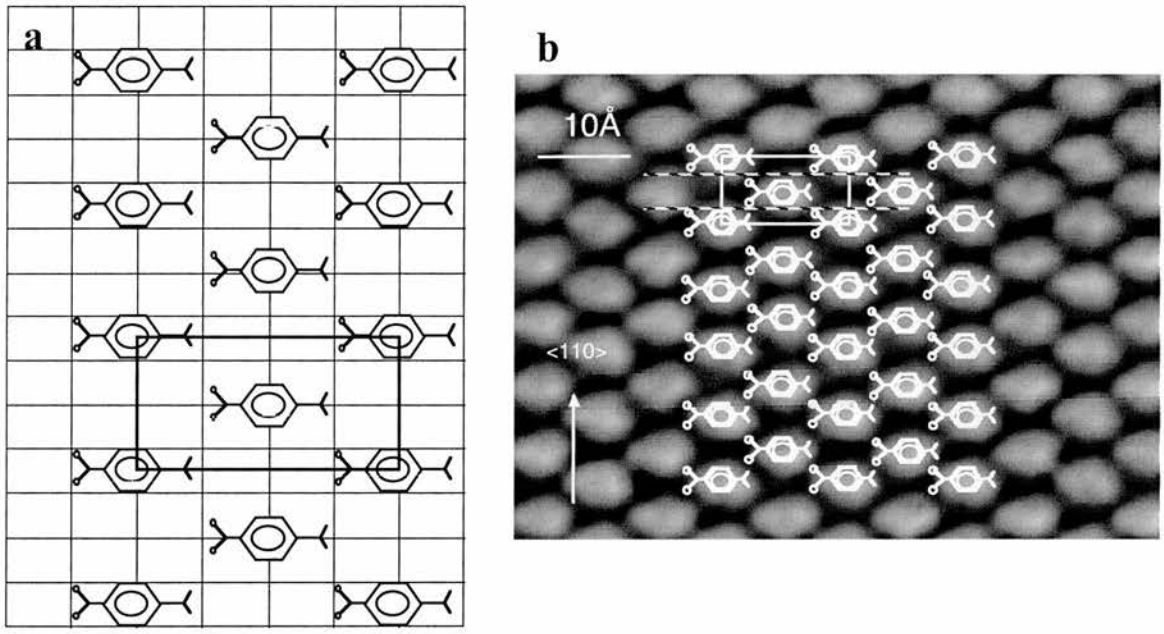

Fig 4.5 a) An STM image (70×50Å), sample bias 0.16V, current 40nA) of the (3×4)g periodic structure of 4-aminobenzoic acid on Cu(110) with structural models. The glide planes are indicated by the dash lines. b) real space model

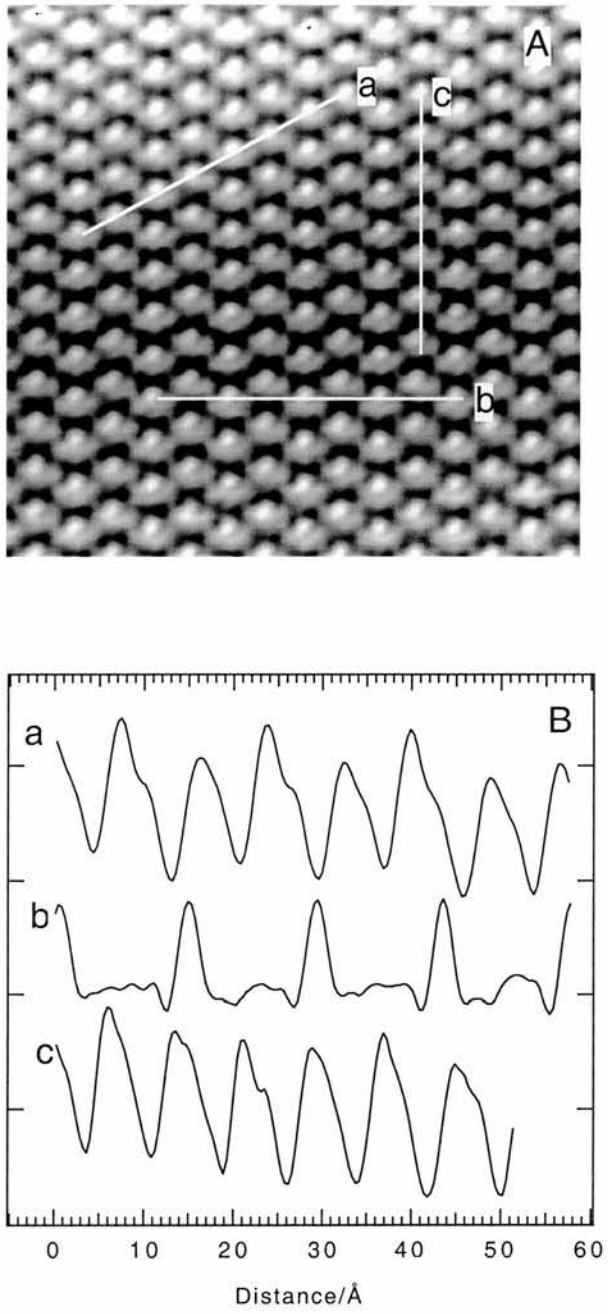

Fig 4.6 a) An STM image (100×100Å, sample bias 0.11V, current 5.35nA) of the (3×4)g periodic structure of 4-aminobenzoic acid on Cu(110) in which the phenyl ring appears to be imaged differently from usual due to a tip effect. b) Measure line profile along a) the (3,4) direction b) the <001> direction c) the <110> direction. Only along the (3,4) direction does the profile show an intensity oscillation.

If the glide plane symmetry is sensitive to the molecular adsorption site, the model in Fig. 4.5b would not give a perfect glide plane symmetry. However, if the adsorbates are shifted by 0.638Å (1/4 of the Cu lattice constant) along the <110> direction, depicted in Fig 4.6c, the two molecules within the unit cell have the same adsorption sites and the unit cell has perfect glide plane symmetry. In this model, two hydrogen bonds of each molecule are not equivelent, one of them crosses over a Cu atom, the other crosses the short lattice space. The difference in this local enviroment may also cause the alternation of intensity of the STM image line profile shown in Fig. 4.6b (a). As there is no direct experimental evidence to show the substrate structure induced by the adsorbate, certain reconstruction of the top layer Cu atoms may also be possible, in which case, the carboxylate group could still bond on the short bridge sites while the unit cell has a good glide plane symmetry. Here, the possibility of reconstruction of the substrate is supplied by the faceting induced by the interaction of the carboxylate group and the Cu substrate[14].

In this model, each H atom of the amino group is close to one of the O atom of the adjacent molecule and each molecule has two hydrogen bonds. There is also a favourable interaction of molecular dipoles. Thus, the formation of this ordered structure would have a considerable enthalpy gain and if this gain is large enough to compete with the entropy loss and assuming a low diffusion barrier at the adsorption temperature, this ordered structure will be occur as islands even at relatively low coverage. Fig. 4.7 shows the STM image with small ordered domains formed with domain boundaries aligned along either (3, ±4), (0, 1) or (1, 0) direction. However, it is found that the domain boundaries along the (3, ±4) directions are more favourable than others. This suggests that the intermolecular interactions along the

(3, ±4) directions are strong and attractive, which is consistent with the presence of hydrogen bonding in this model.

From our HREELS and LEED study, it his found that, at saturation coverage, the surface is fully covered with the flat-lying species and additional upright species without changing of the periodicity. Fig. 4.8 shows the STM image of such a high coverage surface. The upright species can be found as the bright features located on domain boundaries at step edges and surface defects. Frequently, it is found that the upright species form along the (3, ±4) directions, which is due to the fact that most of the domain boundaries are aligned along those directions and form a template to define the alignment of the upright species. Thus the overall periodicity and LEED pattern are unchanged.

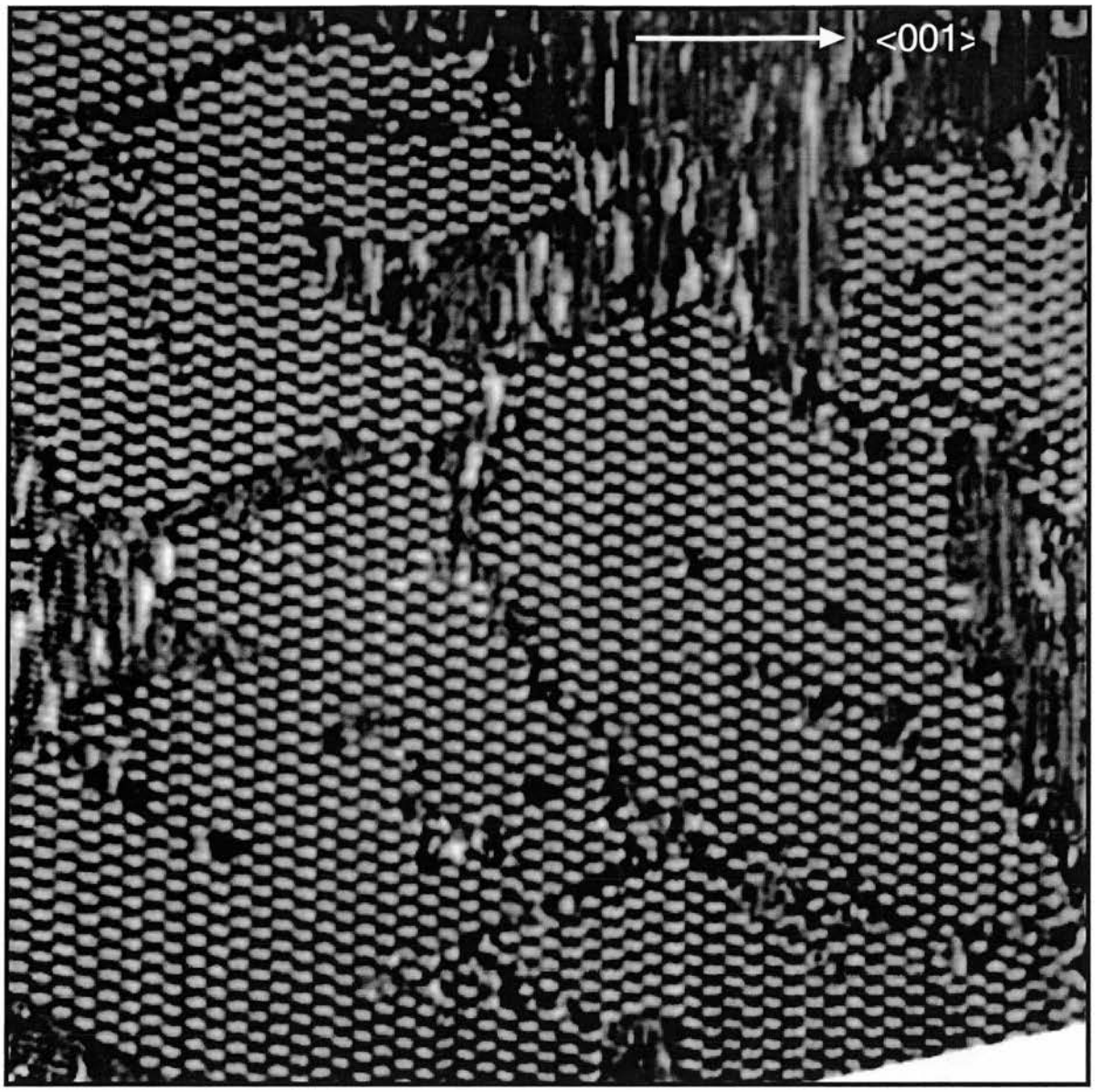

Fig 4.7 a) Low-coverage STM image (400×400Å), sample bias 0.09V, current 2.68nA) of the (3×4)g periodic structure of 4-aminobenzoic acid on Cu(110) showing the boundaries of small domains.

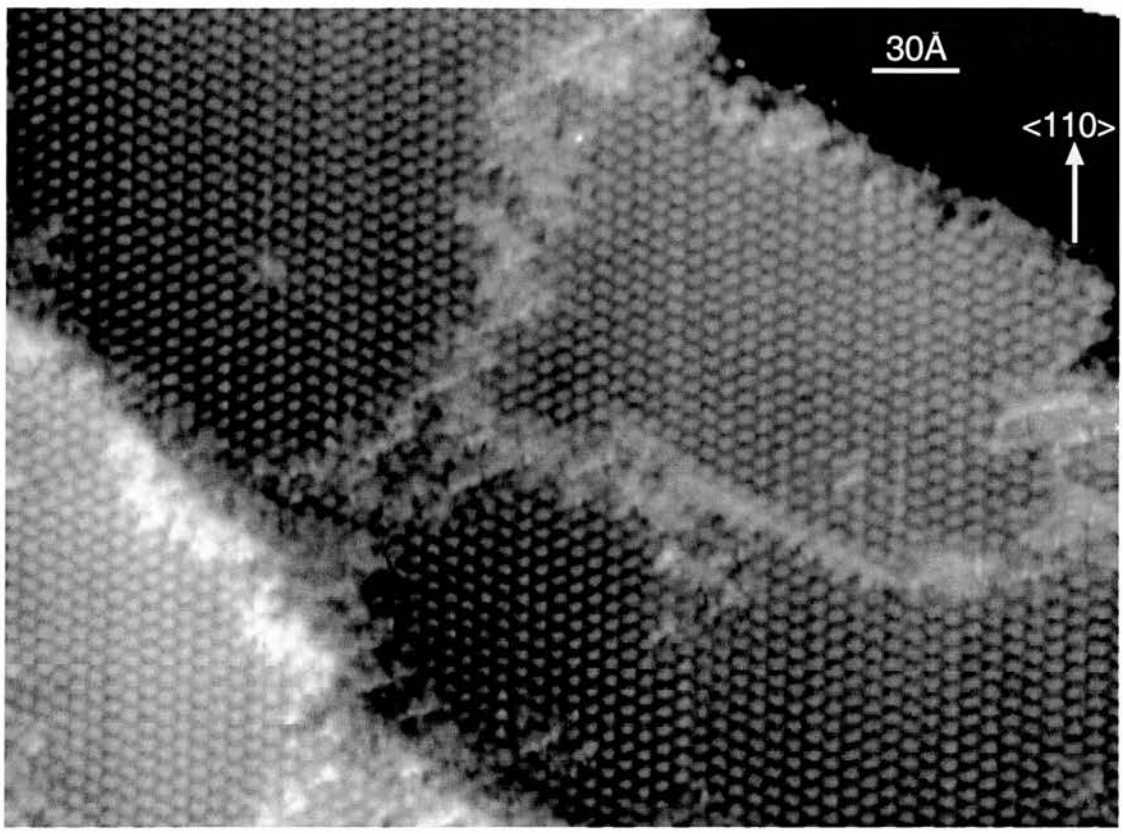

Fig 4.8 High coverage STM image (420×300Å, sample bias -0.18V, current 0.59nA) of the (3×4)g periodic structure of 4-aminobenzoic acid on Cu(110) The bright features are attributed to upright species

Fig. 4.9 shows a sequence of on-specular HREELS spectra as a function of the annealing temperature. All spectra were obtained at room temperature. Prior to any annealing, the surface has a perfect (3x4)g LEED pattern with very low background. This structure will be referred to as "α-phase" and was the subject of the preceeding discussion. The spots are almost as sharp as the substrate spots, which helps to give a very high electron reflectance in the EELS measurement. Thus, the pass energy of both the monochromator and the analyser can be reduced

significantly to allow a resolution of 3.2 meV full width half maximum. The spectrum has four strong bands at 500, 670, 760 and 870 cm^{-1}. The high intensity of vibrational modes below 1000 cm^{-1}, dominated by the out-of-plane CH and NH_2 deformation modes is characteristic of aromatic rings aligned parallel to the surface [1-4,15] and indicates that initially, exposure to p-aminobenzoic acid results in a flat-lying p-aminobenzoate species. Annealing the surface even to 540 K does not increase the intensity of any vibrational modes above 1000 cm^{-1}, which suggests that the molecule remains in the flat-lying geometry at high temperature. The low intensity at 1400 cm^{-1}, the carboxylate symmetric stretch, arises from the few upright molecules which decorate domain walls in the temperature range to 480 K. The frequency of aromatic CH deformation modes are strongly dependent on the electron withdrawing properties of any ring substituent [5]. It is found that if the phenyl ring has a functional group with a lone pair of electrons, for example NH_2, the vibrational mode at 900 cm^{-1} will shift down to 880 cm^{-1} [16]. This normal mode is found to be localised on the ortho and para CH bonds [17] and strongly coupled to the NH_2 out-of-plane wagging mode. Since, in p-aminobenzoate, the para position is bonded by the carboxylate group, here, the peak at 870 cm^{-1} can be assigned as the γ(ortho-CH) mode, which is also consistent with *ab initio* calculations. Both the free molecule in acid and radical forms have been calculated with similar results using the 6-31g basis set with B3LYP DFT method in GAUSSIAN 98 [18]. The localization of each vibrational mode is determined by the major displacement of atoms in the calculation. The modes at lower frequency, for example 760 and 670 cm^{-1}, are less affected by the property of the substituents. These modes are delocalised over most of the CH bonds on the ring [17], although the mode at 670 cm^{-}

[1] has same contribution from ortho-CH. The mode at 500 cm^{-1} is assigned as the out-of-plane skeletal deformation mode involving the CCN bond [19]. All these modes have their dynamic dipole moment perpendicular to the ring and hence contribute to the dipole intensity in EELS from the flat-lying molecule.

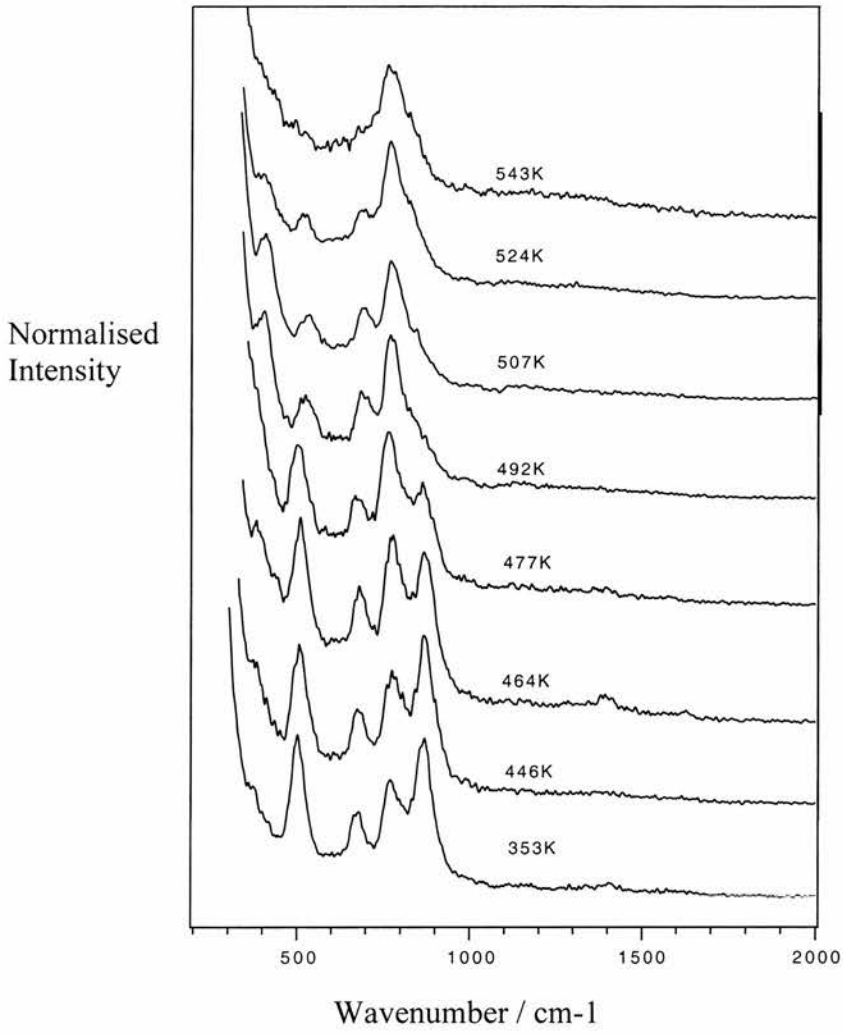

Fig. 4.9 On-specular HREELS spectra recorded as a function of annealing temperature. The spectra were collected at room temperature with a primary energy of 8 eV

At this stage, it has been recognised [20] that the acid proton has been dissociated and the p-aminobenzoate moiety is left on the surface. This species is

analogous to those formed by benzoic acid [8,15], formic acid [21-26] and acetic acid [27-29] on copper and other metal surfaces. On a Cu(110) surface, temperature dependent RAIR spectra[15] showed that benzoic acid deprotonated at 120 K. For p-aminobenzoic acid, here, this is also evidenced by the absence of a γ(O-H) bending vibration, expected at 935 cm^{-1} with an intensity comparable to that of the γ(CH) mode in the free acid [30].

Temperature dependent HREELS measurement shows that the peaks at 500, 670 and 870 cm^{-1}, assigned to the NH_2 and ortho-CH out-of-plane bending modes, reduce their intensities from an annealing temperature of 464 K. The gradual loss of intensity as a function of annealing temperature is directly correlated with the initial desorption of H_2 in the TPD experiments. Annealing above 540 K, all loss peaks disappear, except that at 760 cm^{-1}. This temperature corresponds to the leading edge of the main desorption peak, which accompanies molecular decomposition.

With increasing surface temperature, the (3x4)g LEED pattern of the α-phase disappears, while the EELS spectrum remains the same, until the temperature reaches 464K, whereupon a new phase is observed in LEED and STM. Thus, a substantial restructuring of the surface is necessary during the transition between the p(3x4)g and the new ordered phase. Since there is no change in the vibrational spectra, reordering rather than reorientation occurs at 464 K. The new phase formed at 464K is described in matrix notation as $\begin{pmatrix} 2 & 4 \\ 5 & -2 \end{pmatrix}$, which for simplicity will be referred to as the "β-phase". Simultaneously with the appearance of the β-phase LEED pattern, the intensities at 500 and 870 cm^{-1} decrease relative to those of other vibrational modes. It should be emphasised that the p-aminobenzoate is a rigid and

planar molecule. Thus, if the vibrational intensity variation were purely due to the reorientation of this planar molecule, all the vibrational modes with the same dynamic dipole direction would keep a constant intensity ratio. Therefore, the variation of the vibrational intensities indicates a chemical reaction, rather than reorientation, starting around 450~460K.

TPD data, fig. 4.3 shows that hydrogen has a desorption peak at low temperature, T_{max}=500 K, with a second peak at 570 K. All other species desorb at a peak temperature of 570 K. The desorption of H_2 at 500 K is unlikely to be related to the formation of amide bonds by a condensation reaction between molecules, since no H_2O desorption peak is observed at this temperature. Nevertheless, this initial desorption of H_2 is clearly related to the strong decrease of the vibrational intensities at 870 cm^{-1} and the smaller decrease of the band at 500 cm^{-1}. These two vibrational modes have significant contributions from the NH_2 and the ortho-CH groups.Thus, the dehydrogenation seems to involve these H atoms, rather than the meta-CH bond. Ortho activation is common for substituted benzenes with an electron donating group, for example, -NH_2, -OH or -OR. The sharing of the lone pair electron on the functional group with the π system causes the charge densities at the ortho and para positions to be substantially higher than the meta position, which is also related to the vibrational frequency shift referred to earlier.

The LEED pattern shown in Fig.4.10 was recorded at 23 eV from the saturated surface after annealing to 464K. The open circle in the middle indicates the approximate location of the (0,0) beam; the first order spots of the clean substrate are not visible at such a low beam energy. The structure is relatively complex in comparison with the p(3x4)g, since none of the over-layer lattice vectors

are aligned along the high symmetry axes. Thus, the real space unit cell is better described in a matrix notation $\begin{pmatrix} 2 & 4 \\ 5 & -2 \end{pmatrix}$, where each row represents one of the real space unit cell lattice vectors. Conventionally, the first integer in each row refers to the <110> direction of the copper surface, in units of the interatomic spacing $d_{Cu\text{-}Cu}$ = 2.55Å, and the second refers to the <001> direction with units of $\sqrt{2}d_{Cu\text{-}Cu}$ = 3.61Å. The (2, 4) vector is 15.51 Å long and oriented 70.55° respect to the <110> direction, while the vector (5, -2) is 14.65 Å long and aligned 29.52° respect to <110>.

Since neither of the defining vectors are aligned with the substrate unit cell, two domains are implied, related by reflection across the <110> direction (or the <001> direction). The reciprocal lattice vectors and higher order diffraction spots, within the first order substrate diffraction pattern, are illustrated in Fig. 4.10B and the real space unit cells are shown in Fig. 4.10C. In Fig. 4.10B the solid and dashed meshes correspond to the two domains and LEED spots can be found at the intersections in each mesh. The unit cell is 24 times larger than the underlying substrate unit cell, which is double that of the p(3x4)g unit cell which itself contains two molecules. Compared with the benzoate species, the "footprint" of the flat-lying p-aminobenzoate is slightly larger, thus, a slightly larger unit cell size than the α-phase benzoate (23 times of Cu unit cell) on Cu(110) suggests that the number of molecules per unit cell are the same for p-aminobenzoate and benzoate, i.e. there are four p-aminobenzoate molecules within the unit cell of the β-phase, with a surface coverage of 0.167ML, the same as the α-phase.

Further annealing the surface to 510 K, the LEED pattern changes gradually to a periodicity of $\begin{pmatrix} 1 & 2 \\ 6 & -5 \end{pmatrix}$, as shown in Fig. 4.11, which will be referred to as the γ-phase. It again consists of two domains with sides of length 7.66 Å and 23.66 Å and an included angle of 59.73° resulting in a unit cell which is 17 times larger than the Cu (110) unit cell. Here, we want to emphasize that both β and γ phases have one of their unit cell vectors along the (1, 2) or (-1, 2) direction.

From the β to the γ phase, the unit cell size reduces by 7 Cu atoms, which approximately corresponds to one flat lying molecule. Thus, the γ-phase is likely to have three molecules per unit cell, which is confirmed by the STM images discussed in Sect. 4.4. The local surface coverage increases to 0.176ML. Although most of the diffraction spots can be found at the intersections in meshes formed by $\begin{pmatrix} 1 & 2 \\ 6 & -5 \end{pmatrix}$ matrix, the spots at (±1/3, ±1/5) positions (in the reciprocal space) are elongated. By varying the electron kinetic energy, it was found that the spots splitting is centred along the (±1/3, ±1/5) spots, rather than the (0, 0) beam. This is typical for faceted surface, at which the diffraction from the facet is centred at different (0, 0) diffraction positions. The structure of the γ-phase is formed by dehydrogenation at 510 K. The first H_2 desorption peak in TPD seems to contain several steps corresponding to different phases

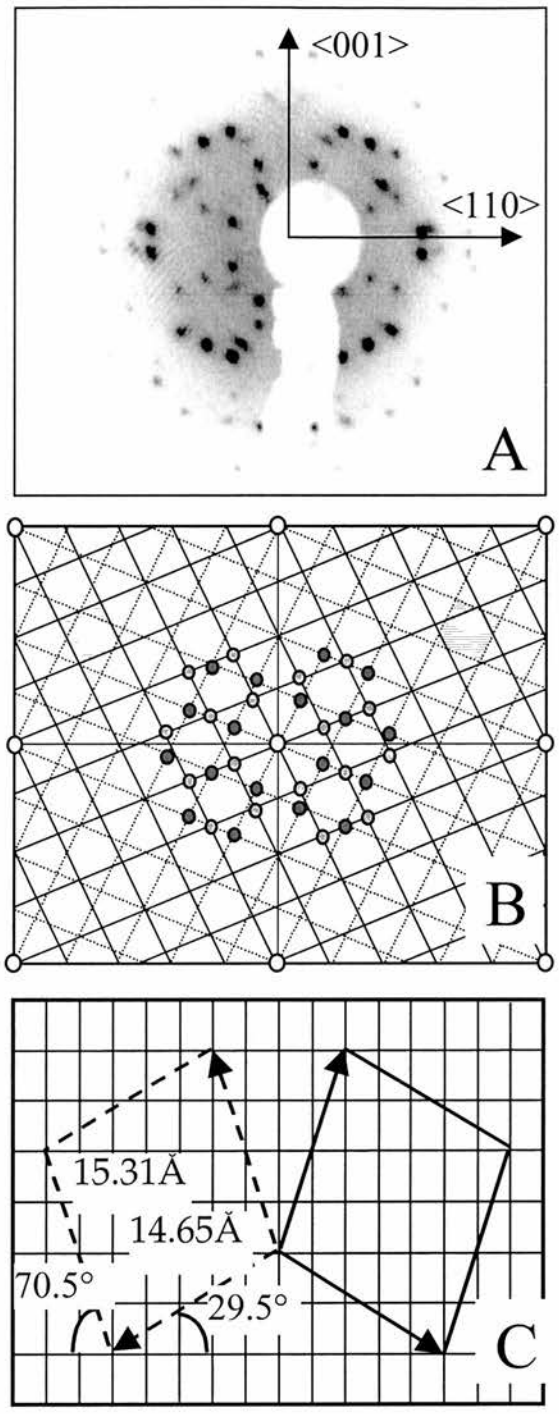

Fig 4.10 A)LEED Pattern of β phase, 23eV B) Overlayer reciprocal lattice unit cells c)Real space unit cells

EELS suggests that at 510K, there is still some ortho-CH left on the surface. By further annealing the surface, the dehydrogenation can be completed at about 540 K, when a final phase, referred as the δ–phase, is formed. However, slightly

above the temperature of 540 K, decomposition and desorption of the whole molecule is initiated, as shown in Fig. 4.2.

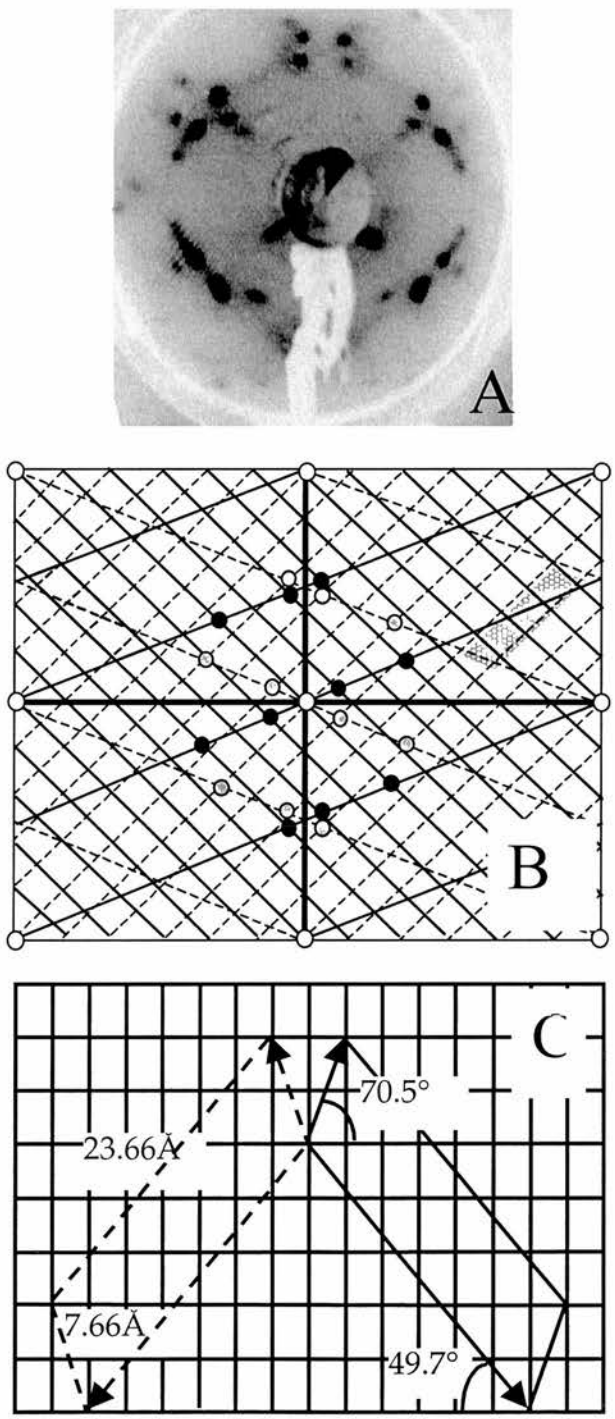

Fig. 4.11 A)Leed pattern of the γ-phase, 15eV B) Reciprocal lattice unit cells of the two domains C) Real space unit cells

Initially, the LEED over-layer spots of the δ phase are weak, so to improve the surface order, the sample was annealed overnight at a fixed temperature 540 K. The LEED pattern, recorded at 35 eV, is shown in Fig. 4.12, in which the real space unit cell is also shown. The unit cell, $\begin{pmatrix} 1 & 2 \\ 4 & -3 \end{pmatrix}$ is formed by two vectors of 7.66 and 14.88 Å in length with an included angle of 62.73°. This angle is only slightly larger than in the γ-phase, and the unit cells again share a common vector, (1, 2). This unit cell is 11 times larger than the Cu unit cell, but smaller than that β and γ phases by 13 and 6 Cu unit cells, respectively. Thus the unit cell probably contains only two molecules corresponding to a local surface coverage of 0.182ML. Increasing the surface coverage from β– (0.167ML) to γ– (0.176ML) and then to δ– phases (0.182ML), is consistent with the dehydrogenation process, leading to a smaller molecular footprint. However, the details of the molecular arrangement within the unit cell and how the dehydrogenation occurs to form different periodic structures are better revealed by high resolution STM.

4.4 STM measurements

While HREELS can give information on molecular orientation and the LEED pattern presents the size and shape of the unit cell, STM images can indicate the number of molecules within the unit cell and frequently even more structural details, depending on the image resolution.

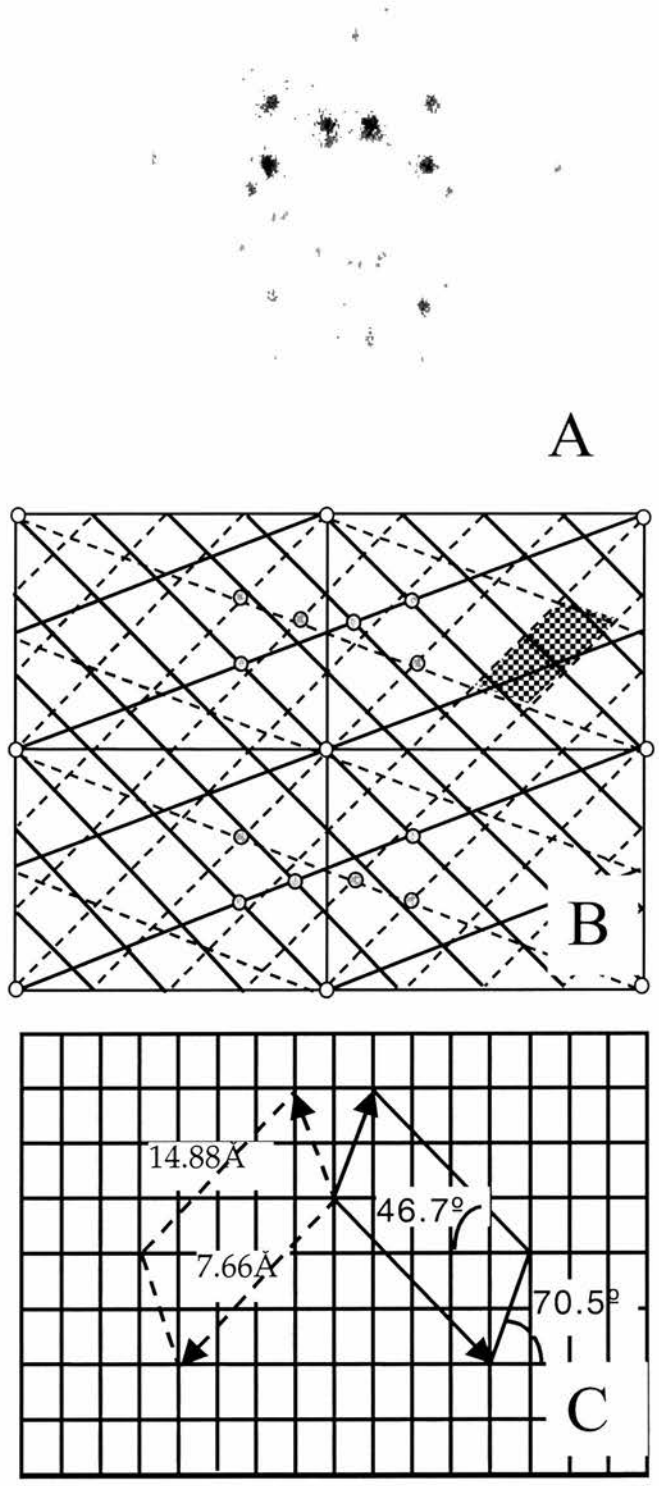

Fig. 4.12 δ phase LEED pattern – sample annealed overnight, 35eV

As previously mentioned, in the p(3x4)g periodicity, all the flat-lying molecules are azimuthally aligned with the principal molecular axis along the <001>

direction and two molecules per unit cell consistent with glide plane symmetry along the <001> direction. A typical STM image of this room temperature structure is shown in Fig. 4.13A with a LEED pattern (Fig. 4.13B) recorded at 31 eV.

Annealing this surface to 464K, the β-phase, $\begin{pmatrix} 2 & 4 \\ 5 & -2 \end{pmatrix}$ periodicity is formed and Fig. 4.14 shows a typical STM image of this phase. The unit cell of the β-phase is marked by the white lines. Near the upper part of the image, some residual (3x4) structure can also be distinguished which is marked by the black lines. Two types of features can be observed in the β-phase unit cell. First is the smaller isolated elliptical shaped feature (two per unit cell) with a dimension of 3.0x5.4 $Å^2$. The feature has its longer axis aligned along the <001> azimuth of the substrate, very similar to the features in the p(3x4)g image. Since the size of this feature matches the "footprint" of the flat lying molecule, we have assigned this as an individual molecule with an orientation inherited from the earlier, room temperature (3x4) structure. There are two such isolated molecules per unit cell. However, instead of being located half way along the (3, 4) vector, the second molecule of this type in the unit cell is found halfway along the (3, 2) vector at a shorter distance of 5.3 Å, compared to 8.2Å, i.e. shifted one substrate unit cell along <001>.

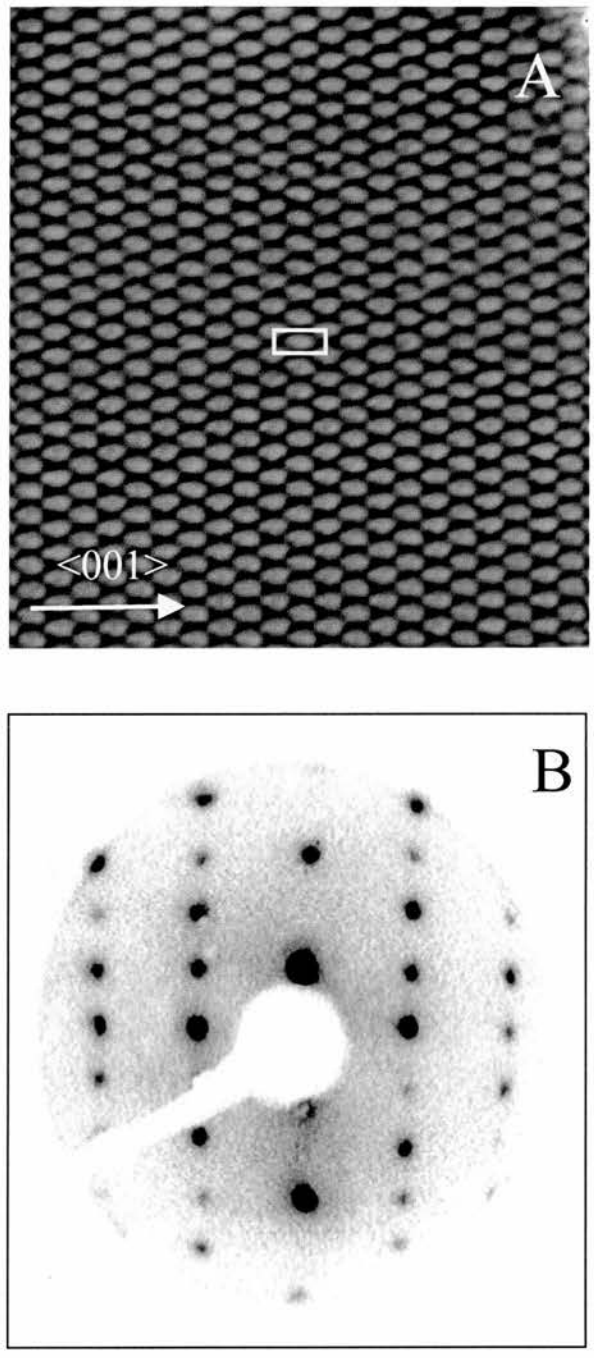

Fig. 4.13 The STM image (170 nmx170 nm, bias=0.16V, tunneling current=40 nA)of p(3x4)g periodicity with B) LEED pattern recorded at 31eV

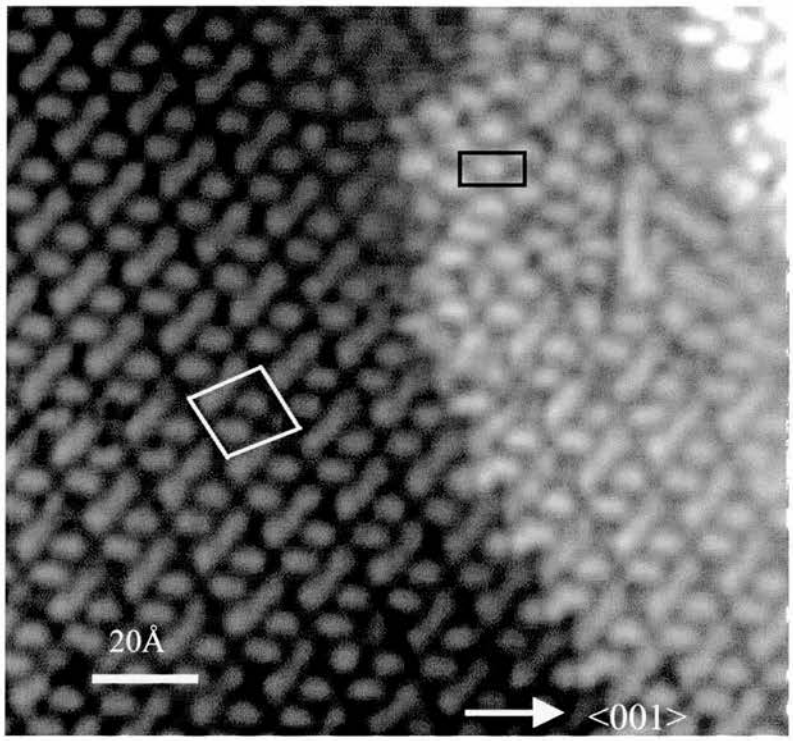

Fig. 4.14 STM image (165Åx140Å, bias=-0.81V, tunneling current=50 nA) shows the $\begin{pmatrix} 2 & 4 \\ 5 & -2 \end{pmatrix}$ structure. Both the residual (3x4)g (black lines) and $\begin{pmatrix} 2 & 4 \\ 5 & -2 \end{pmatrix}$ (white lines) unit cells are indicated.

In addition, a longer feature with a dimension of 3.0x7.5 $Å^2$ and a characteristic "S" shape is also found within the unit cell. The appearance of these features is directly linked to the dehydrogenation reaction, as indicated by TPD and HREELS results. Although the feature of 7.5Å is longer than an isolated molecule, it is shorter than expected for two end-to-end molecules. It suggests that a dimer species is formed. Overall, there are four molecules in each unit cell (one pair and two unpaired), which gives a surface coverage of 0.167 ML (4 molecules per 24 Cu atoms).

Further annealing this surface, a continuous phase transition takes place to the γ-phase with a periodicity of $\begin{pmatrix} 1 & 2 \\ 6 & -5 \end{pmatrix}$. A large area image of this phase is shown in Fig.4.15, while a enlarged smaller area is shown in Fig. 4.16. On these images, bright features are assigned to the presence of upright species along line defects in the $\begin{pmatrix} 1 & 2 \\ 6 & -5 \end{pmatrix}$ structure. The appearance of well defined, faceted step edges can also be found on the right upper corner. Two distinct domain types, related by reflection can be observed in Fig 4.15. The white arrow indicates a boundary between such domains. This boundary is labeled B in Fig. 4.16, where the unit cell is also marked. It can be clearly resolved that there are three features within the new $\begin{pmatrix} 1 & 2 \\ 6 & -5 \end{pmatrix}$ unit cell, of which two are closely packed like a dimer while the third is slightly removed, but linked with one dimer, possibly through H-bonding. The STM unit cell, containing three molecules (one pair and one single molecule), is consistent with our LEED measurement. The surface coverage in the ordered region at this stage is 0.176ML (3 molecules per 17 Cu atoms).

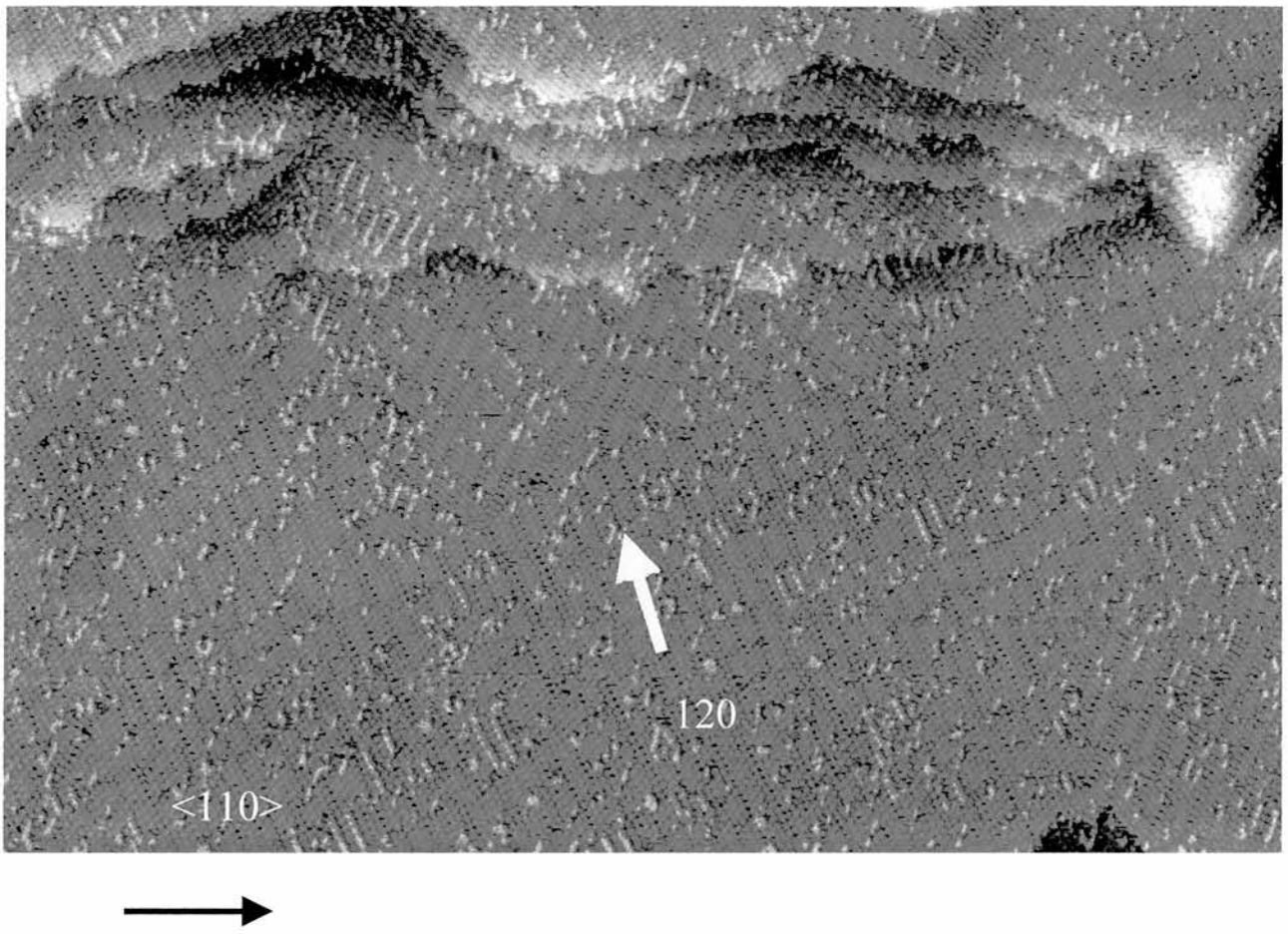

Fig. 4.15 STM image (1320Åx840Å, bias=-0.22V, tunnelling current=0.51 nA) shows the $\begin{pmatrix} 1 & 2 \\ 6 & -5 \end{pmatrix}$ structure. The bright feature corresponds to the upright feature. The domain boundary is indicated with the white arrow

However, on this surface, the proportion of the dimer is about 2/3 of the total molecular species, while in the β-phase, it is about 1/2. It is important to note that, the annealing temperature, rather than the reaction kinetics, determines the degree of the dehydrogenation, since the surface structure is reproducible and independent of the heating rate. The size of the dimer feature is the same as in the β-phase, as is the orientation almost parallel to the (6, ±5) direction.

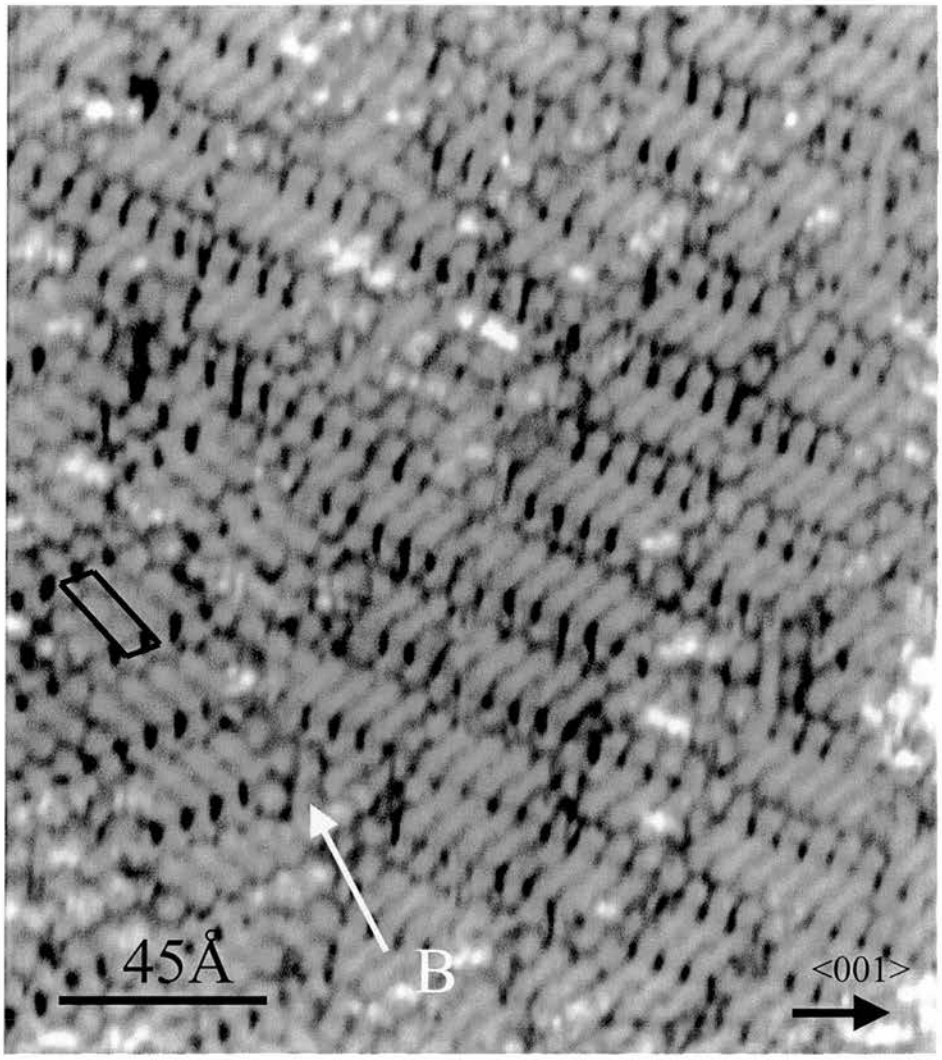

Fig.4.16 STM image (220Åx220Å, bias=-0.22V, tunneling current=0.51 nA) shows a detailed $\begin{pmatrix} 1 & 2 \\ 6 & -5 \end{pmatrix}$ structure with a marked unit cell (black lines). The domain boundary is labeled as B

From the image, it can be found that most of the dimers are attached at one end with a single molecule through the type of link which is aligned along 8° off the <110> azimuth and 45° off the dimer. This link is also found, occasionally, on both sides of a dimer or changing from one row of dimers to the adjacent row, while some of the dimers have no attachment of any single molecule.

Annealing this surface to 540 K completes the dehydrogenation and the first stage of H_2 desorption in the TPD and the δ-phase with $\begin{pmatrix} 1 & 2 \\ 4 & -3 \end{pmatrix}$ periodicity is formed. Figure 4.17 shows an image (350Åx250Å) of this ordered structure. The terrace has a width of only 30Å (shown in the line profile in Fig. 4.17b), but a length of 120Å. Within the unit cell, all molecules are paired into dimers. Again, this dimer feature, has the same dimension and orientation as in the β– and γ–phases. There is no single isolated molecular feature. Although the terraces are small, the periodicity seems not to be limited by or even to recognise the step edges. This is because the location of each step is correlated with the arrangement of the over-layer structure. It is also related to the observed step bunching and faceting. The interactions between adsorbates, as well as between adsorbate and substrate, must be strong enough to cause bunching and alignment of steps into facets that otherwise are thermodynamically less stable for the clean surface. On the right side of the upper part of surface, some of the residual single molecules are still present, which forms a local γ-phase. On this part of the surface, the dehydrogenation is obviously not yet fully complete. The difficulty in achieving a pure δ-phase arises because the difference in the annealing temperature for the γ-phase and the δ-phase is only 30K, while the molecular desorption starts at 550 K, only 10K above the annealing temperature. Thus, although care was taken to anneal the surface slowly, under heating was always a possibility.

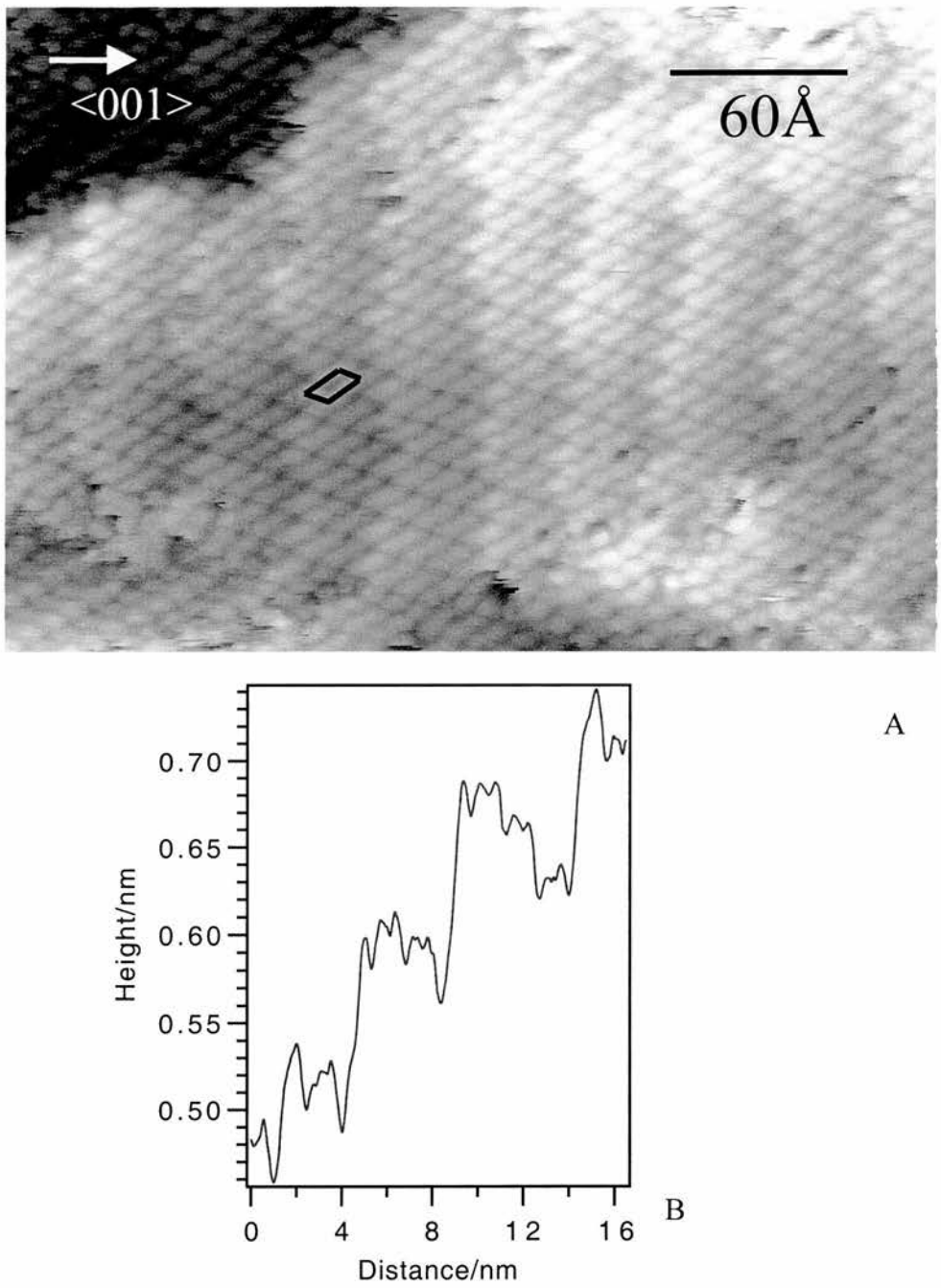

Fig.4.17 A)STM image (350Åx250Å, bias=-1.14V, tunneling current=6.0 nA) shows a detailed $\begin{pmatrix} 1 & 2 \\ 4 & -3 \end{pmatrix}$ structure with elongated terraces along the <110> azimuth. On the right upper of the image, a row of single molecules still can be identified. B) The line profile shows the stepped terrace with a width of 30Å.

4.5. Discussion

Structural models

By annealing the initial (3x4)g surface at 464K, an ordereda $\begin{pmatrix} 2 & 4 \\ 5 & -2 \end{pmatrix}$ structure (α-phase) is identified. It is possible to attribute two distinct features to two molecular types; the isolated elliptical shaped feature, with a dimension of 3.0x5.4 $Å^2$, is assigned as a single p-aminobenzoate molecule, while the longer one with a dimension of 3.0x7.5 $Å^2$ is attributed to a dimer species. TPD shows the desorption of H_2, while EELS spectra indicates a decrease of the loss intensities of vibration modes related to the ortho-CH, NH_2 and CCN out-of-plane bending. Here, it can be emphasised that no other desorption accompanies the H_2 desorption, implying that reaction is limited to dehydrogenation. The possibility that the desorption of H_2 at 460K is due to the deprotonation of the acid can be excluded by comparison with adsorbed benzoic acid [15], where the acid proton is lost at a temperature well below room temperature. Substantial decomposition of the molecule is unlikely on the basis of the limited changes in the EEL spectra. Also, STM shows features readily assigned to molecules and associated dimers, rather than more complex decomposition fragments. Therefore, it can be concluded that, at 464 K, dehydrogenation between two adjacent molecules occurs to form the dimers. From EELS vibrational frequency assignment discussed in Section 4.1, the peaks at 500 and 870 cm^{-1} arises from mixing of the CCN deformation, γ(ortho-CH) and $\gamma(NH_2)$ out-of-plane bending. The decrease of the intensities of these modes suggests that the dehydrogenation is localised on the ortho-H and the NH_2 group. Since the mode at 760 cm^{-1} related to the meta-CH out-of-plane bend, retains a constant intensity

and no peak appears above 1000 cm^{-1}, the molecular geometry is unchanged and other parts of the molecule remain intact. This dehydrogenation process is depicted in Scheme 1. Obviously, the presence of the NH_2 group in the molecule reduces the activation barrier for the dehydrogenation reaction specifically on the ortho site. The dimer is terminated with carboxylate groups on both ends, which stops further dehydrogenation reaction. Meanwhile, a C_2 rotational symmetry is created in the dimer. The CN(H)C bonding structure is typical of that found in a polyaniline structure[31], in which the hydrogen of the para-CH is lost and forms CN(H)C bonding. The occupancy of the para position by the carboxylate group, restricts dehydrogenation to the ortho position. It is plausible that steric consideration in the chemisorbed species favour dimerisation with participation of the NH_2 group of each molecule in the dehydrogenation, rather than polymerisation.

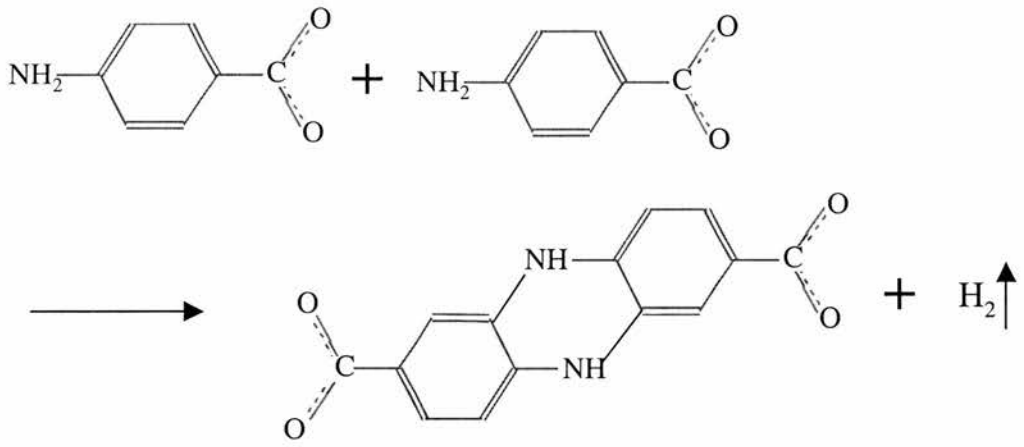

Scheme 1

Based on this experimental evidence and the combination of LEED and STM observations, a model of the $\begin{pmatrix} 2 & 4 \\ 5 & -2 \end{pmatrix}$ structure is suggested and shown aligned with the STM image in Fig. 4.18. In this model, the dimer is formed through the bonding

between the ortho-C and N atoms of both adjacent molecules. Overall, there are 50% of molecules dehydrogenated in the β-phase, which is proportional to the reduction of EELS loss intensity at 870 cm^{-1} at 464 K. The model presented in Fig. 4.19 provides the opportunity for significant contribution from H-bonding between the carboxylate group of the isolated molecule and the amine H of the dimer. However, it should also be realised that to achieve the proposed structure, significant movement, especially rotation of the molecule is critical. This is actually evidenced by the temperature dependent LEED observation of the phase transition. Two types of phase transitions can be recognised. In the first, for example the transition from $\begin{pmatrix} 4 & 3 \\ -1 & 5 \end{pmatrix}$ into $\begin{pmatrix} 4 & 3 \\ -4 & 3 \end{pmatrix}$ and $\begin{pmatrix} 4 & 3 \\ -1 & 9 \end{pmatrix}$ of benzoate on Cu(110) [32], the structures of the different phases are closely related in their ordering. In this case, there are smooth transitions and no disordered stage in between phases. However, here, for the phase transition from (3x4)g into the $\begin{pmatrix} 2 & 4 \\ 5 & -2 \end{pmatrix}$ structure, the (3x4)g LEED pattern disappears before the appearance of the $\begin{pmatrix} 2 & 4 \\ 5 & -2 \end{pmatrix}$ pattern. This transition process can be seen as one, in which, intermediate disordering, due to the large scale molecular movement, is necessary for the formation of the $\begin{pmatrix} 2 & 4 \\ 5 & -2 \end{pmatrix}$ phase.

Although there is no direct measurement of the registration of molecules on the Cu substrate, there is included a Cu substrate mesh in the model in Fig. 4.18. Assuming that each single molecule is bonded to the substrate through the O atoms in the carboxylate group on top of the Cu atoms along the <110> azimuth, it is found that two carboxylate groups of the dimer are also close to the similar adsorbtion site, although the carboxylate groups are not necessary exactly aligned along the <110>

azimuth. Since the molecule is flat lying on the surface, due to the metal surface vibrational selection rule, the vibrational spectrum will not indicate whether the carboxylate group is in a unidentate or bidentate form. On the other hand, STM images also show that each single molecular feature has an elliptical shape with its longer axis parallel to the <001> direction. Of course, there is no experimental evidence to indicate which end is the amino (carboxylate) group. Nevertheless, the opposing direction of the carboxylate groups, similar to that in the dimer, ensures that all the carboxylate groups are bonded on the short bridge sites, and, in turn, H-bonded to the NH group in the dimer, as indicated with the dash line On annealing the surface to 510 K, the ordered structure of $\begin{pmatrix} 1 & 2 \\ 6 & -5 \end{pmatrix}$ periodicity, the γ-phase, is formed. A real space model is proposed in Fig. 4.19. It is assumed that there are three molecules per unit cell, formed by a dimer and a single molecule. The dimer is aligned along the same direction as that in the β-phase. The bonding between the single molecule and dimer can be clearly identified as the bright features between them. However, the single molecule is only able to H-bond to one dimer, while both ends of the dimer can be bonded to a single molecule. Thus, we recognise that each end of the dimer has the same terminating functional group, in this case, the carboxylate group. This dimer model is consistent with continuation of the dehydrogenation reaction proposed in scheme 1. On the basis of this model, the single molecule bonds to the dimer through its amino group. The energy difference for the single molecule to choose which adjacent dimer to bond to must be very small, compared with H bonding between the amino group of the single molecule and the carboxylate group of the dimers. However, the presence of the molecular dipole can influence the alignment of adjacent single molecules, so that a row of

such molecules along the (1, 2) vector have parallel dipoles and always bond to dimers in the same dimer row.

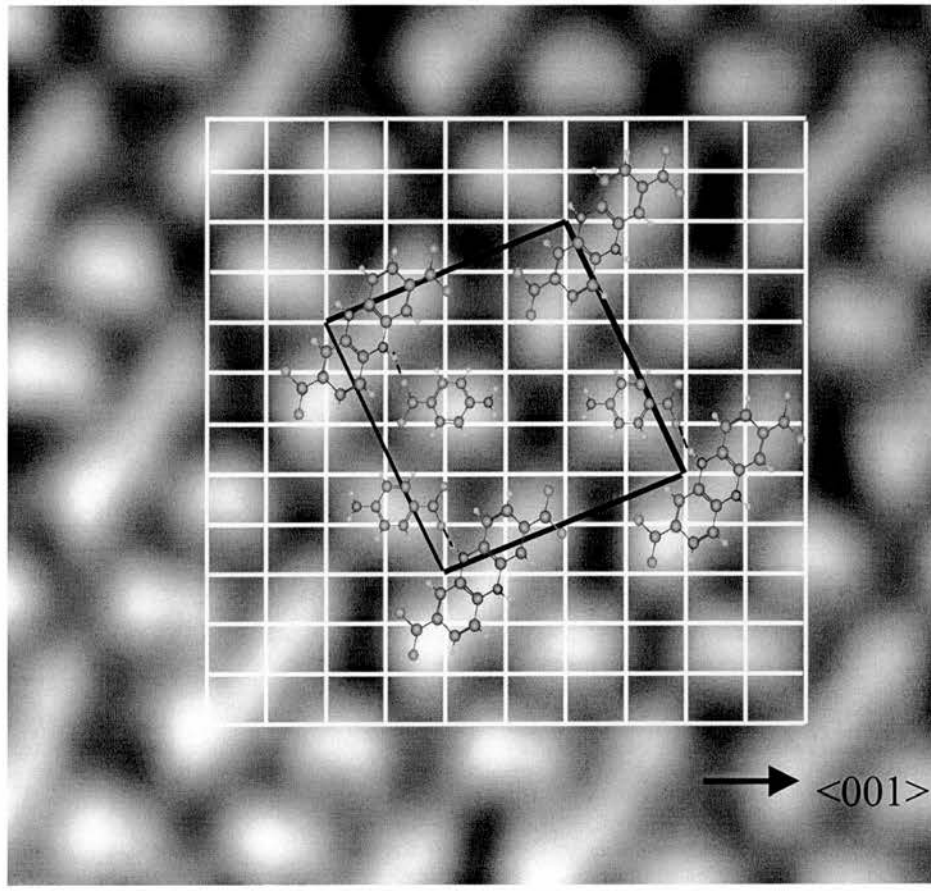

Fig. 4.18 Real space model of the β phase, intermolecular bonding indicated with a dashed line. (60×40Å) area image.

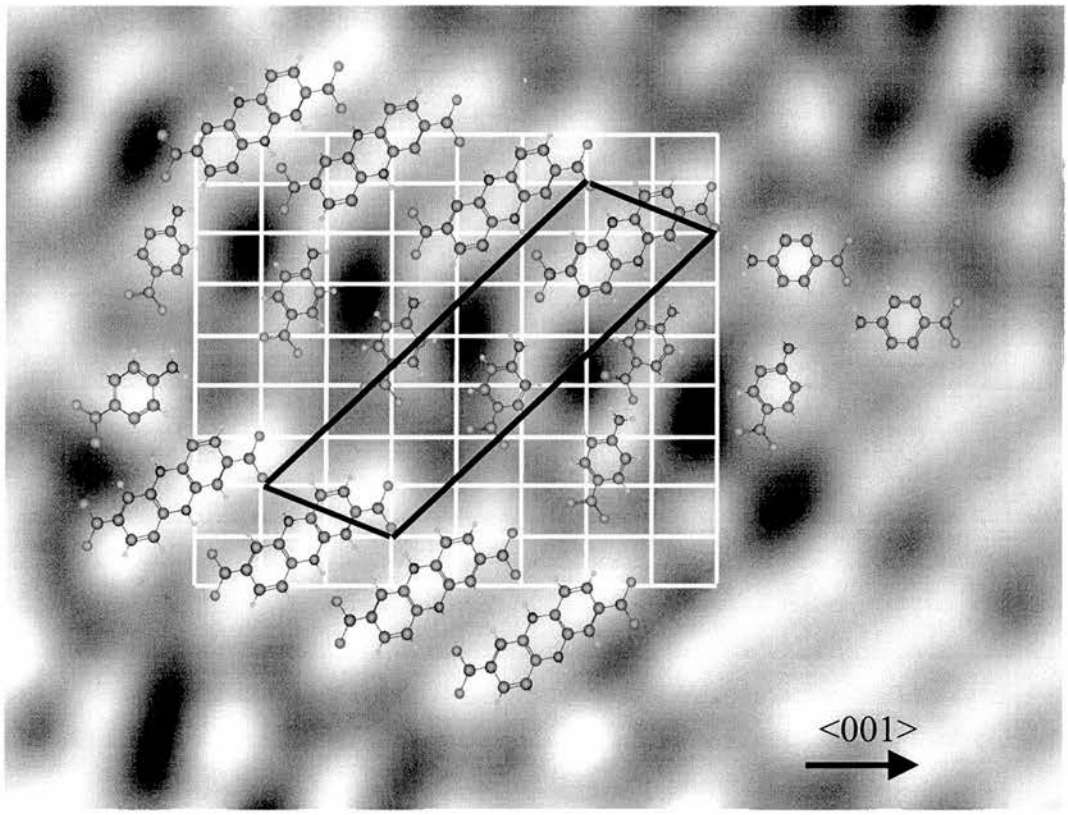

Fig 4.19 Real space model of the γ-phase. (60 ×38Å) area image.

Annealing the surface to 540 K forms the δ-phase, $\begin{pmatrix} 1 & 2 \\ 4 & -3 \end{pmatrix}$. STM images show that all the molecules are now paired into dimers, with the same orientation as that in the β and γ phases. Thus, the dehydrogenation is completed, which gives the highest local surface coverage, 0.182ML. A model is proposed in Fig. 4.20 A large scale search of many STM images found no evidence of any dehydrogenation to form trimers, also supporting the model of dimers terminated with the same functional group, the carboxylate group.

Correlation between phases.

The correlation between β, γ and δ phases is clear. In the β-phase, there are four molecules per unit cell, in which two of them form a dimer, while in the γ-phase, there are three molecules per unit cell formed into a dimer and a single molecule, and in the δ-phase, only a dimer feature is observed. In the β-phase, 50% of molecules are dehydrogenated, while in the γ-and δ-phases, 67% and 100% of molecules dehydrogenate, and the pre-desorption of the H_2 is finally completed at a surface temperature of 540 K. The "footprint" of a dimer is significantly smaller than that of two single molecules, since the intermolecular distance is shorter in the dimer. Thus, from β, γ, to δ phase, the local coverage increases gradually from 0.167, 0.176 to 0.182ML. Of course, total coverage remains unchanged so increases in the coverage in the ordered regions must be offset by decreases at domain boundaries and other defects rich regions. Table 4.1 summarises the observed difference phases as a function of annealing temperature.

The dimer features in these different phases are all oriented along the same direction. The row of dimers in the γ-phase is exactly the same as in the δ-phase, aligned along the (1, 2) vector. The unit cells of these phases are also highly correlated. Fig. 4.21 shows the real space unit cell of each phase on the Cu(110) substrate. All three phases have a unit cell vector aligned along the (1, 2) direction {(2, 4) vector for the β-phase}, which reflects not only the similarity in the intermolecular interactions, but probably also the consistency in the registration of the molecules on the Cu substrate. It can be recognised that it is the H bonding between the O atom of the carboxylate in one dimer with the H atom in the NH

group of the adjacent dimer, and the possibly preferential bonding site for the carboxylate group on the Cu substrate, which determine the position and orientation of the adjacent dimers. H bonding between adjacent molecules was also found for the room temperature (3x4)g p-aminobenzoate on Cu(110). However, in that structure, the H bonding is aligned along the <110> azimuth of the substrate, since carboxylate and amino groups are themselves aligned along that azimuth. However, when the dimer is formed the carboxylate group is not aligned on the dimer longer axis. Therefore, to assure the bonding of the carboxylate group on the short bridge site, the longer dimer axis has to be tilted away from the high symmetry axes of the substrate and the H-bonding is no longer aligned along the <110> azimuth.

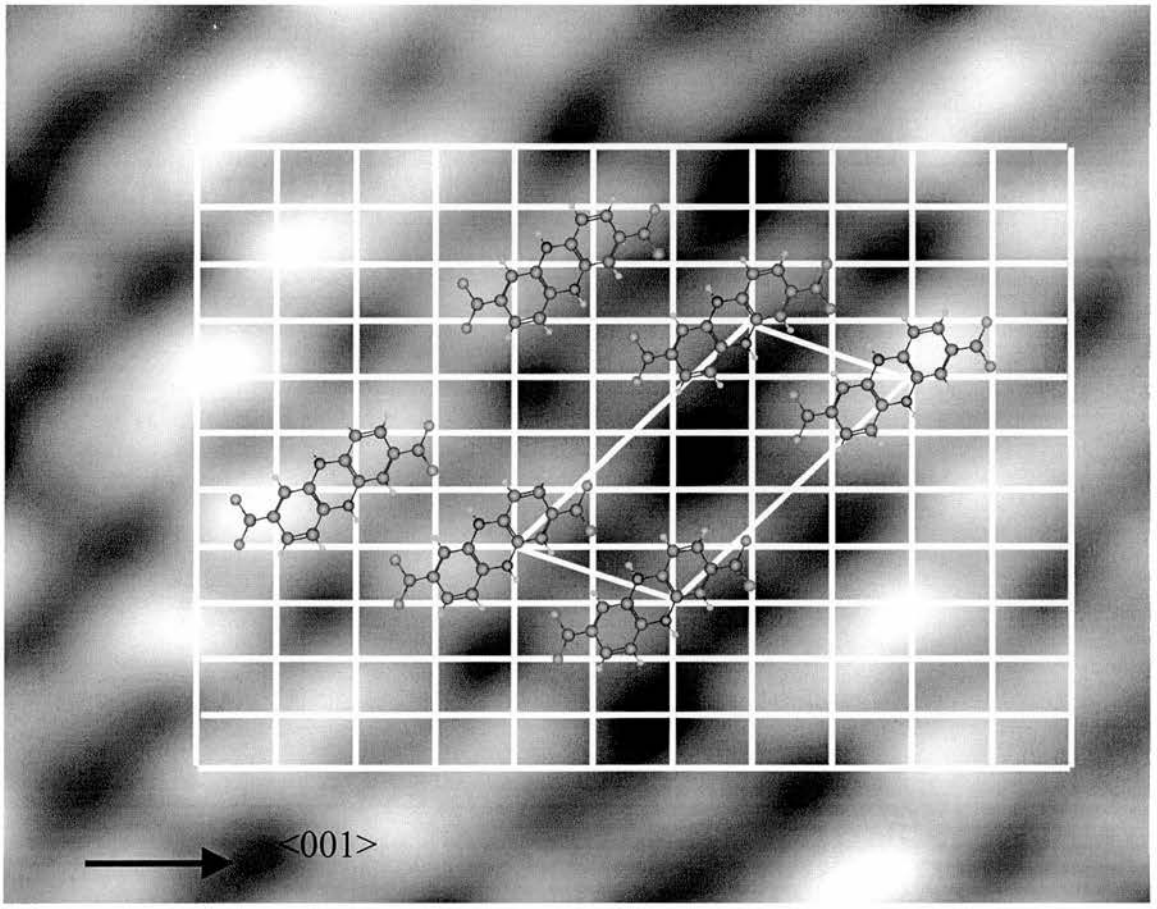

Fig 4.20 Real space model of the δ phase. (50×38Å) area image

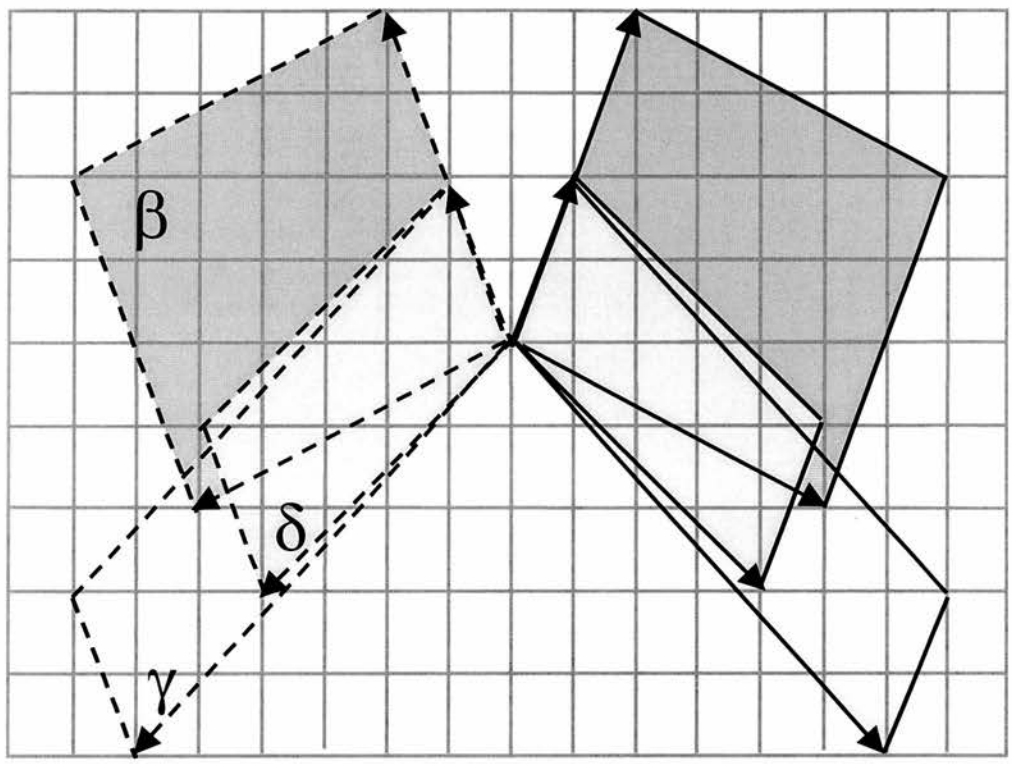

Fig 4.21 Real space unit cell vectors of β, γ and δ phases

Table 4.1. Summary of different phases as a function of annealing temperature

Temperature	300K	464K	510K	540K
Phase	α	β	γ	δ
Periodicity	(3x4)g	$\begin{pmatrix} 2 & 4 \\ 5 & -2 \end{pmatrix}$	$\begin{pmatrix} 1 & 2 \\ 6 & -5 \end{pmatrix}$	$\begin{pmatrix} 1 & 2 \\ 4 & -3 \end{pmatrix}$
Molecules per unit cell	2	4	3	2
Dimers per unit cell	0	1	1	1
"Free" molecules per unit cell	2	2	1	0
Cu atoms per unit cell	12	24	17	11
Total Coverage	0.167ML	0.167ML	0.176ML	0.182ML
Ratio of dehydrogenation	0	1/2	2/3	1

References:

[1]J.C. Bertolini, G. Dalmai-imelik, and J. Rousseau, Surf. Sci. **67** (1977) 478.

[2]N.V. Richardson and P. Hofmann, Vacuum **33** (1983) 793.

[3]B.E. Koel, J.E. Crowell, C.M. Mate, and G.A. Somorjai, J. Phys. Chem. **88** (1984) 1988.

[4]F.P. Netzer and M.G. Ramsey, Crit. Rev. Sol. St. Mat. Sci. **17** (1992) 397.

[5]A. Kuwae and K. Machida, Spectrochimica Acta **34A** (1978) 785.

[6]K. Machida, A. Kuwae, Y. Saito, and T. Uno, Spectrochim. Acta **34A** (1978)

793.

[7]B.G. Frederick, M.R. Ashton, N.V. Richardson, and T.S. Jones, Surf. Sci. **292** (1993) 33.

[8]B.G. Frederick, F.M. Leibsle, S. Haq, and N.V. Richardson, Surf. Rev. Lett. **3** (1996) 1523.

[9]B.G. Frederick, Q. Chen, C.C. Perry, S. Haq, and N.V. Richardson, Polymer-solid interfaces: from model to real systems. Proceedings of the Second International Conference, Namur, Belgium (1996) .

[10]B.G. Frederick, Q. Chen, F.M. Leibsle, S. Dhesi, M.B. Lee, K.J. Kitching, and N.V. Richardson, Surf. Sci. **394** (1997) 1.

[11]D.P. Woodruff, C.F. McConville, A.L.D. Kilcoyne, T. Lindner, J. Somers, M. Surman, G. Paolucci, and A.M. Bradshaw, Surf. Sci. **201** (1988) 228.

[12]T.F. Lai and R.E. Marsh, Acta Cryst. **22** (1967) 885.

[13]F.A. Cotton and G. Wilkinson, Advanced Inorganic Chemistry (John Wiley & Sons, New York, 1988).

[14]F.M. Leibsle, S. Haq, B.G. Frederick, M. Bowker, and N.V. Richardson, Surf. Sci. **343** (1995) L1175

15 Q. Chen, C. C. Perry, B. G. Frederick, P. W. Murray, S. Haq, and N. V. Richardson, Surf. Sci. **446,** 63-75 (2000).

16 N. B. Colthup, Appl. Spectrosc. **30,** 589 (1976).

17 J. R. Scherer, **24A,** 747 (1968).

18 M. J. Frisch, G. W. Trucks, H. B. Schlegel, G. E. Scuseria, M. A. Robb, J. R. Cheeseman, V. G. Zakrzewski, J. A. Montgomery, R. E. Stratmann, J. C. Burant, S. Dapprich, J. M. Millam, A. D. Daniels, K. N. Kudin, M. C. Strain, O. Farkas, J. Tomasi, V. Barone, M. Cossi, R. Cammi, B. Mennucci, C. Pomelli, C. Adamo, S. Clifford, J. Ochterski, G. A. Petersson, P. Y. Ayala, Q. Cui, K. Morokuma, D. K. Malick, A. D. Rabuck, K. Raghavachari, J. B. Foresman, J. Cioslowski, J. V. Ortiz, B. B. Stefanov, G. Liu, A. Liashenko, P. Piskorz, I. Komaromi, R. Gomperts, R. L. Martin, D. J. Fox, T. Keith, M. A. Al-Laham, C. Y. Peng, A. Nanayakkara, C. Gonzalez, M. Challacombe, P. M. W. Gill, B. G. Johnson, W. Chen, M. W. Wong, J. L. Andres, M. Head-Gordon, E. S. Replogle, and J. A. Pople, , Revision A.7 ed. (Gaussian, Inc., Pittsburgh PA, 1998).

19 J. J. C. Teixeiradias, L. Decarvalho, A. M. A. Dacosta, I. M. S. Lampreia, and E. F. G. Barbosa, Spectroc. Acta Pt. A-Molec. Biomolec. Spectr. **42,** 589-597 (1986).

20 Q. Chen, D. J. Frankel, and N. V. Richardson, Surf. Interface Anal. **32,** 43-48 (2001).

21 B. A. Sexton, Surf. Sci.. **88,** 319-330 (1979).

22 B. A. Sexton and R. J. Madix, Surf. Sci. **105,** 177-195 (1981).

23 P. Hoffman, S. R. Bare, N. V. Richardson, and D. A. King, Surf. Sci. **133,** L459-L464 (1983).

24 A. Wander and B. W. Holland, Surf. Sci.. **199,** L403-L405 (1988).

25 T. S. Jones, M. R. Ashton, and N. V. Richardson, J. Chem. Phys. **90,** 7564 (1989).

26 M. Casarin, G. Granozzi, M. Sambi, and E. Tondello, Surf. Sci. **307-309,** 95-100 (1994).

27 M. Bowker and R. J. Madix, Applied Surf. Sci. **8,** 299 (1981).

28 M. Bowker and R. J. Madix, Vacuum. **31,** 711 (1981).

29 S. Bao, G. Liu, and D. P. Woodruff, Surf. Sci. **203,** 89-100 (1988).

30 D. Hadzi and N. Sheppard, Proc. Roy. Soc. (London). **A 216,** 247-265 (1953).

31 R. C. Schomburg and R. L. McCarley, Langmuir. **17,** 1983-1992 (2001).

32 Q. Chen, PhD Thesis, University of Liverpool, 1998

CHAPTER 5 . Adsorption of α-pyridone on Cu (110)

5.1 Introduction

A system of particular interest and potential importance is that of adsorption of nucleic acid bases on various surfaces. These may be suitable candidates for the growth of well defined, crystalline yet ultrathin films, as the molecules' planar geometry and hydrogen bonding interactions could lead to subtle control of the surface structure on the nanoscale as well as producing interesting and novel nanostructures. It is also plausible that the specificity of the base pair interactions could be harnessed for molecular recognition events relevant to biosensors.

It has even been hypothesised that nucleic acid bases on surfaces played a role in the emergence of terrestrial life on Earth[1]. This has led to the investigation of the adsorption of the purines and pyrimidines on surfaces under both ambient and ultra-high vacuum (UHV) conditions. The majority of investigations have been carried out under ambient conditions i.e. monolayer deposition of organic films from solution on substrates such as graphite and MoS_2[2]. The motivation for using ambient conditions of temperature and pressure being that they constitute a more realistic environment for self-assembly. However, a high degree of control in terms of surface coverage, order and molecular orientation can only be achieved under UHV

conditions. Contamination is also substantially reduced in UHV allowing fundamental aspects of adsorbate-substrate interactions and interadsorbate interactions to be the focus of attention.

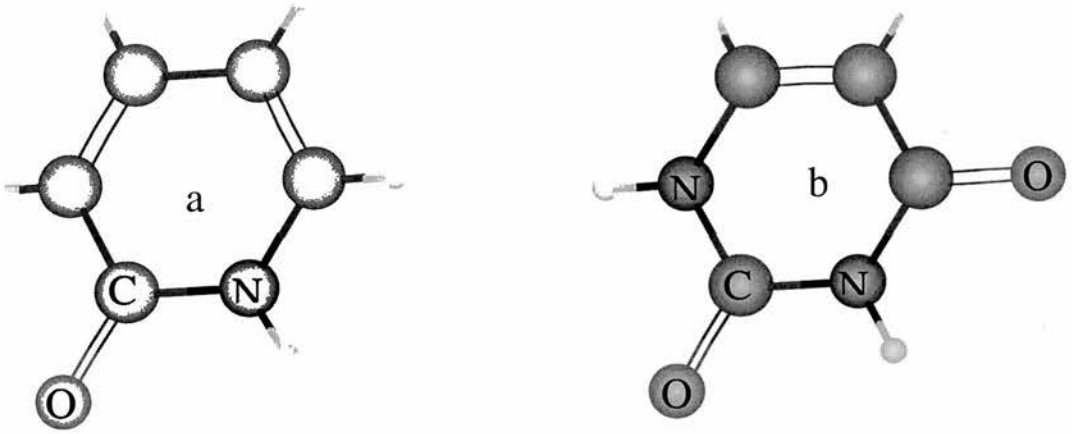

Fig. 5.1. The molecules a) α-pyridone b) uracil

As part of a larger on-going study of nucleic acid bases adsorbed onto Cu(110) under UHV conditions, it was considered useful to investigate simpler analogues as a basis for understanding more complex systems in terms of functionality group influences and the role of hydrogen bonding. One such relevant molecule is α-pyridone which is a close analogue of the RNA nucleic acid base Uracil, Fig 5.1. Indeed, biological structural studies have made use of α-pyridone/(2–hydroxypyridine) as a model system, for example in the investigation

of genetic defects , which are thought to be driven by proton transfer in this type of keto-enol tautomerism[3], Fig 5.2.

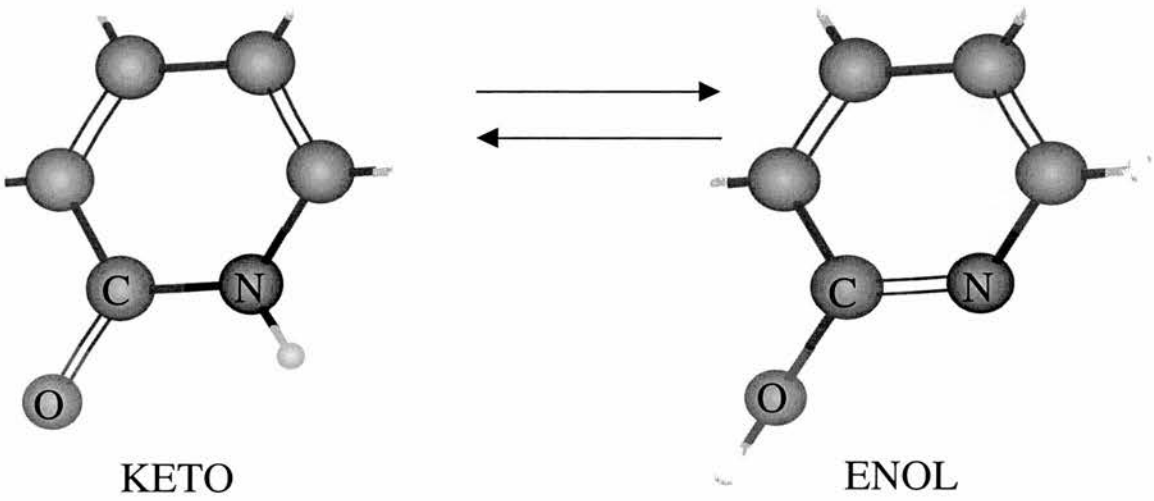

Fig. 5.2 Tautomeric forms of α-pyridone

5.2 Results

Dosing α-pyridone at 300K for 30 minutes caused the (1×1) LEED pattern of the clean Cu(110) surface to fade. However, upon annealing to 590K, a sharp (8×2)gg LEED pattern appeared: figure 5.3. The presence of a glide plane is indicated by the absence of (2n+1)/2 order spots in the <110> direction and a second, perpendicular glide plane is indicated by an absence of (2m+1)/2 order spots in the <001> direction at any incident kinetic energy. The presence of a glide plane requires an even number of molecules in the unit cell and, in the case of a molecule

with symmetry as low as that of α-pyridone, the presence of the second glide plane necessitates a unit cell containing 4, 8 or 12 etc molecules. It also severely limits the possible arrangements of the molecules within the unit cell.

The area of the clean copper unit cell is 9.25Å^2 so that of the (8x2) unit cell is 148Å^2. An intact α-pyridone molecule has a footprint in the range 24Å^2 to 44Å^2 corresponding to the extremes of up-right molecules and flat-lying molecules with the van der Waals' separation, respectively. The unit cell therefore contains four flat-lying or six up-right molecule.

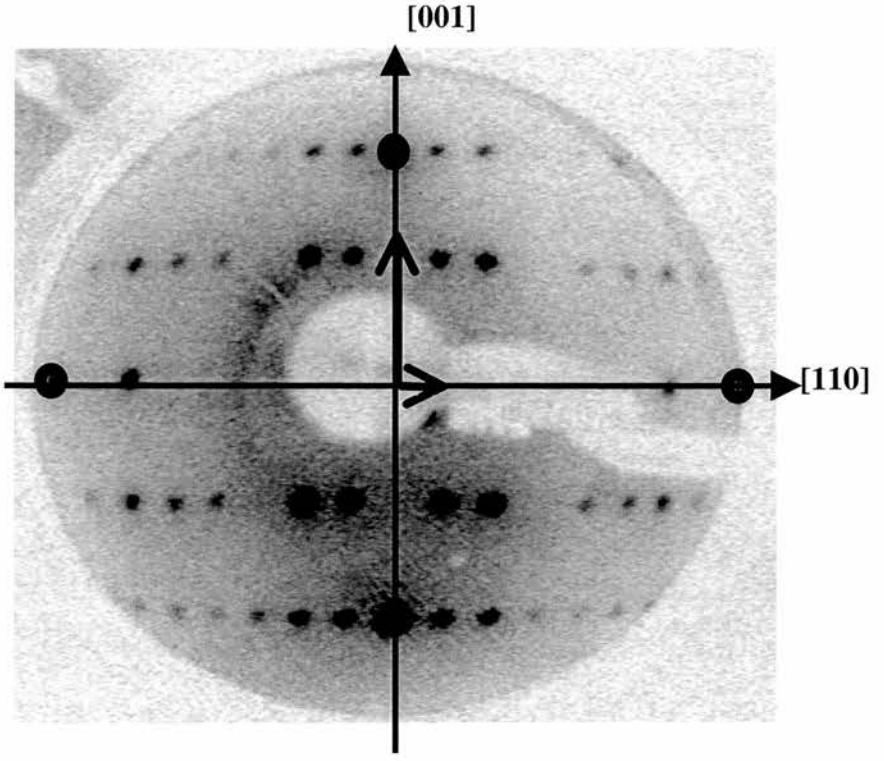

Fig. 5.3 (8×2)gg LEED pattern of α-pyridone / Cu(110). Circles denote integral order spots

Room temperature, scanning tunnelling microscopy studies were carried out to further elucidate the molecular arrangement at the surface. After formation of the (8×2)gg overlayer, the single Cu{110} crystal was transferred through UHV into the adjacent STM chamber for examination. Scanning was performed in constant current mode, 2nA, with a typical bias voltage of –0.3V. Large ordered domains are formed and figure 5.4a shows that the molecules are ordered in a herring bone arrangement compatible with the double glide plane symmetry indicated by LEED.

Measurements of the elongated elliptical features reveal dimensions of approximately 9.5Å. This distance is significant in the fact that it corresponds closely to the length of a hydrogen bonded dimer. It is significantly less than twice the Van der Waals' length of an individual planar α-pyridone molecule because of the interlocking of the heterochiral pair and the closer approach implied by the H-bonding. A typical N-H—O distance would be ca 2.8Å. Such a flat-lying dimer would have a Van der Waals' area of ca 77Å^2 which fits well with there being two such pairs of molecules per unit cell. Figure 5.4b shows a high resolution image with the unit cell superimposed.

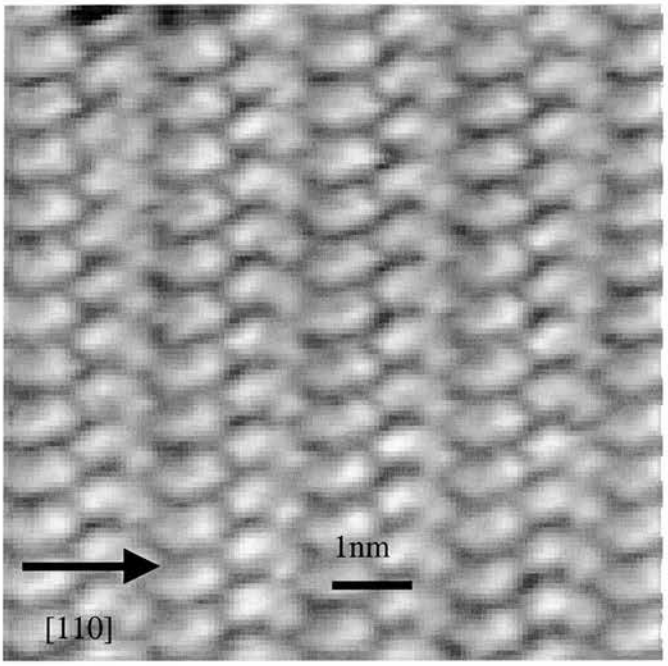

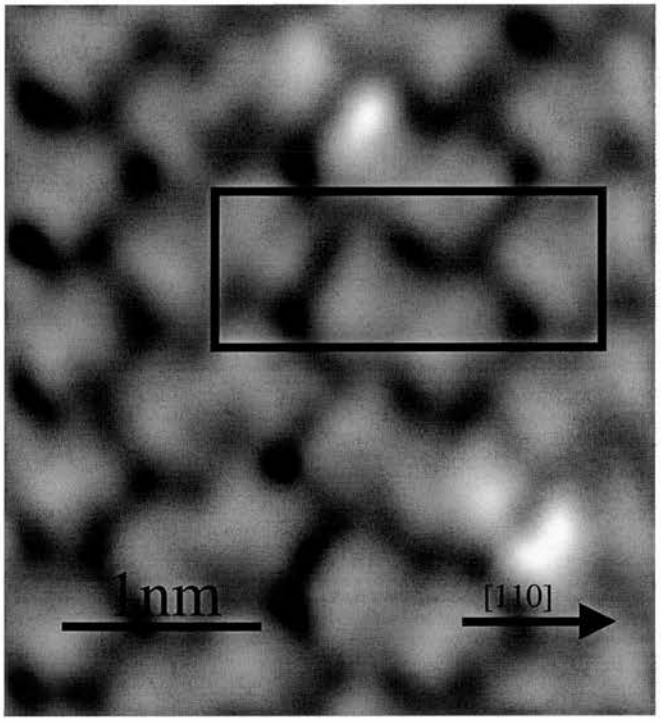

Fig. 5.4 a)Large scale STM image exhibiting herring bone molecular arrangement of α-pyridone / Cu(110) (bias -1.0V, current 0.97nA) b) High resolution STM image with (8×2) unit cell superimposed (bias -0.3V, current 1.7nA)

Energy minimisation calculations of the planar dimer were carried out using Gaussian 98 with a 6-31g basis set. This gave 9.4Å for the dimer length (figure 5.5), although the calculated H- bonded separations of the two N-H--O pairs are surprisingly and probably unreasonably short as well as being unequal. Following structural optimisation of the dimer, the vibrational frequencies were calculated to assist with identification and assignment of the bands in the HREEL spectra.

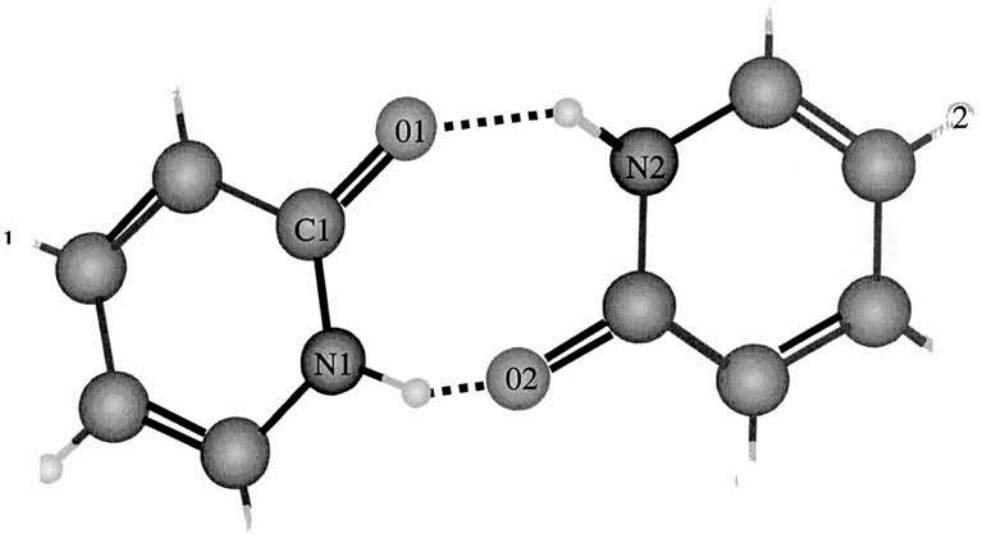

Fig. 5.5 Dimer structure resulting from Gaussian 98 calculation. N2-H-O1 = 2.15Å (170°) and N1-H-O2 = 1.77Å (172°). The dimer length, between the hydrogen atoms marked 1 and 2, is 9.35Å

High resolution electron energy loss spectroscopy (HREELS), was used to characterise the vibrational properties of the adsorbed species and, in turn, to determine, by application of the metal surface dipole selection rule, the orientation of α-pyridone on the Cu (110) surface. Of special interest is the molecular arrangement when the (8×2)gg ordered structure is formed. Therefore, spectra were collected at increasing temperature from that of initial dosing at room temperature to formation of the ordered monolayer at 590K.

Figure 5.6 presents the changes in the HREEL spectra upon annealing. All spectra were collected at room temperature and in the specular direction to ensure that the dipole scattering regime was dominant. Therefore, the metal surface vibrational selection rule can be applied. The loss intensities are normalised against the elastic peak of each spectrum with an offset for a clear view. The measured frequencies, with *our ab initio* calculation result and their assignments, are shown in table 1. The *ab initio* calculation is carried out on a free molecule (in a fully optimised keto form) using the 6-31g basis set and B3LYP DFT method in GAUSSIAN 98[4].

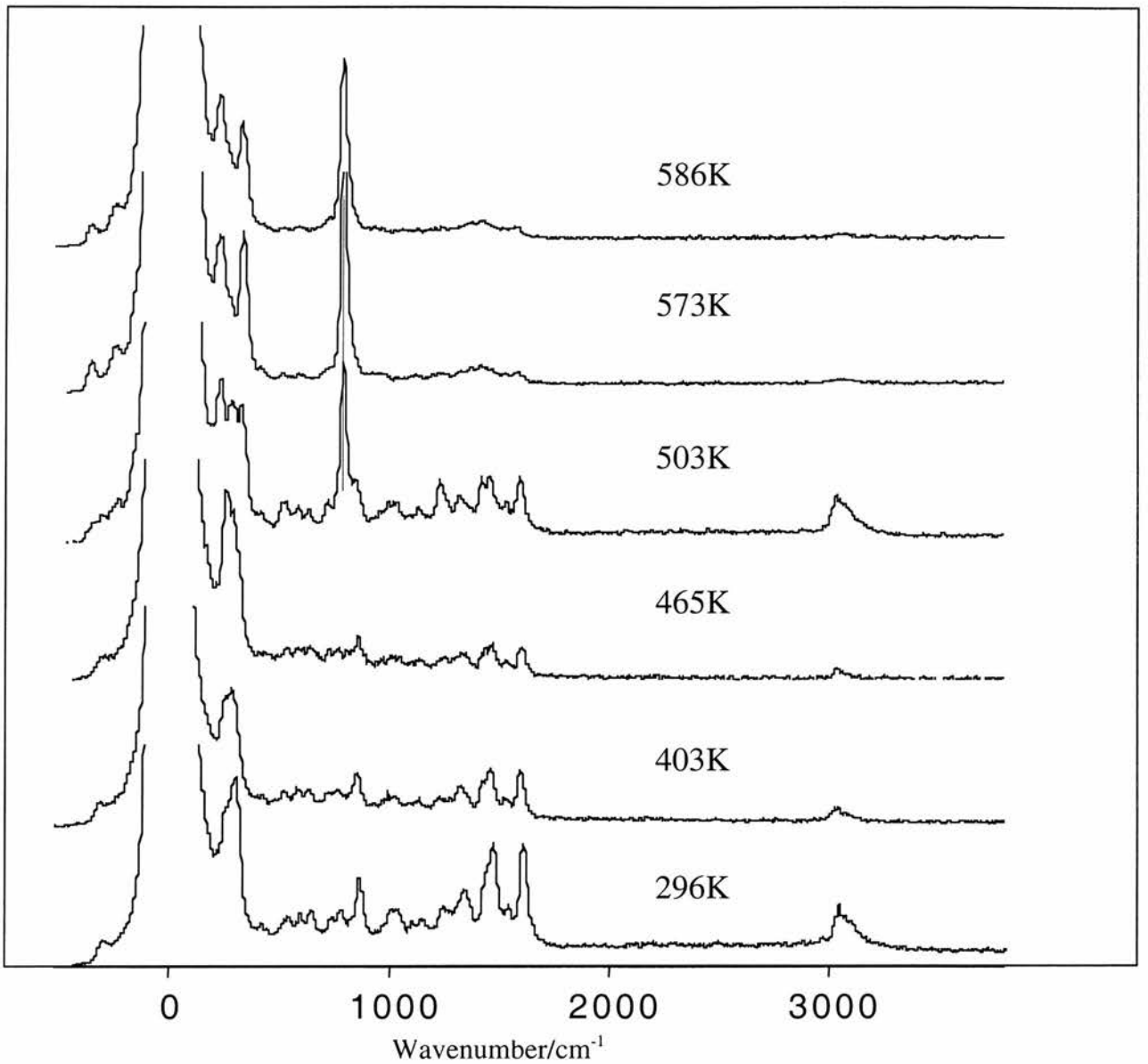

Fig. 5.6 HREEL spectra of α-pyridone / Cu(110) as a function of annealing temperature

It can be seen that, at 300K, several peaks are present with strong loss intensities in the range up to approximately 1700 cm^{-1} and around 3000 cm^{-1}. This spectrum is characteristic of the disordered structure formed immediately after

dosing, corresponding in LEED with disappearance of the integral order spots and the appearance of a higher background intensity. The observation of modes in the higher frequency range >1200cm^{-1}, which correspond to in-plane modes, is strongly suggestive of molecules adsorbed in an upright orientation, although out-of plane bending modes also have significant intensity, e.g. at 867cm^{-1}. Molecules are therefore either inclined to the surface or more likely in a variety of configurations at the surface at this temperature. At this temperature, slightly below the multilayer desorption peak temperature (310K see below), a thin multilayer is still able to be formed. This is clearly evidenced as the surface annealing temperature increases from 330 to 460K, overall loss intensities decreases slightly without changing of the relative intensities.

Between 460 and 500K, all vibrational modes increase their intensities, while the mode at 804cm^{-1} becomes the strongest. This overall increases of loss intensity could be related to the changing of the surface reflectivity. Above 500 K, the vibrational modes above 1000cm^{-1} gradually disappear with the end result being the almost exclusive presence of lower frequency modes (<1000cm^{-1}). In particular, the peak at 804cm^{-1} corresponds to the C-H out-of-plane bending mode which is generally acknowledged as an indication of a flat-lying aromatic ring. Hence, the HREELS data indicates that at 590K, the temperature required to form the ordered

monolayer, the α-pyridone is predominantly flat-lying. The combination of the STM, HREELS and LEED leads us to suggest the dimer based model for the structure of α-pyridone on Cu(110) shown in figure 5.7.

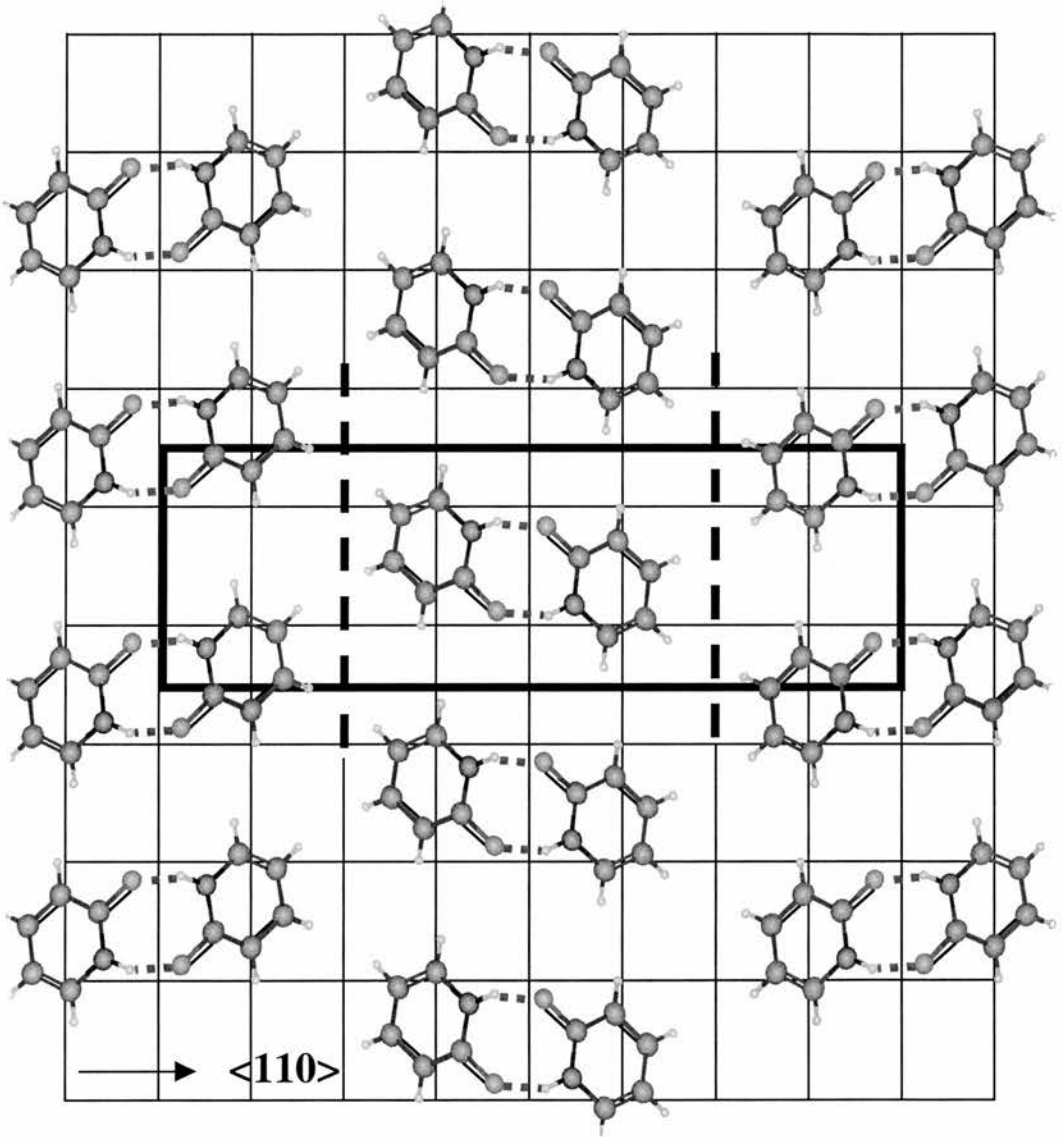

Fig 5.7 Proposed structural model of α-pyridone dimers on Cu(110) surface

To identify the stability of the multilayer and monolayer regimes and to confirm that the ordering of the surface structure is due to rearrangement

within the monolayer rather the desorption of a multilayer or some decomposition process, temperature programmed desorption was employed to explore the thermal stability. α-pyridone was adsorbed on the surface at low temperature, 150K, achieved by mounting the sample on a liquid nitrogen cooled backplate. A linear ramping programme controlled the sample temperature. The thermal desorption data is presented in figure 5.8, where it can be seen that, at all masses investigated, there are two distinct peaks. The intense feature at 310K, can be attributed to the removal of the multilayer. There is a second chemisorption peak at 870K, with almost the same cracking pattern as the multilayer, which is attributed to desorption of the monolayer. The molecular weight of α-pyridone is 95 and the parent ion along with fragments of m/e 27,28,52,42 can be observed in both peaks. *There is no desorption of any species below 850K* The presence of the parent ion in the high temperature peak also confirms that decomposition has not occurred at lower temperatures and that the species in the ordered (8×2)gg surface, formed at 590K, is indeed α-pyridone. A desorption temperature of 870K represents an extremely and surprisingly stable chemisorption system.

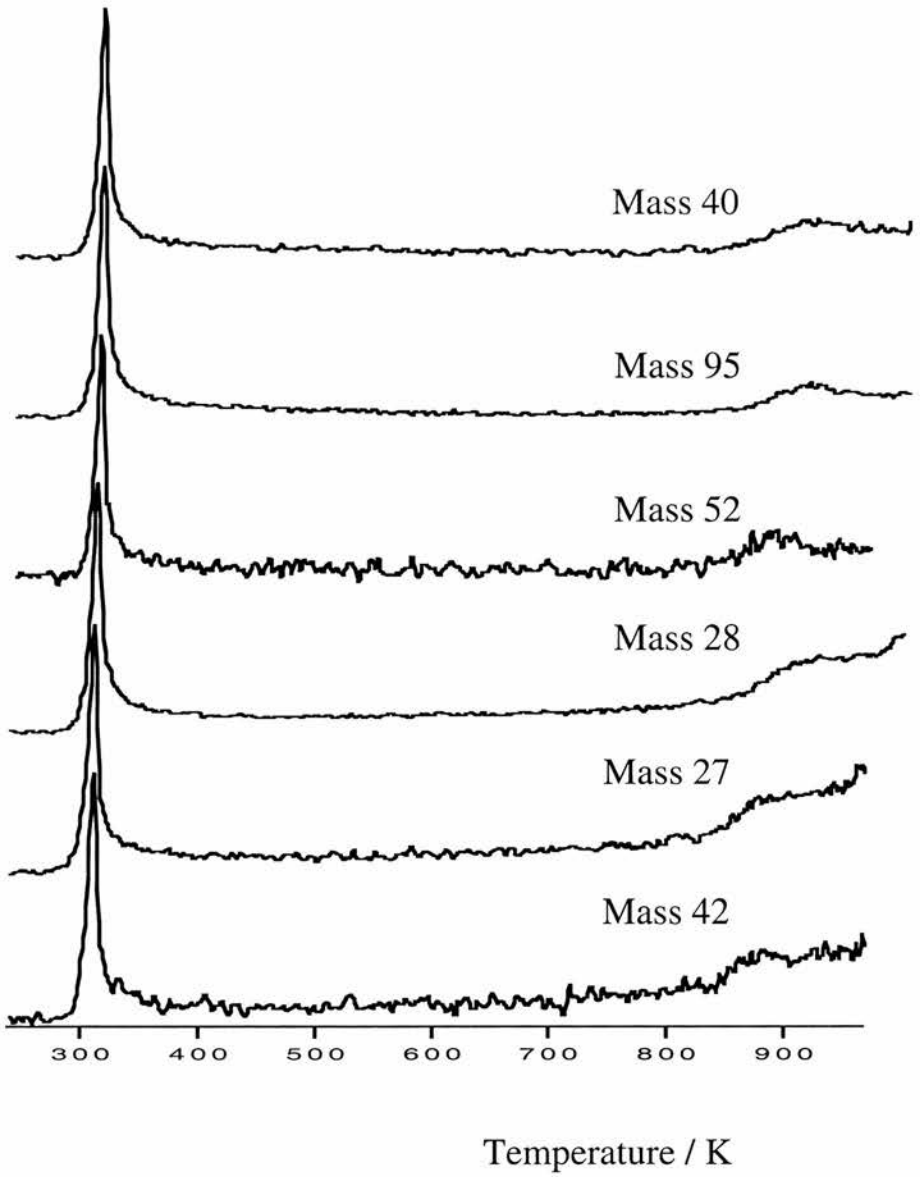

Fig 5.8 Temperature programmed desorption data for α-pyridone on Cu(110)

5.3 Discussion

Since the multilayer desorption occurs at 310K with a tail to lower temperatures, experiments carried out at 295K almost certainly correspond to a more strongly held, chemisorbed monolayer. Nevertheless LEED (and STM) indicate that

this initial structure is not well ordered and annealing at 590K is required to allow reorganisation to a two dimensionally ordered layer. HREELS confirm that the monolayer is not only disordered but also contains molecules, which are also highly tilted with respect to the surface plane or more likely have a range of orientations.

Between 590K and 870K, the surface consists of a (8x2)gg structure with large ordered domains and according to HREELS, the molecular plane lies parallel to the surface and the STM image is consistent with two dimer pairs per unit cell. GAUSSIAN 98 calculations confirm the stability of such dimers in the gas-phase and allow the vibrational modes to be assigned.

The high temperature of the monolayer desorption peak at 870K, suggests that the molecule surface bonding is particularly strong. There are three different bonding modes to the Cu(110) surface as a consequence of the flat-lying geometry. Firstly the de-localised π electron system parallel to the surface. There are also the lone pair electrons from the nitrogen. As a consequence of these two possibilities for bonding it was envisaged prior to the experiments that both upright and flatlying geometries were possible and tilting angles between these extremes. From the HREELS, the pre-annealed surface contains both flat-lying and upright species, thus at this stage bonding through the nitrogen is likely to be dominant. Likewise the oxygen can be involved in both inter – molecular hydrogen bonding and molecule –

surface bonding. This type of phase transition from upright to flat–lying orientations is the opposite of what is expected of a coverage dependent change whereby at low coverage the orientation is flat-lying and increasing the coverage causes the molecules to stand upright as a consequence of steric hindrance. The results of these experiments are differ in nature to the study conducted by Woodruff et al[5] who found that pyridine always adopted an up-right geometry even at low coverage. These measurements were taken using photoelectron diffraction and NEXAFS. They also found that no surface chemical reaction occurred

Under equilibrium conditions the gas-phase α - pyridone exists predominantly in the keto form, figure 5.2. The STM leads us to suggest that dimers form between the α - pyridone molecules on annealling to 590K. Thus we have two N-H...O=C bonds per dimer. *Ab initio* calculations performed using Gaussian 98 confirm that this type of dimer is stable, figure 5.5. The energy minimised structure does present differing lengths for the hydrogen bonds of 2.15A and 1.77A respectively and hence the dimer does not possess perfect C_2 symmetry. In the crystalline state α - pyridone exists exclusively. However in solution the tautomeric form depends on pH. The determination of the keto form has been determined in the crystalline state by the precise location of the Hydrogen in the hydrogen bond, as located by electron density (10). From the STM images this level of detail is not available. It is also

impossible to detect these subtle differences in the hydrogen bonds from surface vibrational spectroscopy because selection rules forbid the in plane modes to be measured. There is some information, however that can be gained, with regards to the tautomeric form, or indeed the hydrogen bonded state of the molecule. At room temperature the HREELS spectra shows a sharp peak at 1720cm^{-1} which has been assigned to C=O stretch. This would only be observable if the molecule was oriented at some tilt relative to the surface (in-plane mode). It can also be inferred that the molecule at this stage is in the keto form. Upon annealing, the peak decreases in intensity and eventually disappears at the temperature required for the formation of the ordered monolayer. This dramatic change would suggest that the C=O moiety is orienting itself flat-lying (to participate in hydrogen bonding) upon annealling. It does not indicate that the C=O is desorped as other peaks in the spectrum would be expected to appear due to the change in molecular structure. In conjunction with the growth of the out of plane-bending mode at 875cm^{-1} ,this development of the C=O peak confirms the model of hydrogen bonded, flat-lying molecules forming the (8×2)gg overlayer.

Table 5.1. Vibrational frequency assignment for HREELS data.

Frequency/cm^{-1}			Symmetry	Assignment
300K	590K annealed	Calculated		
248	242	189	A"	CH wag, CCN bend
302	342	401	A"	NH wag, CCO bend
421		454	A'	$\beta_{C=O}$
537	534	513	A"	Ring buckling,
600		556	A'	$\beta_{C=C}$, $\beta_{C=N}$
646		634	A'	$\beta_{C=N}$
741	738	724	A"	$\gamma_{N=H}$
786		782	A"	$\gamma_{C=H}$
	804	807	A"	γ_{C-H}
867		880	A"	$\gamma_{C=H}$
1021		1020	A'	ν_{C-C}
1102		1124	A'	ν_{C-C}
1147		1194	A'	β_{C-H}
1251		1254	A'	β_{C-H} , ν_{C-N}
1342	1349	1285	A'	β_{N-H}
1441	1440	1423	A'	β_{N-H} , ν_{C-N}
1472		1468	A'	β_{N-H}
1543		1508	A'	β_{C-H}
1610	1589	1593	A'	β_{C-H} , ν_{C-C}
3023			A'	ν_{C-H}
3040			A'	ν_{C-H}

References:

1. J. S. Sowerby, W. M. Heckl, *Origins of Life and Evolution of the Biosphere* **28**, 283-310 (1998).

2. N. J. Tao, Z. Shi, *Journal of Physical Chemistry* **98**, 1464 - 1471 (1994).

3. P. T. Chou, C. Y. Wei, F. T. Hung, *Journal of Physical Chemistry B* **101**, 9119-9126 (1997).

4. Frisch, M. J.; Trucks, G. W.; Schlegel, H. B.; Scuseria, G. E.; Robb, M. A.; Cheeseman, J. R.; Zakrzewski, V. G.; Montgomery, J. A.; Stratmann, R. E.; Burant, J. C.; Dapprich, S.; Millam, J. M.; Daniels, A. D.; Kudin, K. N.; Strain, M. C.; Farkas, O.; Tomasi, J.; Barone, V.; Cossi, M.; Cammi, R.; B. Mennucci; Pomelli, C.; Adamo, C.; Clifford, S.; Ochterski, J.; G. A. Petersson; Ayala, P. Y.; Cui, Q.; Morokuma, K.; Malick, D. K.; Rabuck, A. D.; Raghavachari, K.; Foresman, J. B.; Cioslowski, J.; Ortiz, J. V.; Stefanov, B. B.; Liu, G.; Liashenko, A.; Piskorz, P.; Komaromi, I.; Gomperts, R.; Martin, R. L.; Fox, D. J.; Keith, T.; Al-Laham, M. A.; Peng, C. Y.; Nanayakkara, A.; Gonzalez, C.; Challacombe, M.; Gill, P. M. W.; Johnson, B. G.; Chen, W.; Wong, M. W.; Andres, J. L.; Head-Gordon, M.; Replogle, E. S.; Pople, J. A. Gaussian 98W; Revision A.7 ed.; Gaussian, Inc.: Pittsburgh PA, 1998.

5. T. Giebel, O. Shcaff, R. Lindsay, P. Baumgartel, M. Polcik, A. M. Bradshaw, A. Koebbel, T. McCabe, M. Bridge, D.R. Lloyd, D.P. Woodruff,*Journal of Chemical Physics* **110**, 9666-9672 (1999).

6. H. W. Yang, B. M. Craven, *Acta Crystallographica Section B-Structural Science* **54**, 912-920 (1998).

CHAPTER 6. Cytosine and Thymine Adsorption of Cu(110)

6.1 Introduction

The current state of knowledge regarding the adsorption of pyrimidine bases on surfaces has progressed through the 90's due to the improvement of experimental techniques in particular *in situ* scanning tunnelling microscopy (STM) so as to explore solution deposition, seen as a more realistic model than single crystal UHV systems, for origins of life studies. Tao et al examined the solution adsorption of the nucleic bases on Au (111) single crystals[1]. They found that cytosine spontaneously adsorbed on the surface and formed highly ordered structures with lattice dimensions **a** = 10.5± 0.2Å, **b** = 9.5±0.2Å, γ = 102 ± 3° and oriented at 30± 3° with respect to the gold lattice. It was postulated that this structure forms a planar, two dimensional hydrogen bonded system, similar to the planar layers found in the bulk three dimensional crystals, with two molecules per unit cell. Thymine forms an oblique lattice **a** = 6.5± 0.2Å, **b** = 7.1±0.2Å and γ = 105 ± 5° on Au(111). This smaller unit cell only allows room for one molecule.

Roelfs et al proposed a model based on electrochemical STM results for the adsorption of Thymine on Au (111)[2]. There are three types of adsorption on the (111) surface, one of which is disordered. One of the states is composed of flatlying molecules, hydrogen bonded, and incommensurate with the surface. Another of the states is commensurate, formed by upright molecules coadsorbed with water and in which the thymine molecules are deprotonated. This structure is shown in fig.6.1.

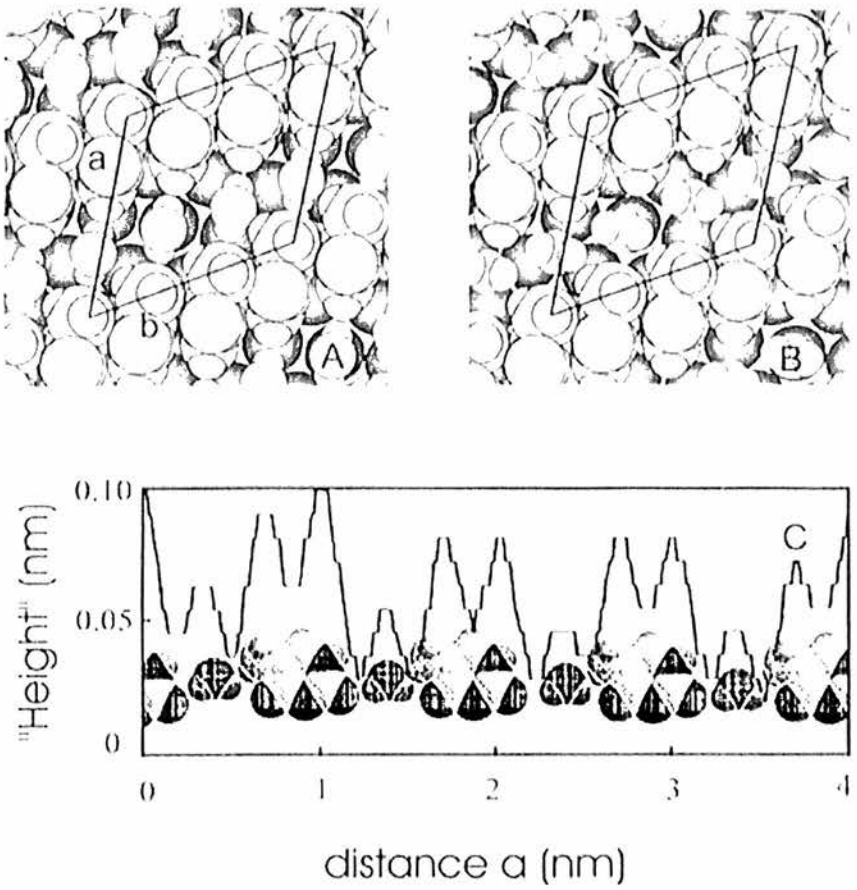

Fig. 6.1 Models for thymine adsorption. Balls represent the Au(111) surface. Thymine and water are represented by space fill molecules a) dioxotautomeric form b) enolic form c) cross section through the STM image and the model along the a axis [2]

Another investigation into the structure of adlayers of cytosine formed on Au(111) by Wandlowski et al found that the molecule co-ordinated through one of the nitrogens to the gold atom[3]. The lattice formed had unit cell dimensions **a** = 7.3± 0.3A, **b** = 8.7±0.3A and $\gamma = 50° \pm 5°$. When comparing the different two dimensional

structures, in terms of lattice cell dimensions and packing arrangements, it is important to consider the structure of the three dimensional crystals. This data, obtained by X-ray diffraction is presented in Table 6.1

Table 6.1 Three dimensional crystal structures for the pyrimidine bases

Base	Lattice Dimensions /Å	Description
cytosine[4]	a = 13.041 b=9.494 c = 3.815	Orthorhombic Hydrogen bonded network
thymine[5]	a = 12.87 b=6.83 c = 6.70 $\beta = 105°$	Monoclinic Hydrogen bonded network π stacking between layers

In this chapter the behaviour of the nucleic acid bases cytosine and thymine adsorbed onto Cu(110), fig. 6.2 will be described

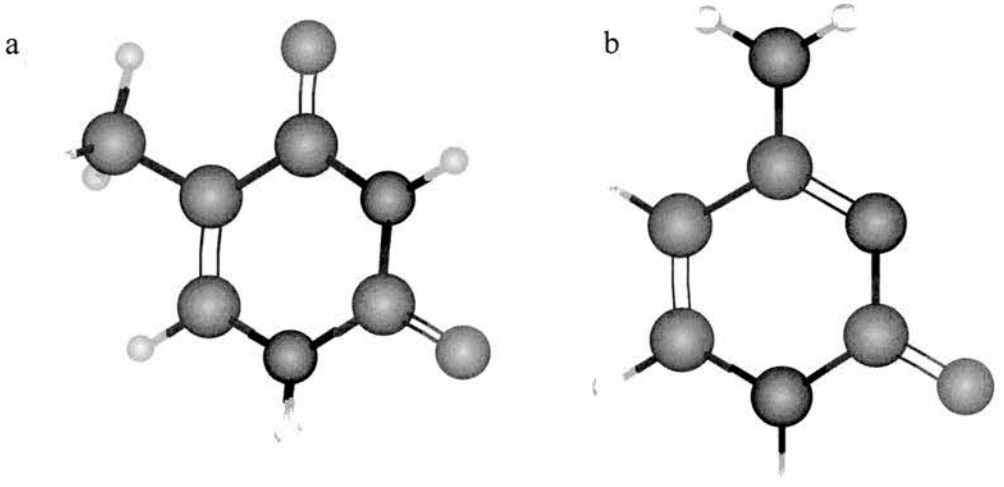

Fig. 6.2 a) Thymine b) Cytosine

The aforementioned studies were performed in the liquid phase and this restricts both the resolution of the STM and also the control, in terms of surface coverage of the adsorption process. Hence phase transitions that might be temperature and coverage dependent (as in the case of amino-benzoic acid), see chapter 4, could be explored under UHV conditions. It is with this improved "accuracy" and "visibility" that these systems will be studied in the proceeding chapter.

6.2 Experimental

Cytosine or thymine was introduced into the vacuum chamber by means of a seperately pumped doser attached via a gate valve through which the powder sample is evaporated at a temperature of 370K . Upon dosing and increase in pressure from 5×10^{-10} to 1×10^{-9} mbar was realised. Mass spectroscopy was used to monitor the sample pressure during dosing. The Cu (110) single crystals were cleaned by cycles of Argon ion bombardment (typically, 500 eV, 20 $\mu A\ cm^{-2}$) and annealing to 800K

6.3 Cytosine results

The first aim was to achieve low coverage of the adsorbate on the surface. Dosing cytosine onto the Cu(110) held at 390K for 10 minutes caused the (1×1) LEED pattern of the clean surface to fade. Upon annealing to 370K, a sharp (6×6) LEED pattern appeared fig. 6.3. It was then judged that a well ordered structure had formed, estimated by the time of dosing to be a low coverage regime, and so the system was ready for further examination. The sample was then transferred under vacuum, to the STM chamber. STM tips were made of, electrochemically etched

tungsten. The most striking features of the STM images are the ordered structures that form well defined islands, fig. 6.4. Coverage of the surface by the islands is estimated to be 40% and so is confirmed to be a relatively low coverage system. The structure within the islands was found to be (6×6) in agreement with the LEED results.

The ordered overlayer within the (6×6) unit cell contains twelve approximately elliptical features, fig. 6.5. Dimensions of the ellipses were measured to be 4Å for the major axis and 3Å for the minor. Within a large unit cell area of 322 $Å^2$, the features are arranged in zigzags, adjacent chains being slightly out of phase with each other.

A longer dosing time resulted in saturation coverage of the monolayer. For this purpose it was found that 30 minutes dosing was sufficient to obtain complete coverage of the surface as observed by STM. Again the (6×6) structure is obvious but this time there are no islands, just domains of the ordered overlayer, fig. 6.6. On closer inspection a subtle difference is apparent in comparison with the low coverage (6×6) structure, despite the fact that the dimensions of the ellipse like features are the same for both coverages. However, the difference is hard to describe completely as the middle row between two more "prominent" rows is considerably less distinct.

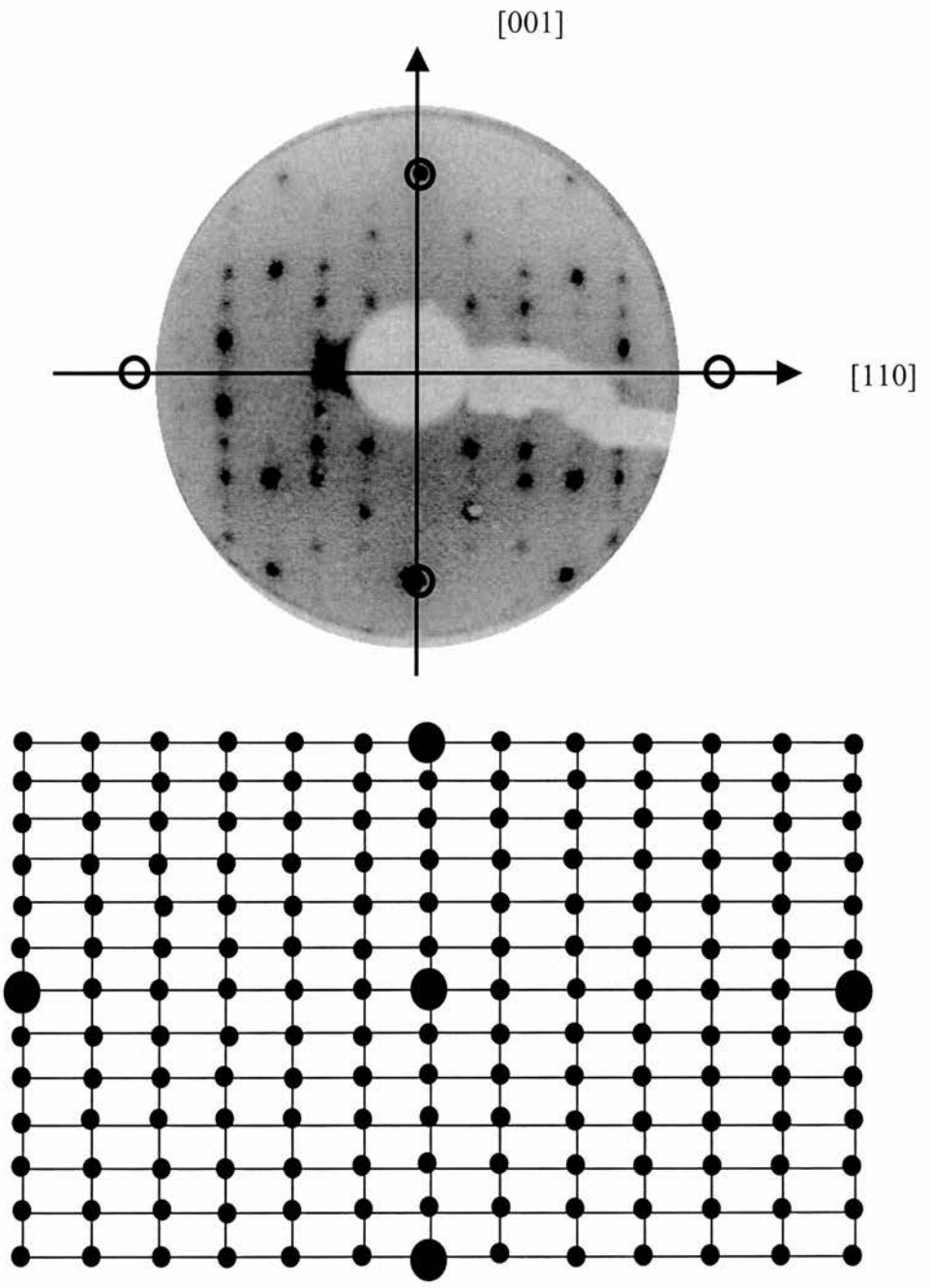

Fig. 6.3 LEED pattern of cytosine/Cu(110) annealed to 370K, 41e. Circles denote the positions of integral order spots. b) Idealised (6×6) LEED pattern

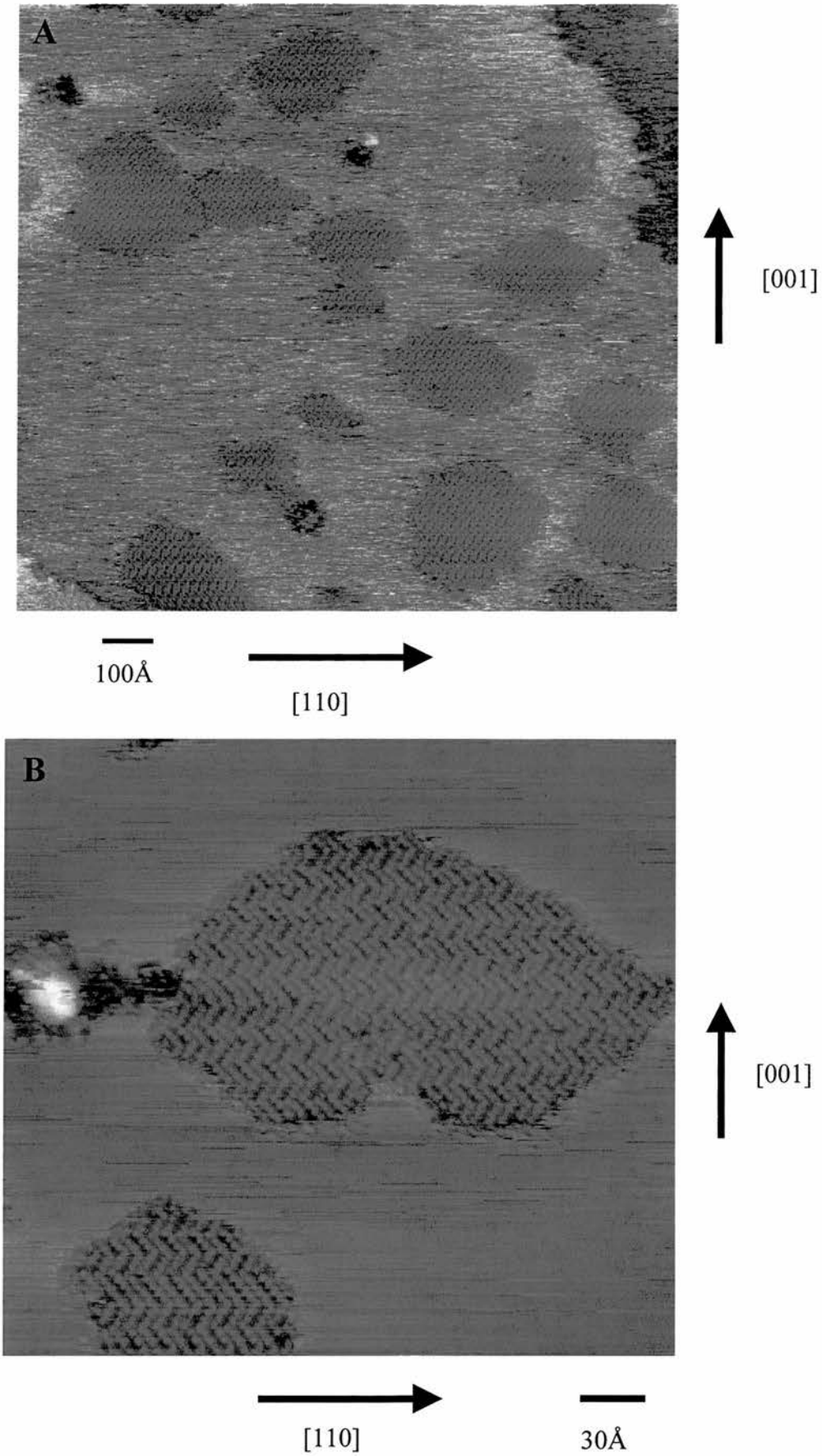

Fig. 6.4 STM images in the low coverage regime presenting islands of ordered (6×6) structure. Tunnelling conditions; A -0.14V, 0.75nA, B 1.4V, 0.34nA.

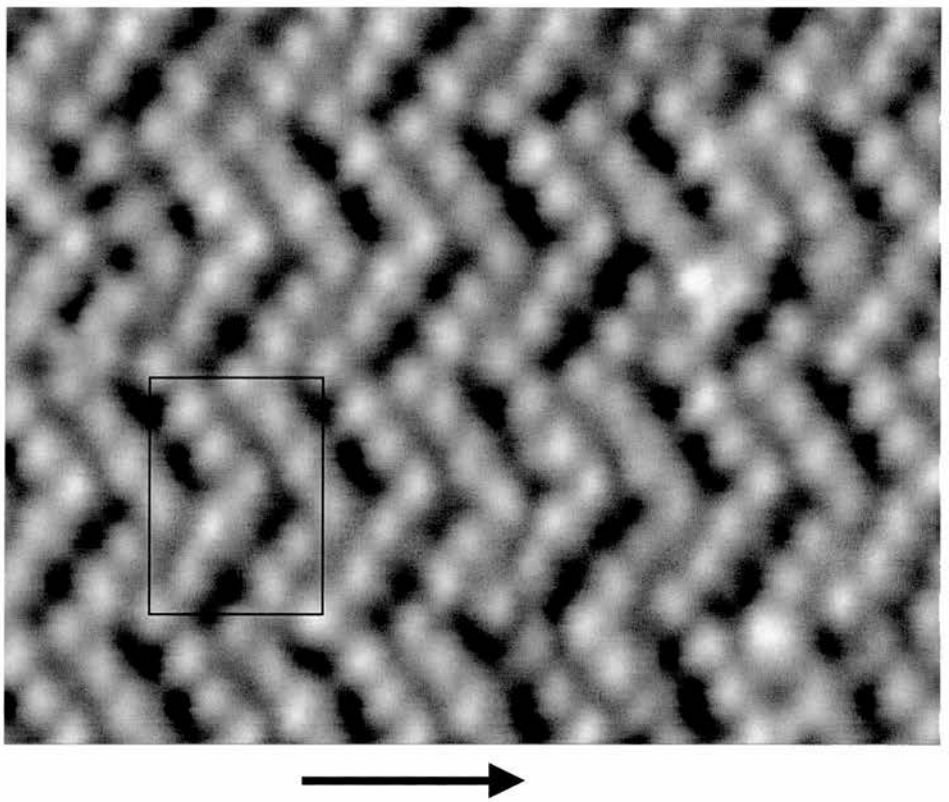

Fig. 6.5 STM image (80×65Å), sample bias -1.3V, current 0.8nA of cytosine/Cu(110) at low surface coverage showing the(6×6) unit cell containing 12 molecules.

Upon further heating to 480K, a sharp (6×2)gg LEED pattern appeared The presence of one glide plane is indicated by the absence of (2n+1)/2 order spots in the <100> direction and a second, perpendicular glide plane is indicated by an absence of (2n+1)/6 order spots in the <001> direction, fig. 6.8. The presence of two glide planes limits the possible configurations of the molecules within the unit cell, based on LEED data alone. The size of the unit cell is 110.5Å^2. After annealing to 480K, quite a different structure is found under examination with STM to that found before annealing. The (6×2)gg unit cell can be recognised, fig. 6.9, containing six features

which can be seen to consist of four within the cell and four at the middle of the edges. The largest width of each feature is uniform throughout the unitcell, with a dimension of 2.6Å although the ones at the middle of the unit cell edges as drawn in fig. 6.7 are rather less distinct than the others.

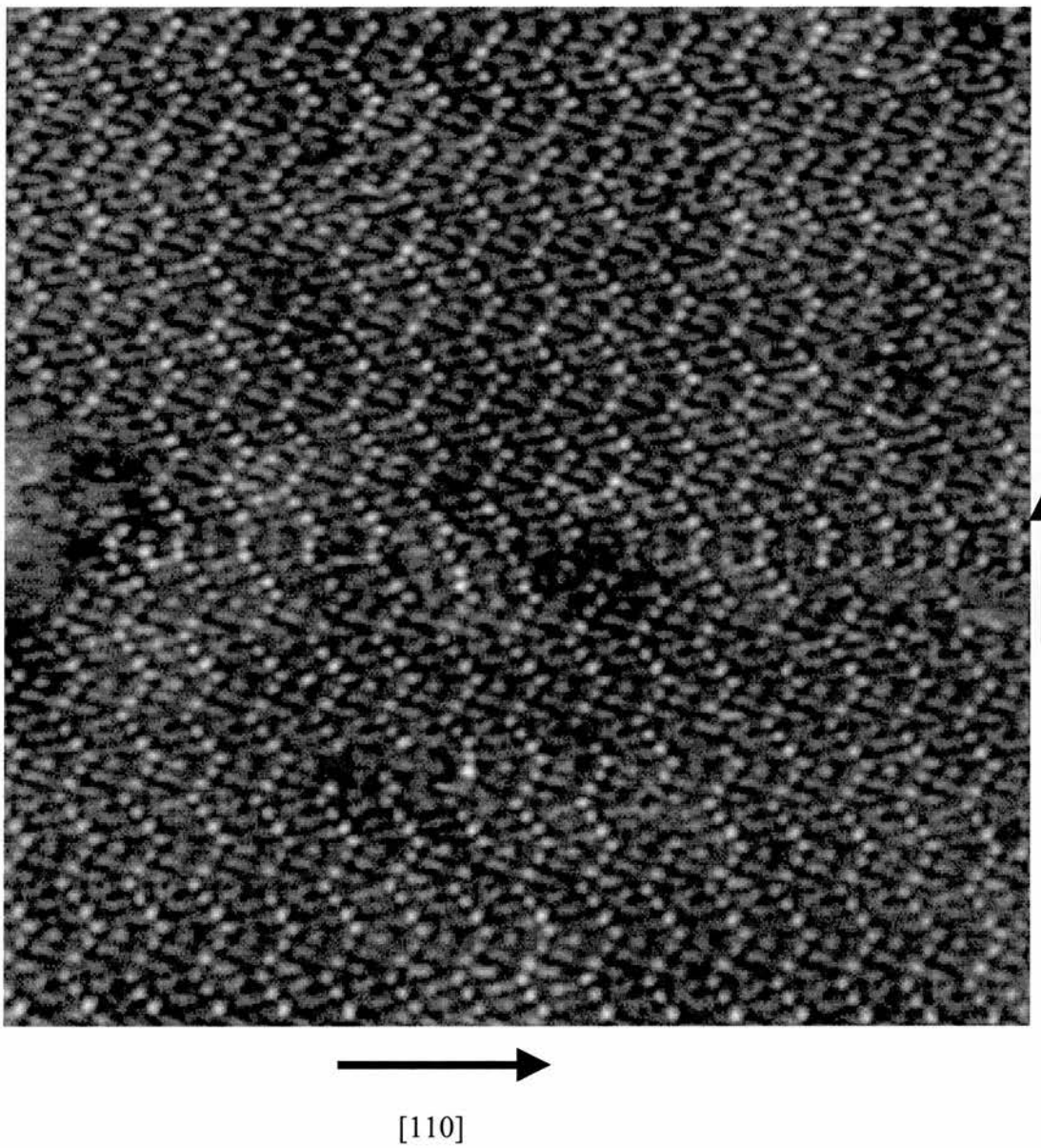

Fig. 6.6 An STM image (26×26nm), sample bias -0.07V, current 0.3nA of an ordered region of thehigh coverage (6×6) structure of cytosine on Cu(110).

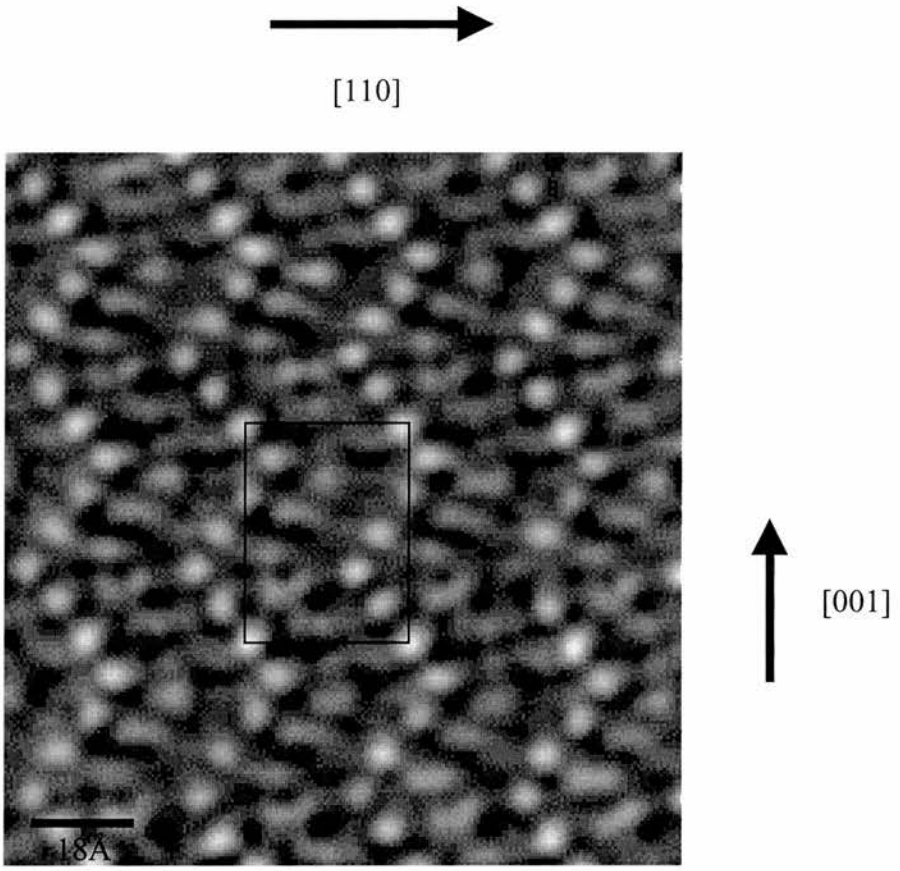

Fig. 6.7 STM image (60Å×70Å) of the high coverage showing the (6×6) unit cell of cytosine/Cu(110)

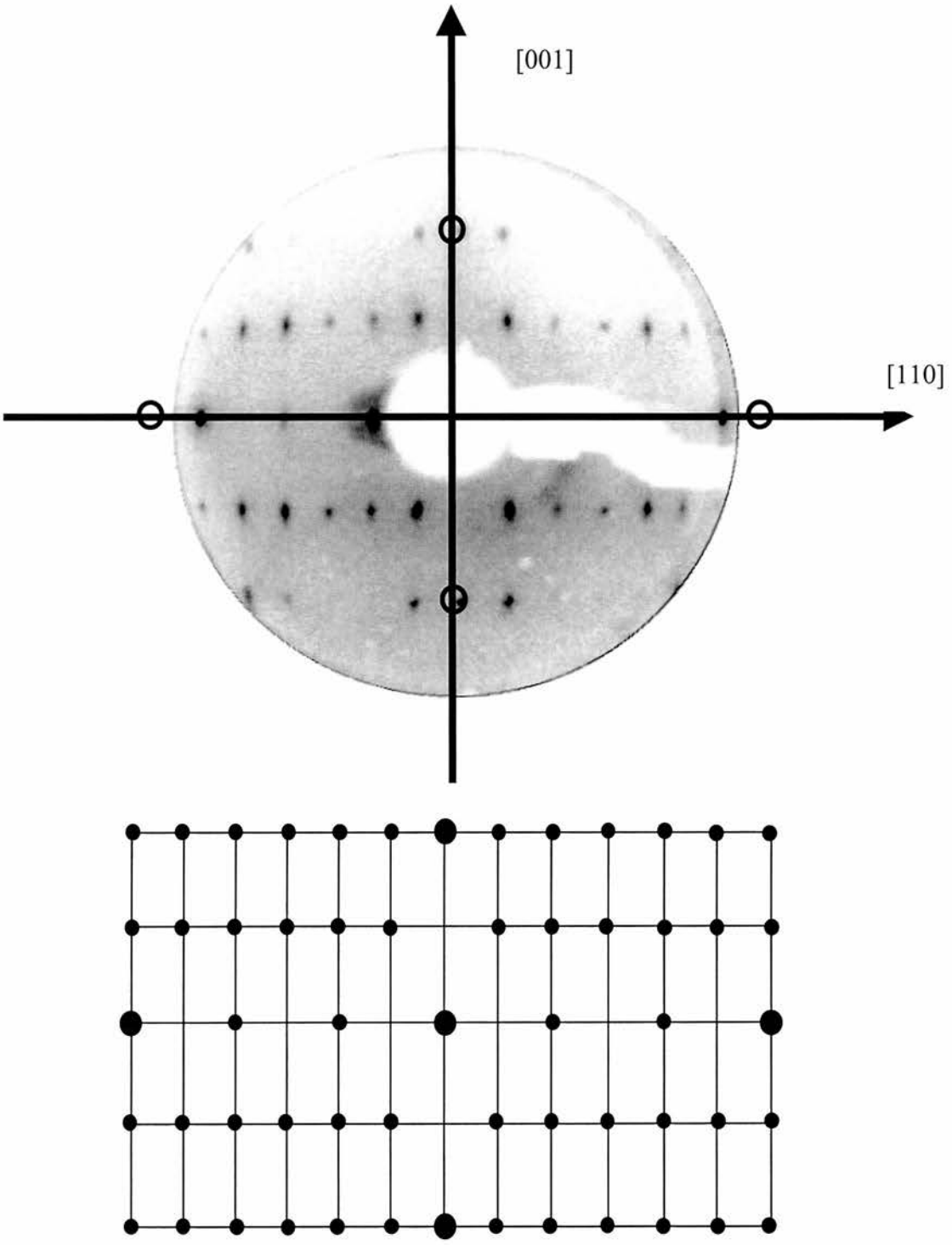

Fig. 6.8 a)LEED pattern of cytosine/Cu(110) annealed to 480K, 50eV b) Idealised (6×2)gg LEED pattern

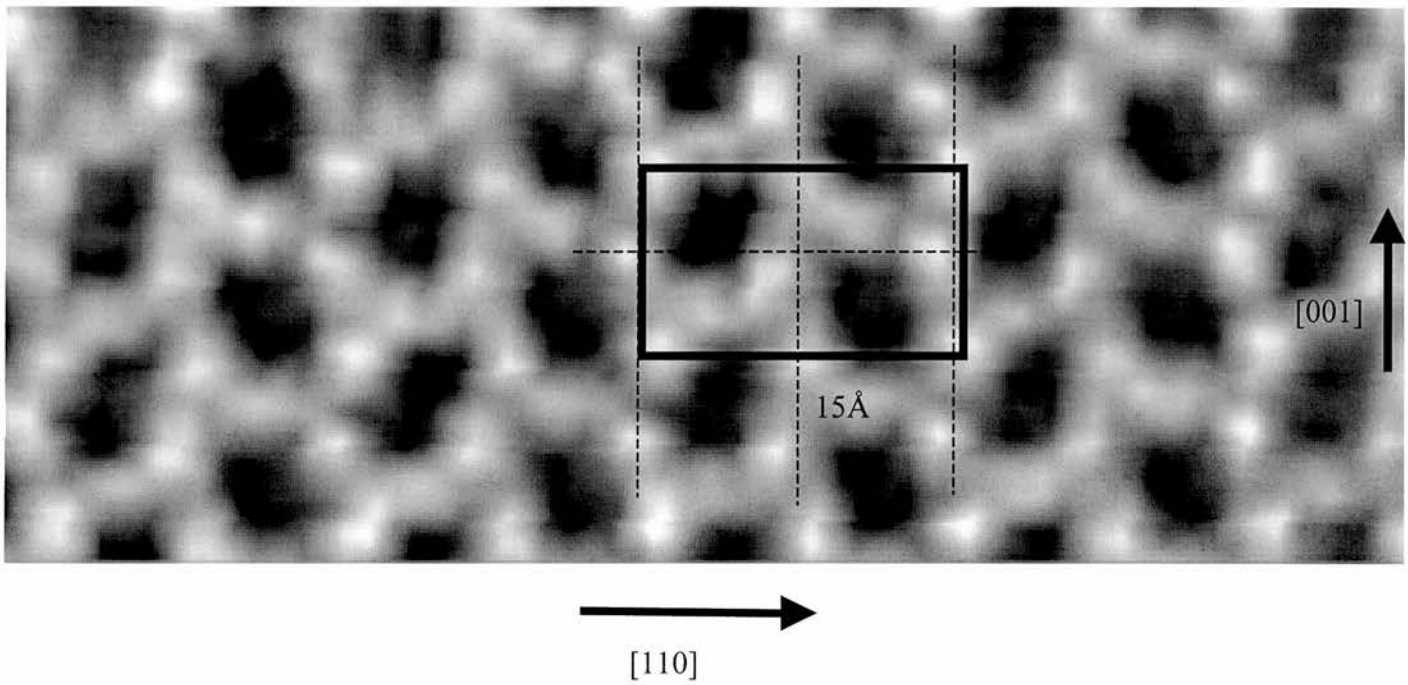

Fig 6.9 STM image (60Å×22Å) of the (6×2)gg cytosine/Cu(110) overlayer with unit cell superimposed showing the glide lines. Sample bias is -0.1V and feedback current is 5.14nA

A series of HREELS spectra were taken in order to observe the initial orientation of the molecules on the surface and the changes which could be induced through the initially deposited monolayer and the (6×2)gg overlayers, fig. 6.9. At room temperature, the surface structure is not ordered and there is no corresponding LEED pattern. Through the series of spectra upon annealing, fig. 6.10, there is a development of the peaks at 1566cm^{-1} and 1610cm^{-1}. Another evolution is that of the intensities of the two adjacent peaks at 1359cm^{-1} and 1450cm^{-1} which start with the room temperature structure with the higher wavenumber mode dominating and

upon increasing the temperature the two peaks equalise in intensity. At the temperature at which the (6×2)gg forms, the most intense peak is that at 1610 cm^{-1} which is more than four times more intense than the neighbouring 1566 cm^{-1}, the next strongest vibration.

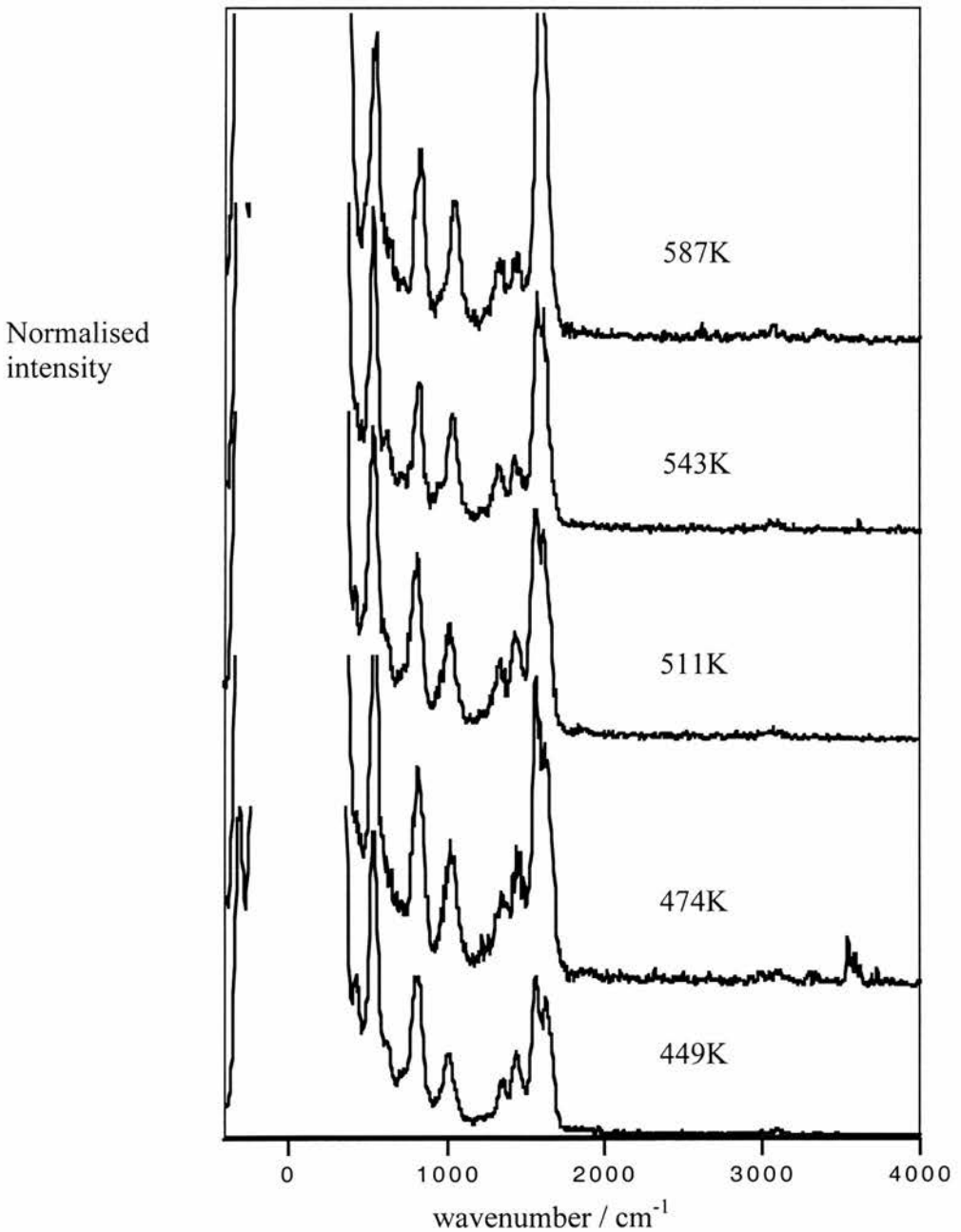

Fig 6.10 HREELS Spectra of cytosine/Cu(110) upon annealling

Thermal desorption curves were taken by linearly ramping the sample temperature from 200K to 900K and monitoring the desorption by a mass spectrometer. The spectrum, fig. 6.11, shows evidence of a small peak at 400K which could be attributed to the desorption of the multilayer peak formed at low temperature. Although the multilayer peak is small, the experiment was repeated several times to confirm the peak. Only the m/e of 27 which could be the HCN fragment exhibited a distinct peak. This monolayer desorption was found to begin at 640K.

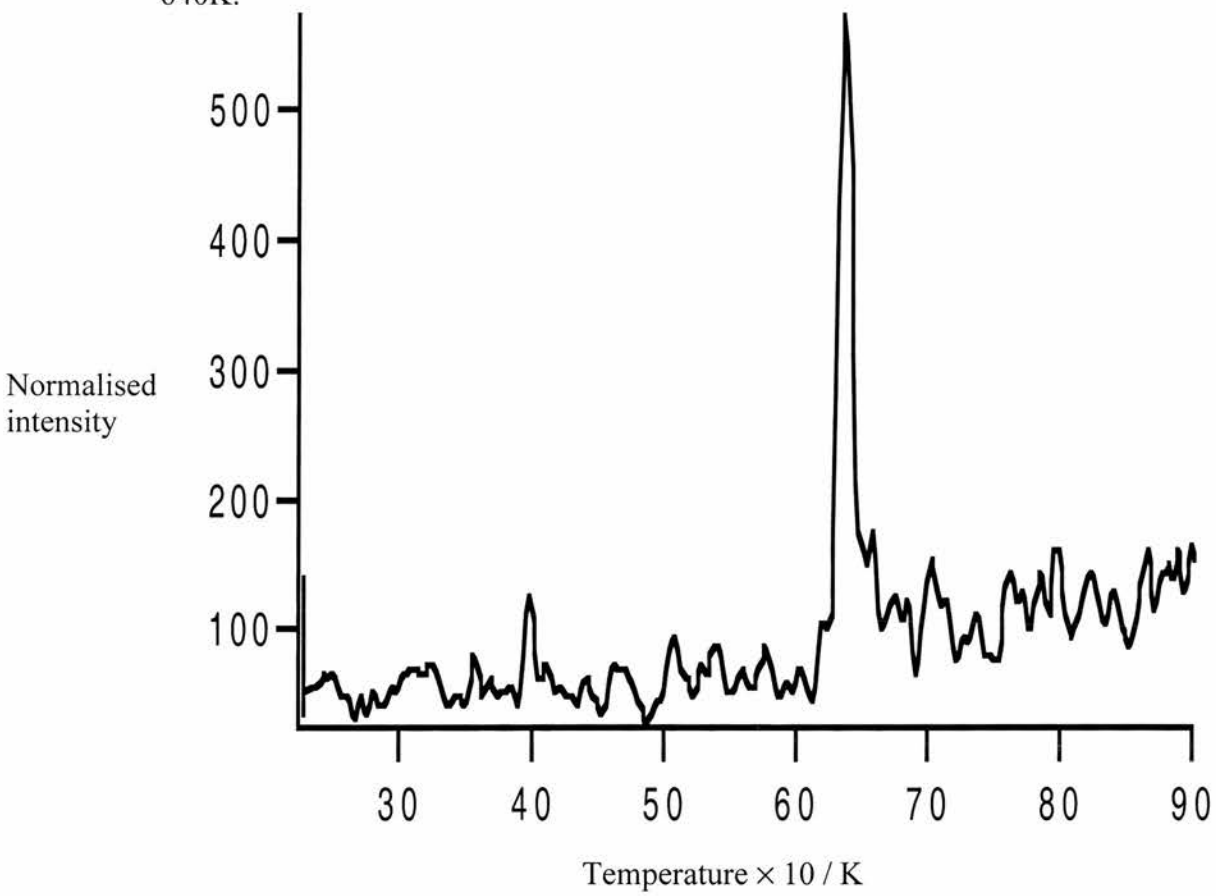

Fig 6.11 TPD Spectrum of cytosine adsorbed onto Cu(110). The mass recorded is 27, probably corresponding to HCN

6.4 Discussion

It is suggested that the (6×6) out of phase structure obtained in islands at sub-mono-layer coverage of cytosine can be considered to consist of upright / tilted cytosine molecules, 12 within a unit cell, fig.6.12. There are two pieces of evidence that are consistent with the molecules being in an upright orientation. The first is the HREELS spectra. Here there are some weak out of plane modes but the overall picture is dominated by in-plane bands. Band assignments and a comparison of calculated and experimental frequencies are given in table 6.2. Calculations are based on *ab initio*, Gaussian 98 calculations of the free molecule. Especially dominant are the CH_2 in plane and C=0 modes. The band at 1611cm^{-1} has been assigned to the NH_2 scissoring vibration. The calculated intensity for this mode is very strong as is the case with the experimental results. It can be suggested therefore that the NH_2 group remains intact and in an upright orientation. From the spectrum, it is also evident that the carboxyl group remains in its entirety as the C=O bend at 534cm^{-1} has an intensity 4/5 of the magnitude of the NH_2 scissoring. There is some evidence for deprotonation of the nitrogen as the NH bending modes are significantly weaker than their calculated equivalents and even significantly weaker than the C=O bend. Secondly in favour of upright molecules, STM measurements show that the unit cell is not large enough to accommodate twelve planar molecules. The (6×6) unit cell has an area of 331 Å^2. The molecular footprints, are 18.8 Å^2 and 46.4 Å^2 respectively for the upright and planar case, based on the van der Waals' radii of the dimensions within the molecular plane and a π stacked diameter of 3.4Å perpendicular to the molecular plane, fig 6.13. Measurement of the features

themselves reveals an ellipse with major and minor axis of 4 and 3Å respectively. Of course this may not be the whole molecule that the STM tip is imaging since, the tunnelling may occur through only part of the entity. Adjacent zigzags are translated alternately by the vectors (3, -1) and (3+1) in relation to the substrate lattice.

Similarly the (6×6) phase produced at higher coverages consists of the same number of upright molecules. It is proposed that the cytosine molecules are π stacked along the rows of the zig zag. This would make sense as the measured distance between features in the lattice is comparable to a π stacking distance and hence also the interplanar spacing in the three dimensional crystal. Turning our attention to the (6×2) gg structure we again propose a structure with upright molecules, fig 6.14.

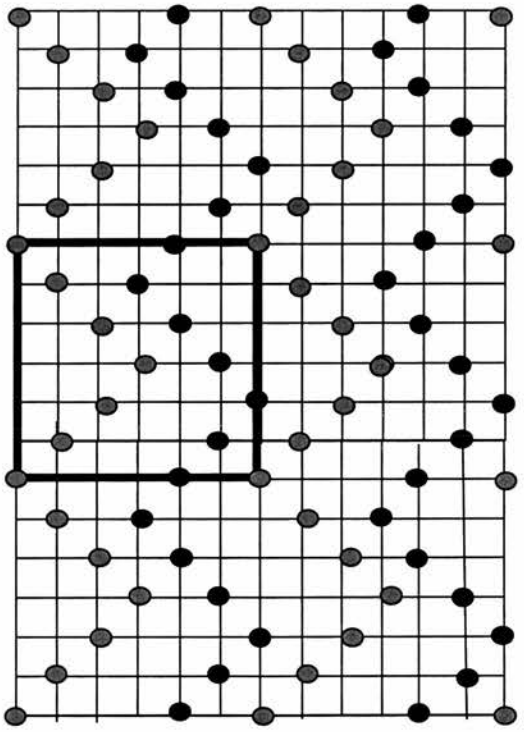

Fig. 6.12 Low coverage (6×6) organisation of cytosine molecules on Cu(110) illustrating the zig-zag arrangement of cytosine molecules within the unit cell.

Table 6.2 Frequency assignments for Cytosine

Calculated vibrational frequencies/cm-1	Scaled frequencies (90%)/cm-1	Calculated IR intensities /kmmol-1	Experimental frequencies/cm-1 Room temperature	Assignment
-204	-184	219.0		γ NH_2 wag
139	125	1.5		ring buckling
203	183	13.2		ring buckling/C- NH_2 wag
357	321	3.8	314	C=O bend/ C- NH_2 bend
394	355	18.9		ring buckling/γC- H wag
530	477	3.5	534	C=O bend/ NH_2 rock
541	487	5.0		NH2 twist/γC- H wag/γN- H wag
542	488	2.3		ring distortion
577	520	1.9		ring distortion
629	566	69.5	638	γN- H wag
732	659	25.2		γC- H wag/γN- H wag
761	685	20.5		γC- H wag/ring buckling
770	693	4.0		ring distortion/C-N stretch
770	693	35.9		γ C=O wag/ring buckling
919	827	3.6	830	ring distortion/ NH_2 rock/C-H bend
958	862	0.3	946	γC- H wag
987	888	0.0		ring distortion/C-H bend
1082	974	40.6	1038	NH_2 rock
1129	1016	4.2	1166	C-H bend/ N-H bend
1217	1095	42.0		N-H bend/C-H bend
1266	1139	32.8	1322	C-N stretch/ C-H bend/ N-H bend
1365	1229	32.4		C-H bend/ N-H bend
1445	1301	80.8	1434	N-H bend
1518	1366	98.5		C-H bend/ NH_2 scissors
1575	1418	161.0	1566	C-H bend
1639	1475	158.6	1610	NH_2 scissors
1705	1535	460.8		C-C stretch/C-H bend/N-H bend
1818	1636	617.8		C=O stretch/N-H bend

3209	2888	4.4		out-of-phase C-H stretch
3236	2912	4.0		in-phase C-H stretch
3625	3263	103.3		symmetric NH_2 stretch
3636	3272	53.5		ring N-H stretch
3769	3392	48.5	-	asymmetric NH_2 stretch

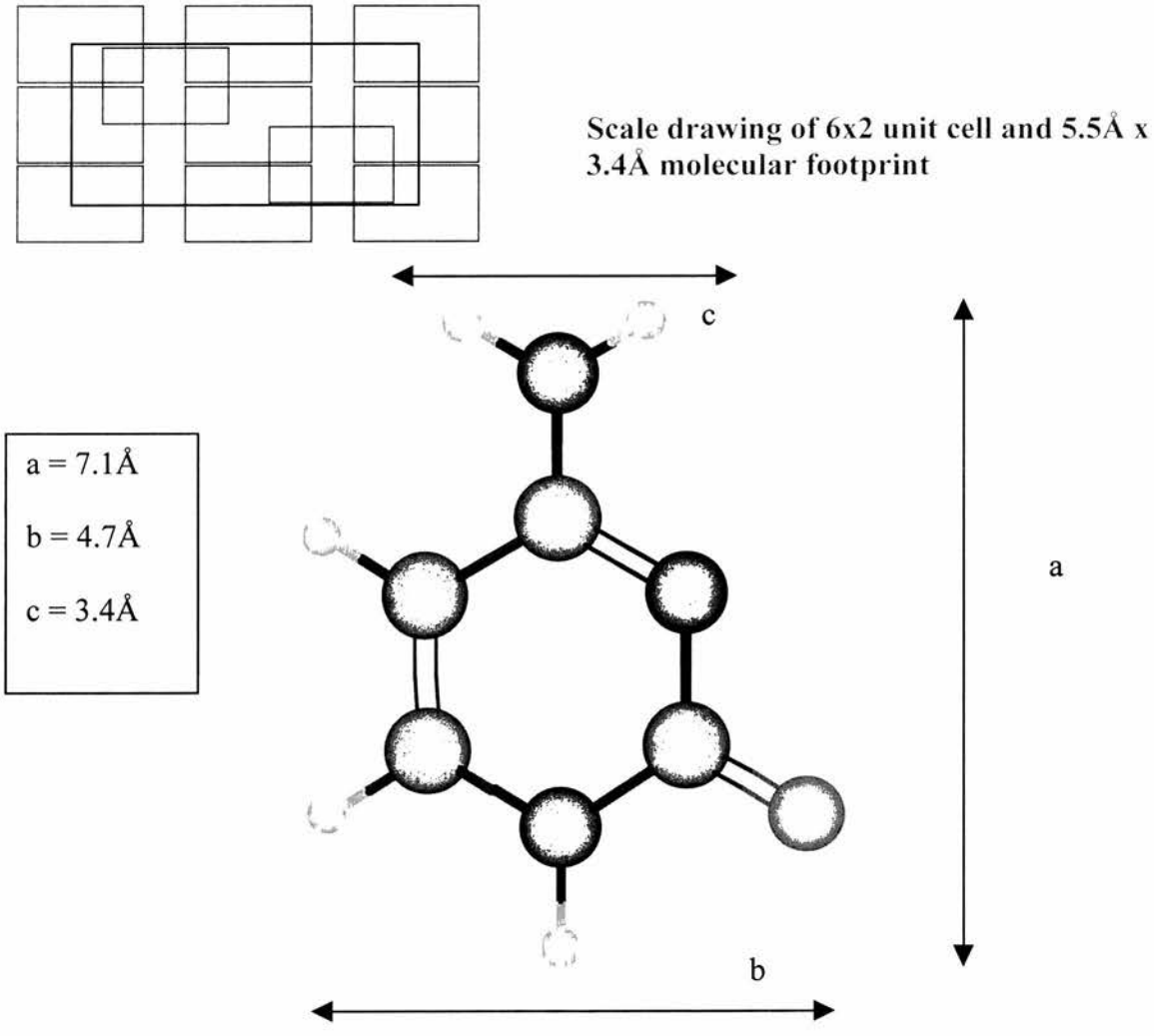

Fig 6.13 Molecular footprints of cytosine excluding Van der Waals radii

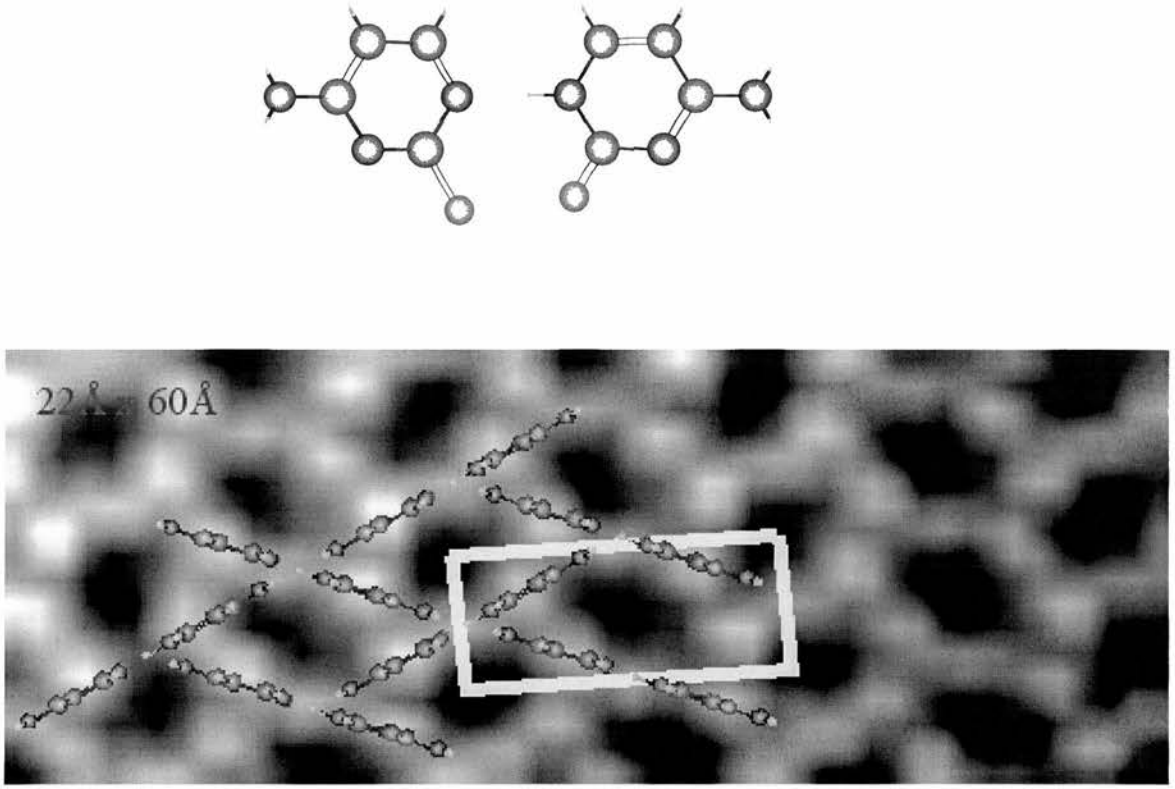

Fig 6.14 High resolution image of cytosine with model superimpoosed

The symmetry requirements of the two glide planes impose the conditions that the molecules should be head to tail in the rows along the [100], fig 6.14. These π stacked zig zags also have another feature which has a slightly different shape and dimensions. This we propose is the dimerisation between adjacent zig zags. In this model it is suggested that one of a pair of cytosine molecules is deprotonated, fig 6.15. There is some evidence for this from the HREELS data, in the very low intensity of the N-H in-plane modes.The dimerisation of these molecules allows a delocalisation of the negative charge. Thus the dimer bonds to the copper substrate through the oxygen atoms of both molecules.

It is also of note that both the (6×6)gg and (6×2)gg have the same area density the first being with 12 molecules/ unit cell and the second with 4 molecules/unit cell

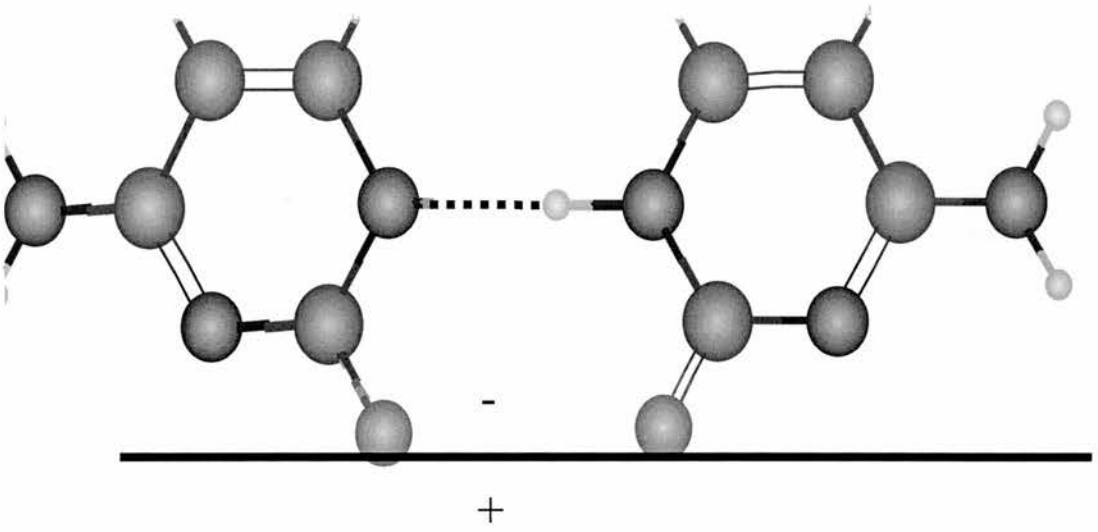

Fig 6.15 Proposed mode of adsorption to the copper surface illustrating the formation of delocalised negative charge, and hence bonding through the oxygen atoms to the copper surface

6.5 Thymine Results

Dosing Thymine at 390K for 30 minutes caused the (1×1) LEED pattern of the clean Cu(110) surface to fade. Upon annealing to 500K a sharp (6×2)gg LEED pattern appeared The presence of one glide plane is indicated by the absence of (2n+1)/2 order spots in the [001] direction and a second, perpendicular glide plane is indicated by an absence of (2n+1)/6 order spots in the [110] direction, Fig. 6.16. The

presence of two glide planes limits the number of molecules and their possible configurations within the unit cell, based on LEED data alone. As with the case of α - pyridone and cytosine the size of the (6×2) unit cell is 110.5Å^2

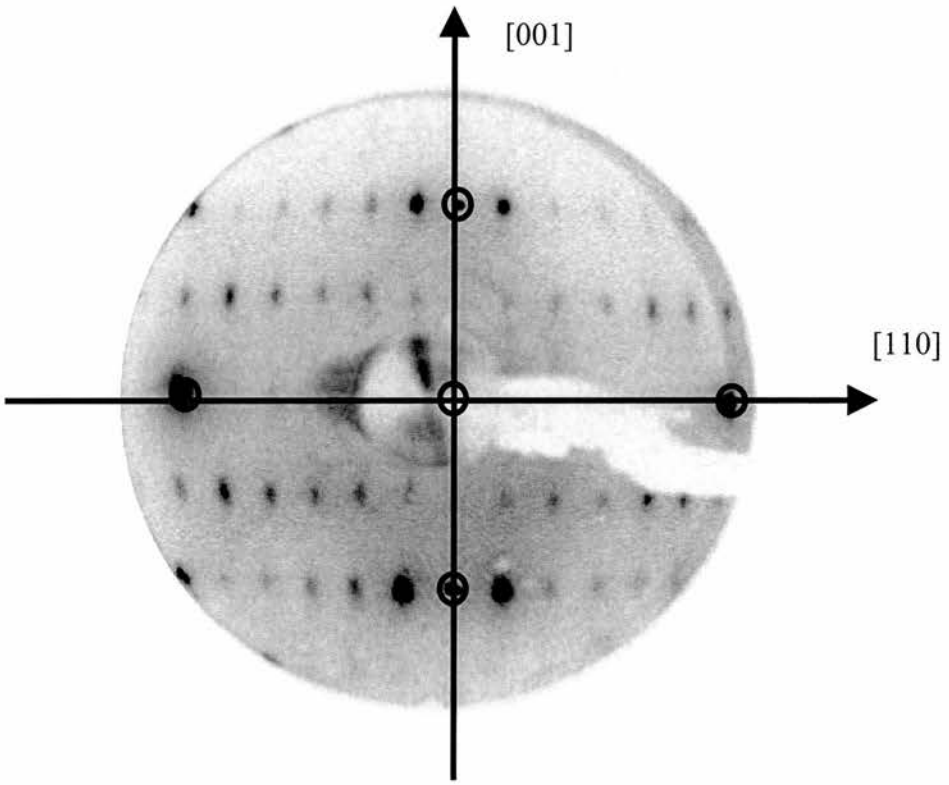

Fig. 6.16 LEED Pattern of thymine on Cu(110) annealed to 500K, 50eV

A large area STM image shows that the (6×2)gg seems to be high coverage and that the molecules do indeed form well ordered monolayers. There appears to be a small amount of a second phase present and this is thought to be contamination emanating from by products in the chemical synthesis of thymine, fig 6.17. On the larger scale the unit cell can be recognised, fig 6.18. This entity contains 6 features which as, drawn, can be seen to consist of three internal, 4 corner and 4 edge

features. The largest width of each feature is uniform throughout the unit cell, at a dimension of 2.6 Å

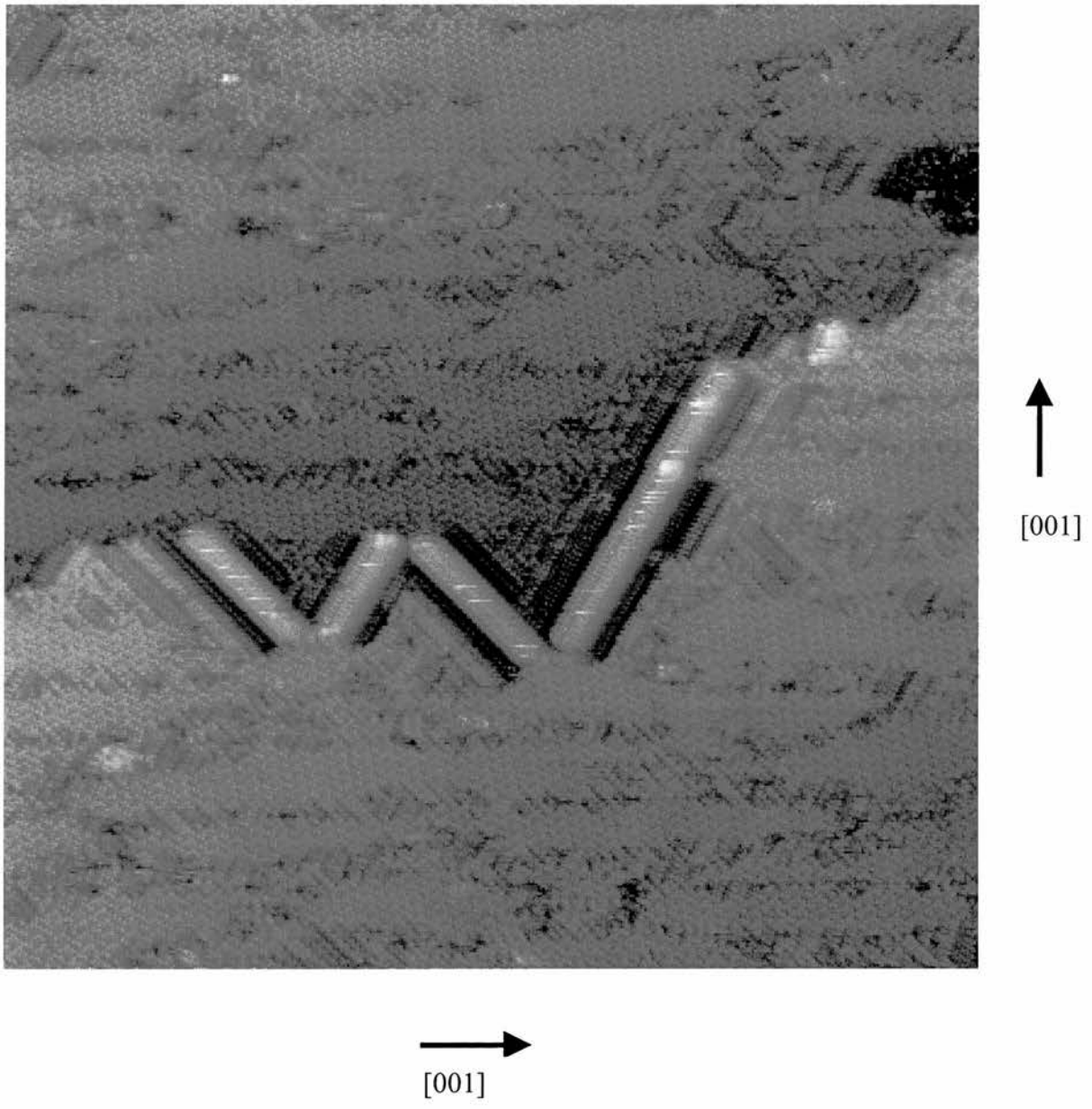

Fig 6.17 STM image (680Å×680Å) of thymine/Cu(110),voltage -1.37V, current 0.43nA . The large V shaped features are thought to be contamination as a consequence of by products in the production route of thymine.

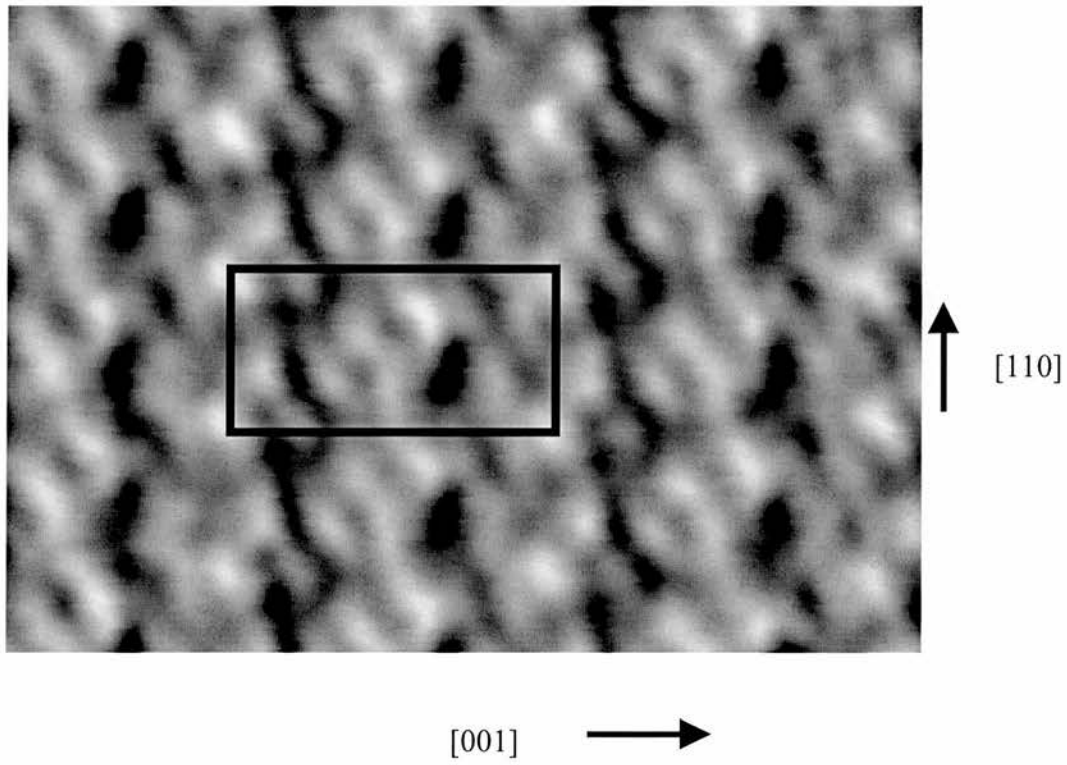

Fig. 6.18 STM image (45Å ×32Å) of thymine/Cu(110) showing the (6×2) unit cell. Voltage -1.48V, current 1.00nA

A series of HREELS spectra, fig. 6.19,were taken in order to observe the initial orientation of the molecules on the surface and the change that could be induced upon annealing. Band assignments and a comparison of calculated and experimental frequencies are given in table 6.3. Calculations are based on ab initio, Gaussian 98 calculations of the free molecule A distinctive evolution is apparent. This evolution is dominated by the development of three peaks assigned to in-plane

modes, two of which are characteristic of CH_3, and hence are characteristic of thymine as opposed to the other bases. The1544 cm^{-1} band which becomes extremely sharp and strong is attributed to the in-plane CH_3 bending mode and the 1445 cm^{-1} is characterisic of the out of phase C-H bending mode. Also apparent is the growth of the 1221 cm^{-1} band which is assigned to in-plane C-H stretching vibrations of the ring.

From the STM images it can be considered that there are 5 sub-units, one at each corner, and one central one related by reflection and thus satisfying the glide plane requirements. It is plausible that the sub-units are made up of two thymine molecules. Each one appearing as a bright oval like feature adjacent to a thinner, shorter blob. The bright feature could by the ring and the thinner one the CH group. Thus two molecules form a complex, one with the CH group tilted, the other with this group more flat lying.

Again as with the case of cytosine, only the HCN peak can be detected by TPD, fig. 6.20, which concludes a temperature of 700K for a monolayer desorption peak.

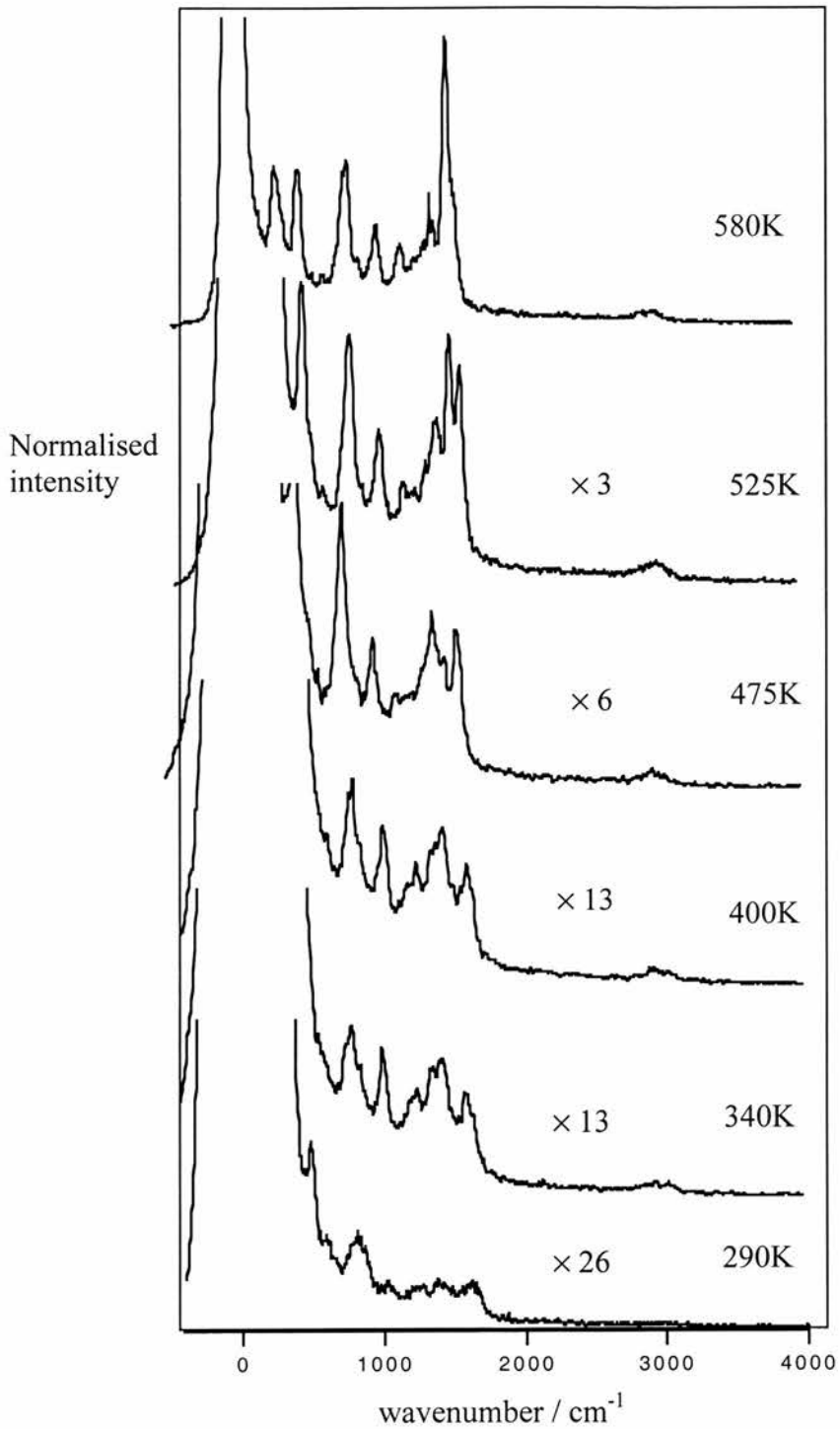

Fig. 6.19 HREELS spectra of thymine on Cu(110) upon annealing

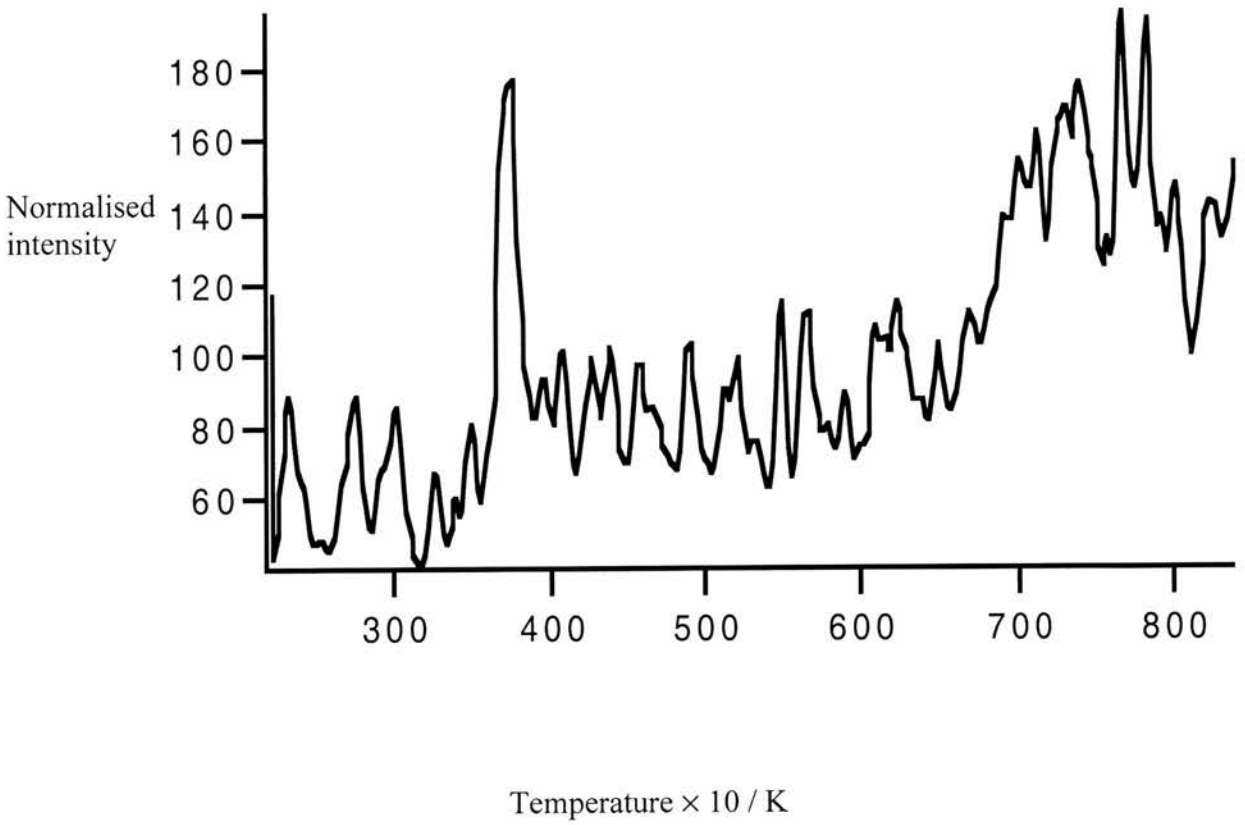

Fig. 6.20 TPD spectrum of thymine on Cu (110). Mass 27 is shown which is assumed to be characteristic of HCN. Both physisorption and chemisorption peaks are apparent

Table 6.3 Frequency assignments for thymine

Calculated vibrational frequencies/cm-1	Scaled frequencies (90%)/cm-1	Calculated IR intensities /kmmol-1	Experimental frequencies/cm-1 Room temperature	Assignment
-135	-122	0.0		CH_3 rotation
122	114	0.2		C-C wag / C=O wag
179	167	2.9		ring buckling/ C=O wag
300	279	3.5		CH_3 rock
325	302	1.9	330	CH_3 rock/ C-C wag
389	361	22.0		C=O bend
421	392	9.2		ring buckling
468	435	19.2		ring distortion
552	513	6.8	495	C=O bend/ring distortion
611	569	0.5		ring distortion/N-H bend/C-H bend
658	612	97.5	669	γN-H wag
732	681	4.6		γN-H wag/ring buckling
741	689	4.8		ring distortion
765	712	28.7		γN-H wag/ring buckling
813	756	3.6		ring distortion
836	778	206.2	843	γN-H wag/ring buckling
938	872	9.7	918	γC-H wag
977	909	2.3		CH_3 bend/N-H bend
1046	973	14.3	1052	CH_3 bend/N-H bend
1185	1102	20.0		C-N stretch/N-H bend
1226	1141	109.8	1221	N-H bend/C-H bend
1246	1159	9.9		C-C stretch/CH_3 bend
1395	1297	40.4		C-H bend/N-H bend
1427	1327	12.9		N-H bend/C-H bend
1441	1341	90.1	1445	N-H bend
1462	1360	10.1		CH_3 bend
1504	1399	25.9		N-H bend/CH_3 umbrella
1537	1429	12.5		CH_3 umbrella
1551	1442	11.5		CH_3 bend
1694	1575	35.4	1544	C=O stretch,/N-H bend
1721	1600	392		C=O stretch,/N-H bend

1767	1643	663		C=O stretch,/N-H bend
3049	2836	30.3		CH_3 symmetric stretch

Calculated vibrational frequencies/cm-1	Scaled frequencies (90%)/cm-1	Calculated IR intensities /kmmol-1	Experimental frequencies/cm-1 Room temperature	Assignment
3106	2889	21.5		CH_3 asymmetric stretch
3160	2939	0.8		CH_3 asymmetric stretch
3236	2912			C-H ring stretch
3620	3367	56.1		N-H stretch
3657	3401	85.0		N-H stretch

6.6 Thymine Discussion

Each feature of the STM image can asigned to an upright/tilted molecule, rather than to a planar orientation from simple coverage considerations. The total area of the unit cell is 110.5Å^2 and the molecular foot print of a planar molecule would be 39.0Å^2, Fig. 6.21. Thus for four molecules the planar arrangement would require a unit cell area of at least 156Å^2

Measurement of the features from the STM image allows four molecules per unit cell. There are two rows of molecules per unit cell and the upright/tilted molecules are π stacked along the (100) direction. This π stacking is a consequence of the head tails arrangement of molecules along a <110> row in a column and the alternate orientation of neighbour molecules, as regards the position of the methyl group gives rise to the glide plane symmetry. Added to this the distance between molecules in a row can be estimated to be 3.5Å which is an appropriate value for π stacking. The heads to tails arrangement has also been proposed as a possibility for the adsorption of thymine on Au(111) in solution by Nichols et al, fig 6.22. They

also go on to propose that the thymine is vertically adsorbed bonding to the gold with an oxygen and deprotonated nitrogen atoms.

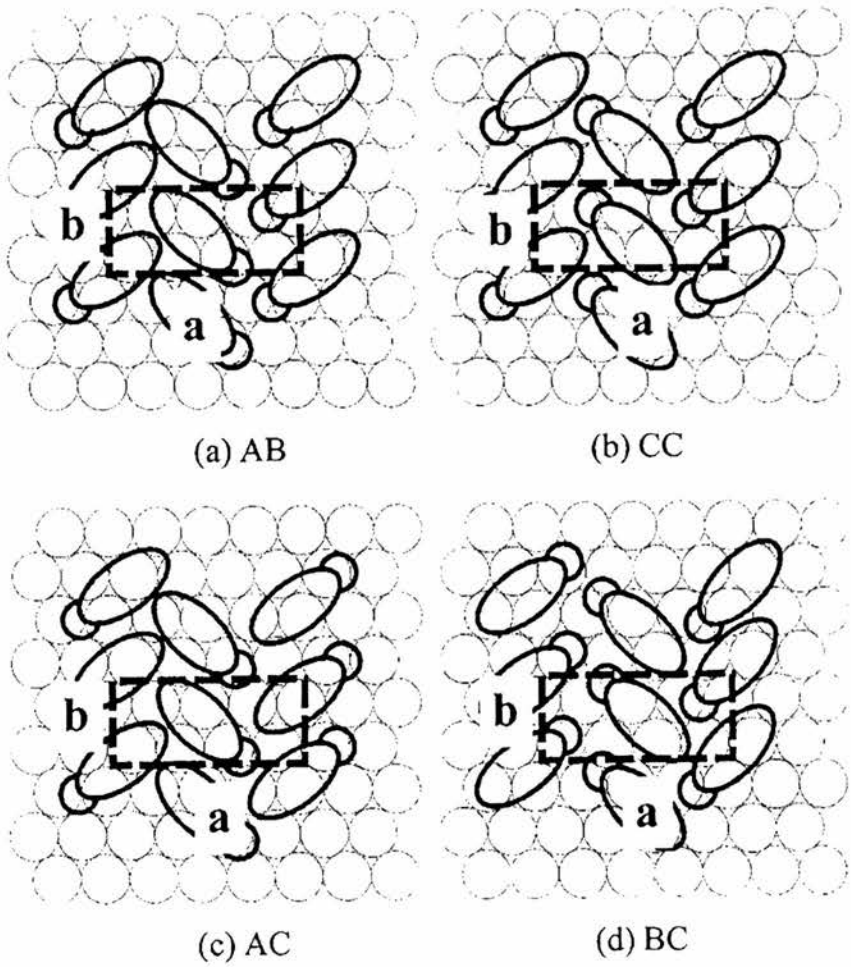

Fig. 6.21 Illustration showing some possible different configurations of thymine. Different stacking possibilities are considered: "head to head", "tail to tail", "tail to head" [2]

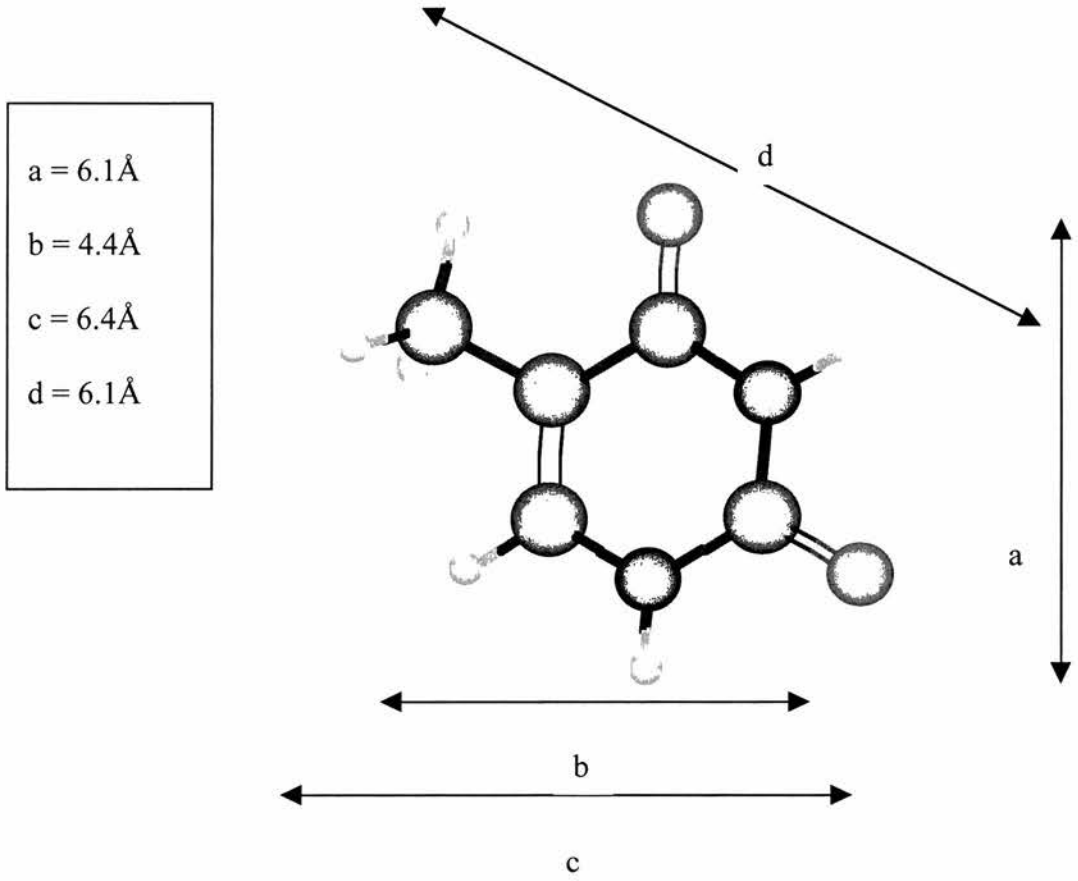

Fig 6.22 Molecular footprints of thymine excluding Van der Waals radii

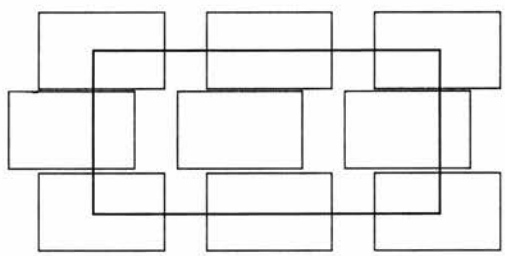

Fig 6.23 Scale drawing of (6×2) unit cell and 5.4Å×3.4Å molecular footprint which illustrates the feasibility of the thymine molecules being able to fit the unit cell in an upright manner

The model consists of four molecules per unit cell with two rows per unit cell. The upright or slightly tilted thymine molecules are π stacked along the [100] direction. This is not closely related to the three dimensional crystal structure as determined by x-ray diffraction which proposes that the aromatic rings are not directly above each other, i.e. no π stacking.

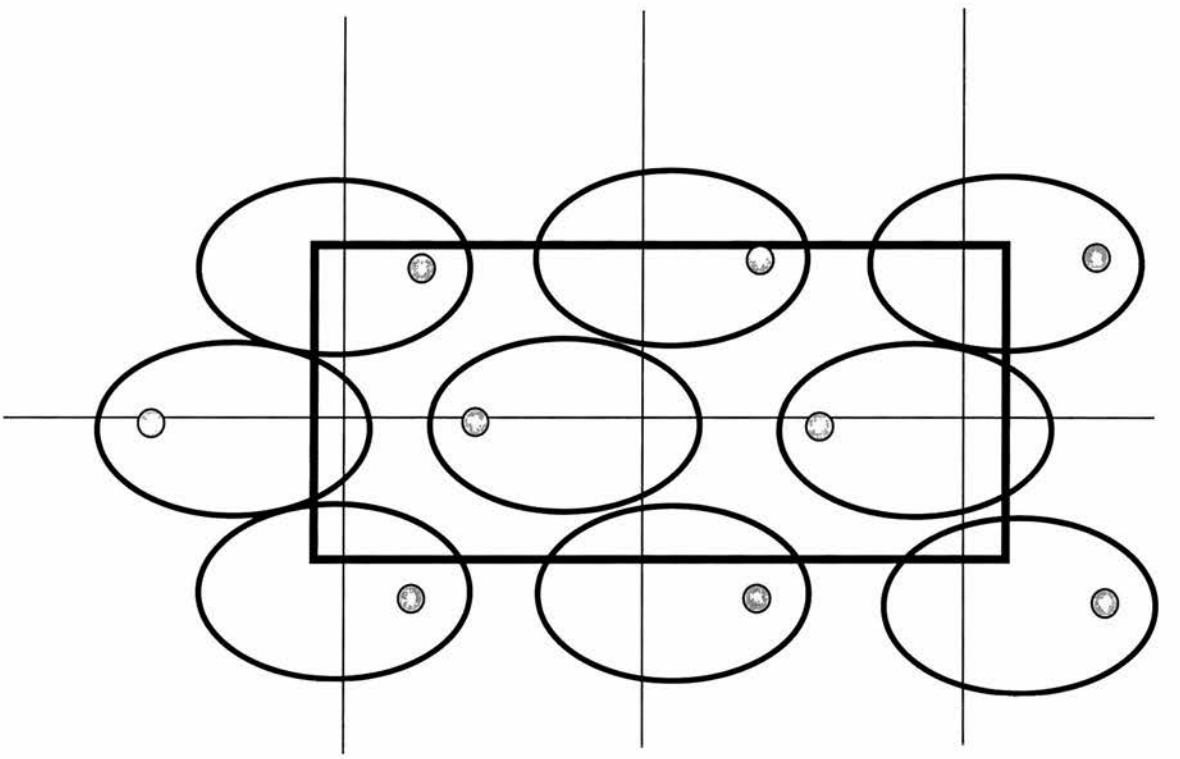

Fig 6.24 Head to tail arrangement of molecules along rows in [100] direction as required by glide plane symmetry with four molecules belonging to a unit cell

For this upright model to be correct it must be possible to see the in-plane modes characteristic of thymine in the HREELS spectra. This is the case with the in plane mode at 1445cm^{-1}, the CH_3 bend, being particularly strong, with an intensity relative to the C=O bend far larger than the same ratio for the calculated data. The CH_3 rock at 330 cm^{-1} and the C=O bend at 495 cm^{-1} have the same strong intensity. All of the aforementioned peaks grow in intensity upon annealing reaching the maximum in terms of sharpness and intensity at the temperature at which the (6×2)gg structure appears in the LEED. Thus it can be suggested that initially the monolayer is disordered and the formation of an ordered structure is almost exclusively based on a reordering of the surface, not a reorientation as primarily the intensities of the peaks change, not so much the positions.In the model, fig.6.25 the rows of upright molecules are seperated and with alternate CH_3 groups pointing inwards or outwards. Therefore it can be concluded that the molecule should have some tilted orientation when the 6×2 gg structure is formed as there is a corresponding presence of strong in plane and out of plane modes.Another possibility which could be considered on the evidence of the spectra alone is that a combination of flat-lying molecules and upright molecules co exist and hence contribute to out-of-plane and in-plane features respectively.

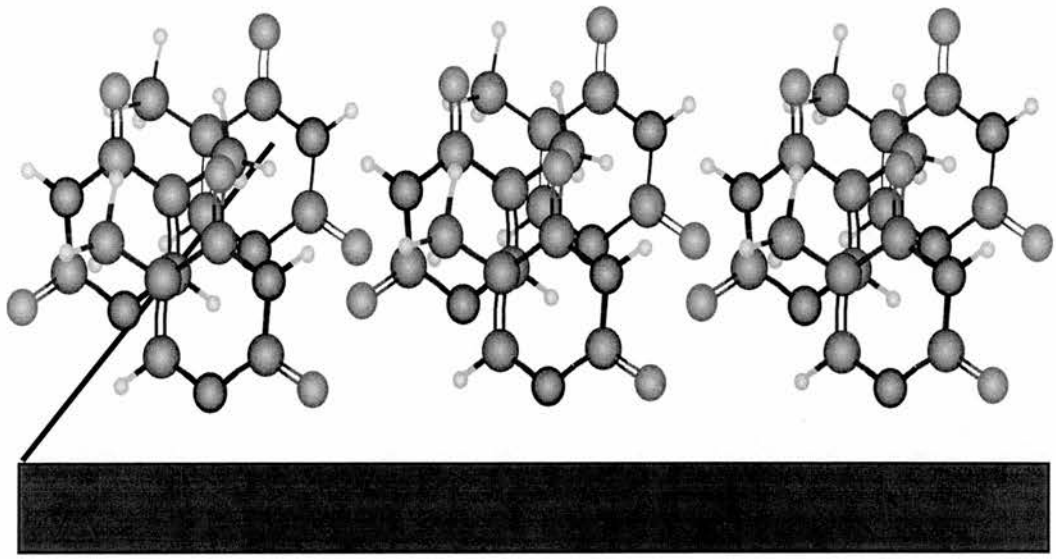

Fig 6.25 Model of thymine molecules for the (6×2)gg structure. Alternate molecules within a π stacked row have either the CH_3 group pointing inwards or outwards respectively

References:

1. Tao, N.J., DeRose, J.A. & Lindsay, S.M. *Journal of physical chemistry* **97**, 910 (1993).

2. Roelfs, B., *et al. Journal of physical chemistry B* **101**, 754 (2001).

3. Wandlowski, T., Lampner, D. & Lindsay, S.M. *Journal of Electroanalytical Chemistry* **404**, 215-226 (1996).

4. Barker, D.L. & Marsh, M.E. *Acta crystallographica* **17**, 1581 (1964).

5. Ozeki, K., Sakabe, N. & Tanaka, J. *Acta crystallographica* **B25**, 1038 (1969).

CHAPTER 7 . Self-assembly of Adenine on Cu(110) Surfaces

7.1 Introduction

Previous studies of the self-assembly of adenine have focused on graphite or Cu(111) surfaces under either liquid or ultra high vacuum conditions. On graphite surfaces [1-4], with the scanning tunneling microscopy (STM), atomic force microscopy (AFM) and/or low energy electron diffraction (LEED), a commensurate rectangular unit cell with two glide planes, containing 4 adenine molecules, was found, while on the Cu(111) surface [5,6], STM studies show only short range ordering into a parallel one dimensional chain or a two dimensional honeycomb structure at 70K. In those studies, relying on the topographic height measured from STM images, it was assumed that the molecule is lying flat with the molecular plane parallel to the substrate. Of course, the variation of tip height in an STM image, that is required to maintain constant conductivity at the particular tunnelling conditions, may not be suitable for determining the physical dimension of the adsorbed molecule. Therefore, other surface spectroscopic methods should be introduced in order to confirm the molecular orientation. Vibrational studies are ideally suited to the determination of molecular orientation. Both semi-empirical PM3 [6] and molecular mechanics simulations [1] have been applied to some possible models with extended hydrogen bonding in the adenine layer. However, none of these models can satisfactorily fit the STM observations.

The free, planar adenine molecule has a single mirror plane, which gives rise to a C_s point group, and may be regarded as a prochiral molecule. Thus, once it is adsorbed onto a solid surface in such a way that breaks the molecular mirror plane, the adsorbed species becomes chiral. Since there is necessarily a racemic mixture of enantiomers on the surface, the two dimensional unit cell formed by these chiral adsorbates could be either achiral, by mixing molecules of opposite chirality within the unit cell, or chiral with separated distinct enantiomer domains. The unit cell of adenine on graphite [1] has p2gg symmetry, thus the unit cell is achiral and must contain an equal number of enantiomeric molecules within the unit cell. In this study, the Cu(110) surface was used, which has a lower symmetry, C_{2v}. It is shown that the adsorption of adenine on these surfaces forms enantiomerically separated domains at various surface coverages, in which there is no mirror (glide) plane symmetry within the unit cell. Moreover, the direction of the adenine rows is strictly correlated with the chirality of the molecules forming the row.

Although the vibrational spectrum of the free adenine molecule has been extensively studied by Fourier transformed infrared spectroscopy (FTIR) [7,8], Raman [8,9] and inelastic neutron scattering [9], there is no report of the vibrational analysis of the adsorbed adenine species. The vibrational analysis is important evidence to confirm not only the molecular orientation, but also some detailed internal structural information. Here, is presented an electron energy loss spectroscopy (EELS) measurement of the adenine molecule adsorbed on the Cu(110) surface. Vibrational analysis suggests that, rather than simply flat lying on the substrate, adenine is somewhat tilted with a significant bonding between the NH_2 group and the Cu

substrate. This structure is confirmed by cluster *ab initio* calculations using the 6-31g basis set with B3LYP DFT method in GAUSSIAN 98 [10].

7.2. Experimental

Adenine was dosed onto the surface by vacuum deposition at a temperature of 370K. The crystalline solid was pumped overnight on a gas line, attached to the chamber via a gate valve. Dosing was carried out with the Cu(110) sample at room temperature with a dosing pressure *ca.* $5x10^{-10}$ mbar. After being dosed at room temperature, the Cu(110) sample was slowly heated to 430K while monitoring by LEED. After the ordered phase is formed, the sample was allowed to cool down to room temperature for STM or EELS measurements.

7.3. Results

The LEED pattern shown in Fig. 7.1A was recorded at 54 eV from the adenine saturated surface after annealing to 430K. The open circle in the middle indicates the approximate location of the (0,0) beam. The first order spots of the clean substrate are clearly visible with the <110> azimuth aligned along the horizontal direction. The structure has only one of the overlayer lattice vectors aligned along the high symmetry axes of the copper substrate. Thus, the real space unit cell is most conveniently described in matrix notation $\begin{pmatrix} 1 & 2 \\ 6 & 0 \end{pmatrix}$, where each row represents one of the real space unit cell lattice vectors.

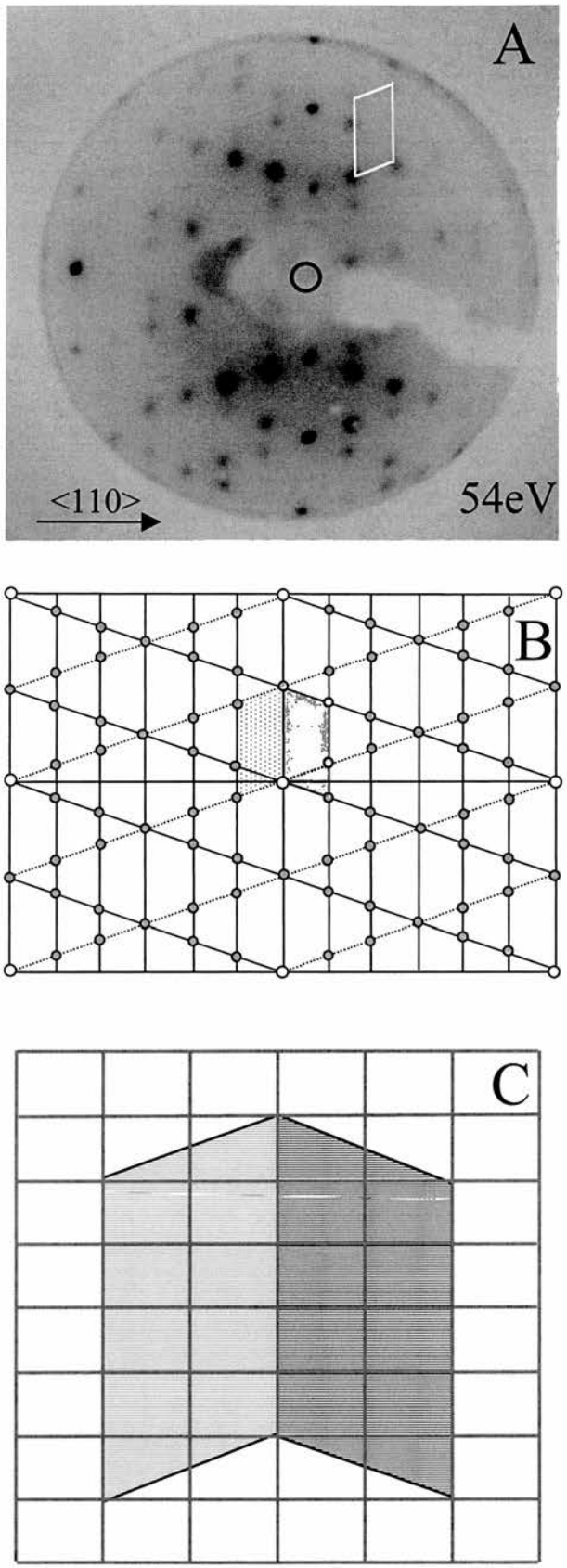

Fig 7.1 A) LEED pattern of Adenine on Cu(110), 54eV B) Associated reciprocal lattice unit cells C) Real space unit cells

Conventionally, the first integer in each row refers to the <110> direction of the copper surface, in units of the interatomic spacing d_{Cu-Cu} = 2.55Å, and the second refers to the <001> direction with units of $\sqrt{2}d_{Cu-Cu}$ = 3.61Å. The (1, 2) vector is 7.76 Å long and oriented 70.55° respect to the <110> direction, while the vector (6, 0) is 15.3 Å long and aligned along the <110> azimuth. Since one of the defining vectors is not aligned with the substrate high symmetry azimuth, two domains are implied, related by reflection across the <110> direction (or the <001> direction). The reciprocal lattice vectors and higher order diffraction spots, within the first order substrate diffraction pattern, are illustrated in Fig. 7.1B and the real space unit cells are shown in Fig. 7.1C. In Fig. 7.1B the solid and dashed meshes correspond to the two domains and LEED spots can be found at the intersections in each mesh. The unit cell is 12 times larger than the underlying substrate unit cell, with a size of 110.5 $Å^2$. Since there is no mirror plane symmetry within the unit cell, the overlayer structure formed by adenine is chiral. However, the two reflection correlated domains have opposite chirality. Therefore, with domain averaging, the surface appears to be achiral. This phenomenon suggests a mechanism for the introduction of a localised chiral symmetry break by the spontaneous 2D-crystallization and self-assembly of these prebiotically available molecules on inorganic surfaces and may have some role in the origin of biomolecular optical asymmetry [11].

The STM image of the saturated surface is shown in Fig. 7.2. Two reflection related domains can be clearly identified. At some of the domain boundaries, disordered molecules can also be found. Within each domain, molecules form rows along the (±1, 2) directions, while along the <110> direction, the adjacent rows have a

separation of 15.3Å. Most of the domains have an elongated shape with their longer dimension parallel to the <110> direction.

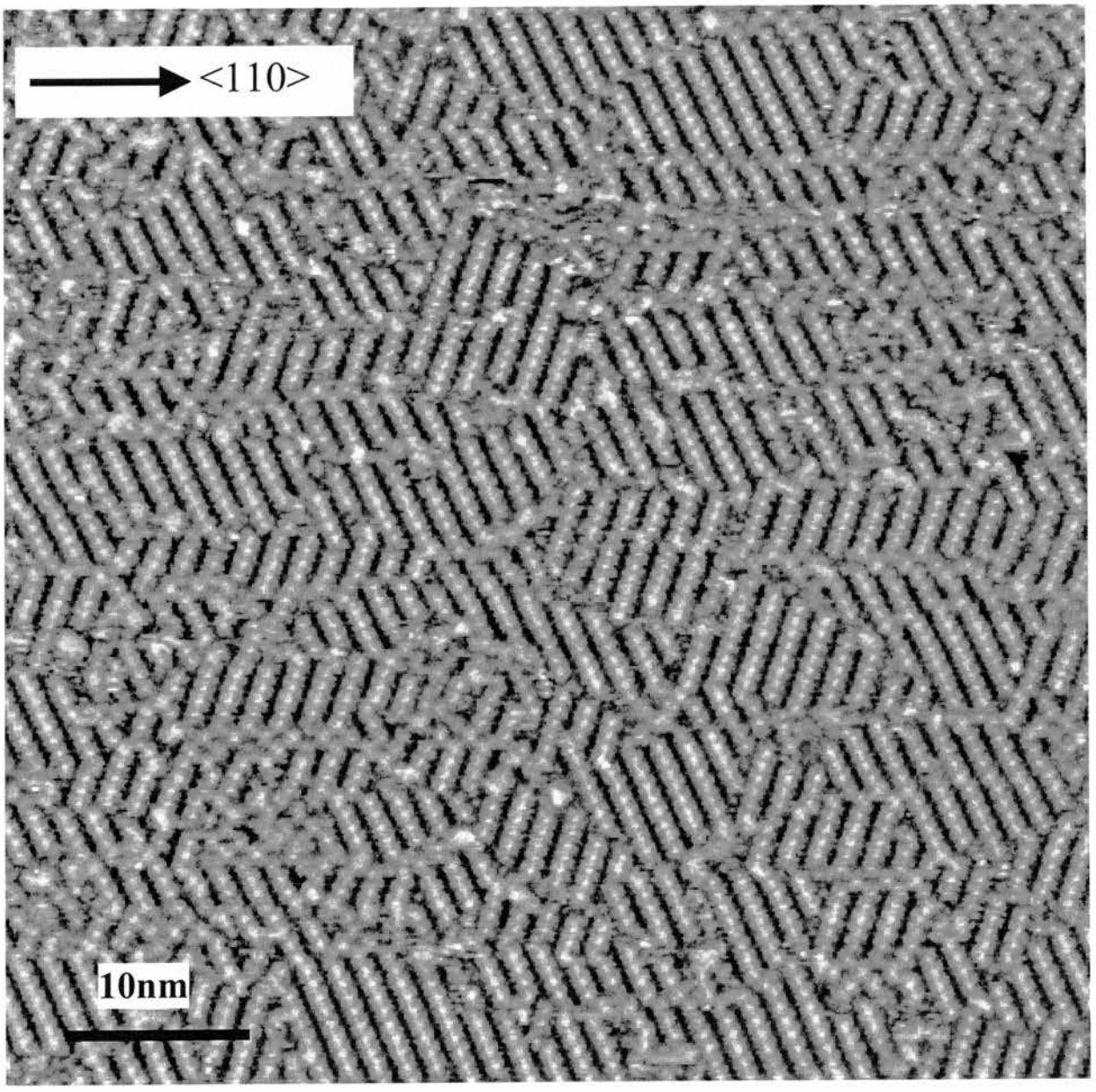

Fig 7.2 The STM image (60nmx60nm, sample bias=-0.16V, tunneling current=2.38nA) of ordered adenine on Cu(110) at saturation coverage

Although one of the unit cell vectors is parallel to one of the high symmetry axes, <110> azimuth, it is clear that the unit cells, described as $\begin{pmatrix} 1 & 2 \\ 6 & 0 \end{pmatrix}$ and $\begin{pmatrix} 1 & -2 \\ 6 & 0 \end{pmatrix}$, in each domain do not have any mirror plane symmetry. Therefore the highest possible symmetry of the unit cell can only be C_2. Different preparation approaches have been investigated in order to achieve larger sized domain, but without success so far. The saturated surface coverage has only been achieved by dosing with the sample at room temperature to form a multilayer structure followed by annealing at 430K. The multilayer desorbs at about 380K, which is very close to dosing temperature of adenine, 370K. It is also observed that, if the molecule is dosed at a sample temperature above the multilayer desorption temperature, 380K, the sticking coefficient becomes too low to form the ordered overlayer. Thus it is suggested that the strong attractive intermolecular interactions, rather than the molecular-substrate interaction, stabilise the adsorbate and are responsible for the formation of the ordered structure.

The growth of this well ordered domain can be monitored by coverage dependent LEED and STM measurements. Fig.7.3. shows an electron diffraction pattern of a low coverage surface annealed at 430 K, recorded at 45 eV. Rather than well defined spots, only stripes along the (±1, 2) directions can be observed, which is one of the unit cell vectors of the surface at saturation coverage shown in Fig. 7.1A. This suggests that, even at low coverage, after annealing, long range ordering is still achieved along the (±1, 2) directions, but not along the (6, 0) direction. The ordering of adenine at low coverage indicates a relatively strong attractive intermolecular

interaction along the (±1, 2) directions. This intermolecular interaction is also responsible for the formation of ordered domains at higher coverage.

Fig 7.3. LEED pattern of low coverage adenine on Cu(110) recorded at 45eV. The substrate orientation is the same as in Fig.7.1

All the diffraction stripes have their profile width similar to that of the spots of the saturated surface in fig. 7.1A, which suggests a similar degree of the ordering between the saturated and low coverage surface along the (±1, 2) directions. The lack of any ordering along the <110> azimuth may indicate very weak, or even, repulsive intermolecular interactions along this direction.

The detailed low coverage overlayer structure can be clearly identified by STM images, shown in fig. 7.4. Here, the STM images were recorded on surfaces prepared

at different coverages, 8%, 35% and 65% of the saturated coverage. Surfaces with different coverage are achieved by control of the exposure time.

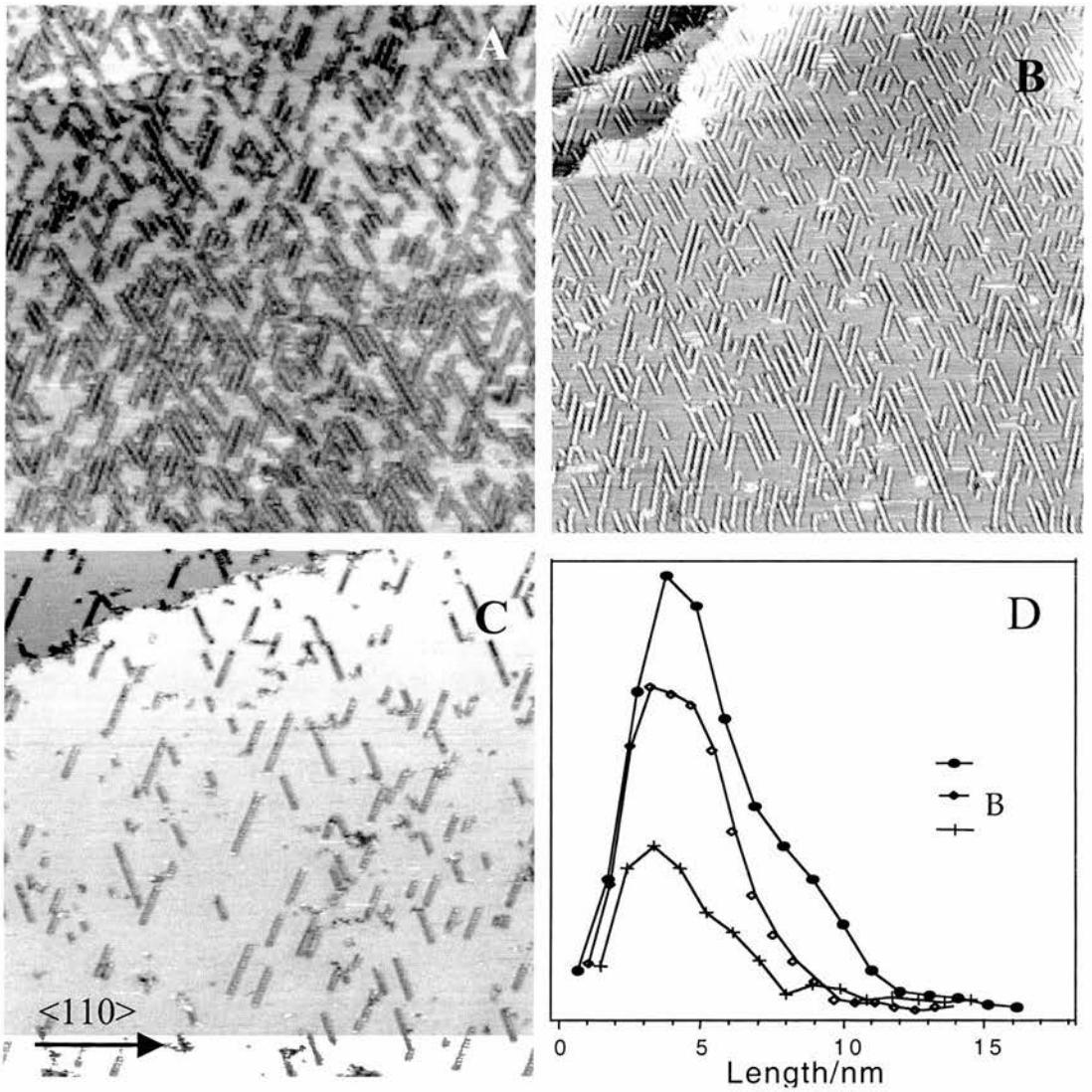

Fig 7.4 STM images (100nmx100nm) as a function of surface coverage. A) Image of the surface with a 65% of saturation coverage, recorded with a sample bias=-0.04V and tunneling current=0.84nA. B) Image of the surface with a 35% of saturation coverage, recorded with a sample bias=-1.07V and tunneling current=1.24nA. C) Image of the surface with an 8% of saturation coverage, recorded with a sample bias=-1.31V and tunneling current=0.07nA. D) The length distribution of molecular chains in image A, B and C.

The actual coverage is directly measured from the STM images by counting the number of individual features. Relative to the substrate, the molecular features in these three STM images show different contrast, which corresponds to the difference in their electronic conductivity. It is suggested that this is due to the variation of the tip condition between different images. Molecules can be adsorbed on the tip, which has been shown previously to reverse the contrast in many cases [12-14]. With an adenine molecule adsorbed on the W tip, the tunneling junction will be formed as Cu-Adenine-Adenine-W, in which a higher resistance could be responsible for the depression of the molecular features in the image. Here it could be that this depression is due to the electronic effects rather than the height effects.

All the images of Fig 7.4 show isolated molecular rows growing along the (±1, 2) directions which is entirely consistent with the LEED observation. There is a very low population of other isolated, molecular size, features even at very low coverage. The molecular row features are stable to a maximum tunneling current of 3.5nA at 10mV bias. The stripes along the scanning direction are probably due to the tip induced diffusion of individual molecules. Dosing the molecules at a sample temperature of 370K, or annealing the surface at 460K overnight does not increase the length of molecular chain and domain size. With increasing coverage, the length of the rows does not increase only their number. Fig 7.4D shows the length distributions as a function of coverage, which are directly measured from images in fig 7.4A, 7.4B

and 7.4C. All the distributions have an average length of 38Å, which corresponds to 5 unit cells along the (±1, 2) directions. All distributions have similar distribution width.

The overlayer structure is commensurate with the substrate structure, with no significant aggregation of the adsorbates on the step edges. The growth of the two dimensional domains can be identified as a coverage driven process, since the ordering of chains along the <110> azimuth can only be found at high coverage. This growth behaviour clearly indicates a diffusion limited mechanism, indicating a strong adsorbate-substrate interaction, which is also consistent with the fact that the domain size cannot be increased with thermal treatment of the substrate.

Fig 7.5 shows the image of a small area (100Åx100Å) at high resolution. Each row has a measured width of 7.5Å. The unit cell along the (1, 2) directions has a length of 7.65Å and contains two parallel, elongated features, which gives rise to a C_2 rotation symmetry. This symmetry property confirms that each domain is chiral, since the chiral domain cannot have mirror plane symmetry and an achiral domain cannot have C_2 symmetry. These features are elongated along the direction 57° away from the chain direction, 13° from the $<\bar{1}10>$ azimuth, with a dimension of 6.5Å, which is close to the longest dimension of free molecule. The closest distance between adjacent molecular rows along the <110> azimuth is about 15.3Å. This distance

corresponds to the six-fold periodicity. At this distance, the gap between the rows shows a lower tunneling conductivity with its feature darker than either the clean Cu surface or the adenine molecule.

While the electron diffraction pattern presents the size and shape of the unit cell with further details of molecular structure in the STM images, such as the number of molecules and their relative position, HREELS can give information on molecular orientation and the bonding geometry.

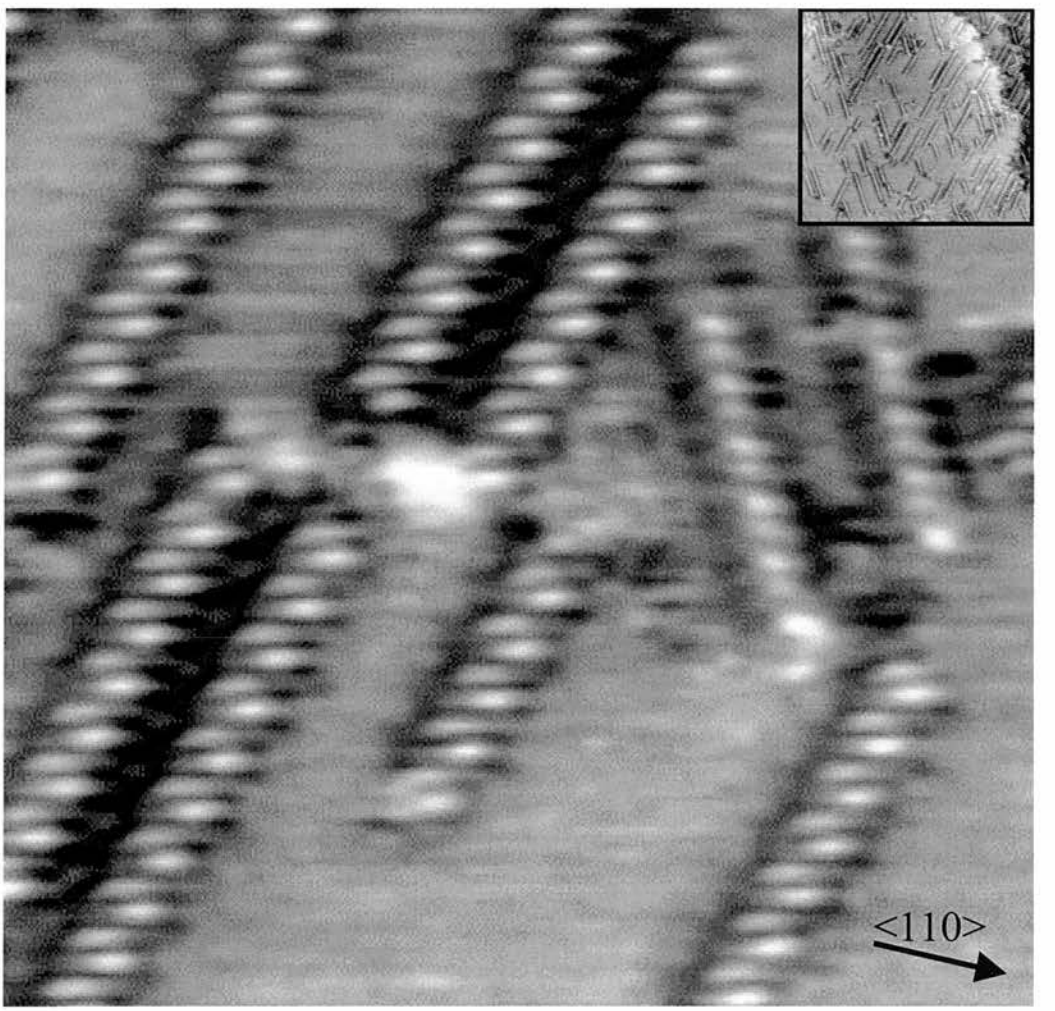

Fig 7.5 Small size STM image (10nmx10nm, tunnelling current=0.63nA, bias=-10V) at low coverage with molecular resolution

Figure 7.6 shows the on-specular HREELS spectrum of ordered adenine on Cu(110), with a primary energy of 8 eV. The surface was annealed to 430 K to achieve the ordered structure with a high reflectivity for electron scattering. Since the spectrum was recorded in the specular direction, the dipole selection rule for scattering at metal surfaces can be applied. Only those vibrational modes which have their dynamic dipole perpendicular to the surfaces can be excited in the dipole scattering. The recorded spectrum has strong loss peaks at 376, 574, 645, 764, 842 and 1441 cm^{-1}, accompanied by weak modes at 496, 931, 1098, 1146, 1288, 1384, 1534, 1557 and 1629 cm^{-1}. The strong loss intensities for the frequencies below 1000 cm^{-1}, including most of the out-of plane wag and torsion modes, suggest that the molecular plane is almost parallel to the substrate. However, if the molecular plane were perfectly parallel to the substrate, the modes above 1000 cm^{-1}, which are contributed by the in-plane vibrational modes should have zero loss intensities, since their dynamic dipole moments would be parallel to the substrate. The peak at 1441 cm^{-1} is associated with the C-NH_2 stretching. The relatively high intensity of this mode suggests that the C-NH_2 bond is not parallel to the substrate. Thus, either the C or N atom in the C-NH_2 group must have sp^3 rather than co-planar sp^2 hybridisation.

On the basis of the infrared spectra of the adenine molecule in the gas phase, in an Ar matrix [15,16] and from theoretical calculations [17], it is found that the free adenine molecule is almost planar with the strongest vibrational mode at 1629cm^{-1},

assigned to the NH_2 scissoring mode and frequently found to be intense in many molecules containing the NH_2 group. The low intensity of this mode for adenine on Cu(110) indicates either the NH_2 group has dissociated or the NH_2 group is almost parallel to the substrate. Temperature programmed desorption studies show that there is no desorption associated with the dissociation of NH_2 group below 430K, the annealing temperature. Thus it can be concluded that the NH_2 plane is close to parallel to the substrate, while the C-NH_2 bond is tilted away from this plane. Therefore, the adsorption geometry of adenine can be determined as both the purine and NH_2 planes are almost parallel to the substrate while the C-NH_2 bond is tilted out of this plane. In this geometry, the N atom in the amino adopts a pyramidal sp^3, rather than a planar sp^2, hybridization with an N-Cu bond slightly tilted away from the surface normal in such a way that the NH_2 plane is parallel to the substrate. A more detailed adsorption structure will be discussed in association with theoretical modelling results described in the following section. The low frequency strong peak at 376 cm^{-1} does not belong to the free adenine molecule. It certainly can be assigned to a molecule-substrate stretching mode. However, to identify whether it is bonded to the Cu substrate through the purine ring or the NH_2 group, which gives a strong dynamic dipole in the surface normal direction, an *ab initio* calculation is required which allows the bonded molecule to relax fully on a large Cu cluster.

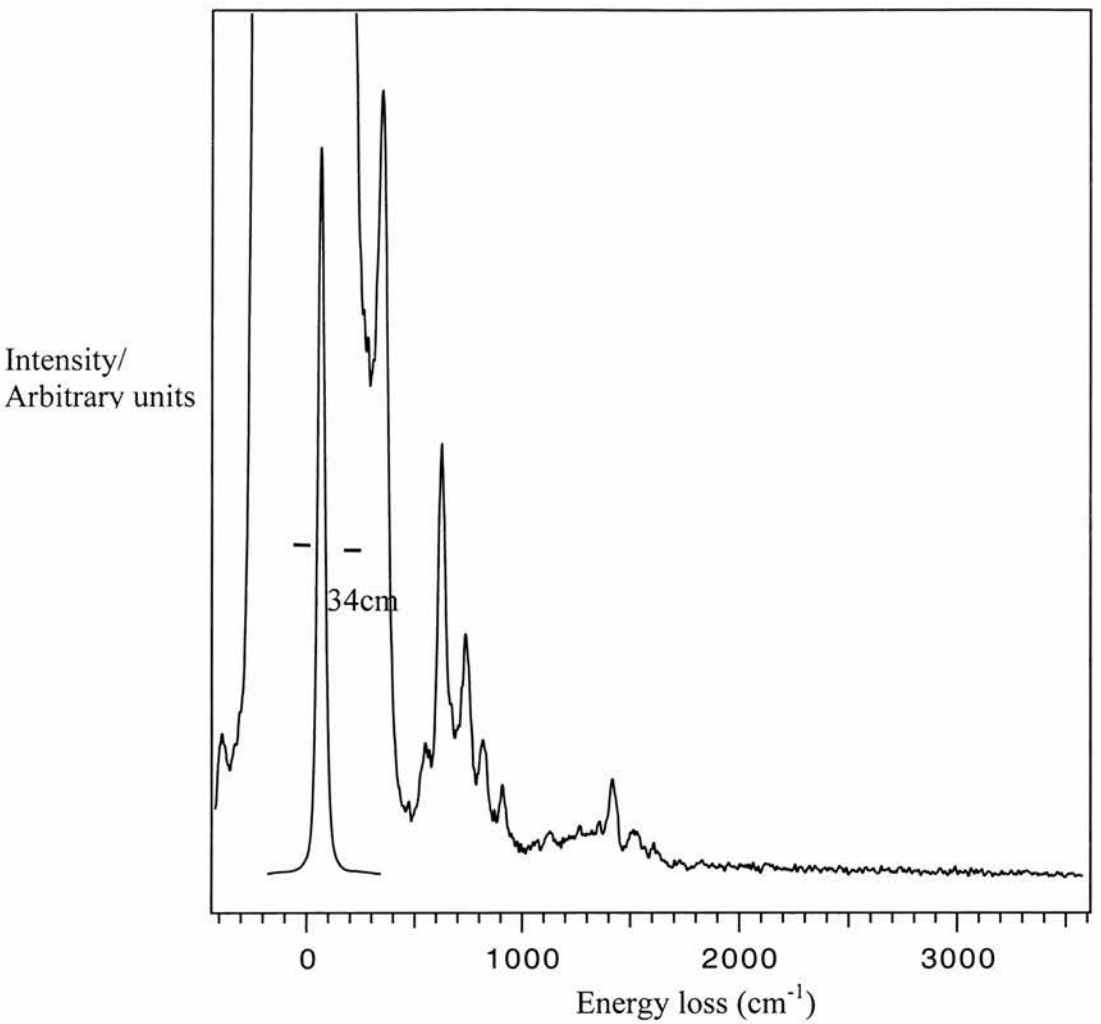

Fig 7.6 High resolution EELS spectrum of ordered $\begin{pmatrix} 1 & 2 \\ 6 & 0 \end{pmatrix}$ adenine on Cu(110) with a primary energy of 8eV

7.4 *Ab initio* calculation.

To confirm the deformation of the molecular plane and to identify the bonding between the adenine and the Cu substrate, *ab initio* calculations of a model, including one adenine molecule and 16 Cu atoms, have been carried out with Gaussian 98W [10]. The input structure of the adenine molecule was initially optimised separately with the

B3LYP method and a 6-31g basis set. The 16 Cu atoms were chosen to form a single layer of a Cu(110) face with (4x4) structure. The initial molecule is almost a planar structure with out-of-plane variation less than 0.1Å, which is consistent with previous calculations [18]. Relative to the substrate, initially, the molecule is assumed to be parallel to the substrate at a vertical distance of 2.0Å. Fig. 7.4.1a shows this input structure with the underlying Cu cluster.

To understand the energetically favourable adsorption structure, a full optimisation of the adenine structure has been done with a fixed Cu cluster structure. Limited by the computational resource, we use an effective core potential for the Cu atoms and sto-3g basis set for other atoms. Fig. 7.4.1b shows the optimised structure.

In this optimised structure, the purine ring is still planar, while the N atom in the NH_2 group has clearly been modified from the original sp^2 into sp^3 hybridisation, in which the N-H bond length reduces from 1.08Å to 1.03Å. The nearest distance between the N atom in the NH_2 group and the Cu atom is 2.2Å, which is very close to Cu-N bond length in organometallic complexes [19]. The molecular plane is tilted about 18° off the substrate plane, which is consistent with the strong vibrational loss intensities of the out-of-plane modes in EELS. The absence of NH_2 stretch modes is also consistent with the fact that the plane of the NH_2 group is found to be parallel to the substrate.

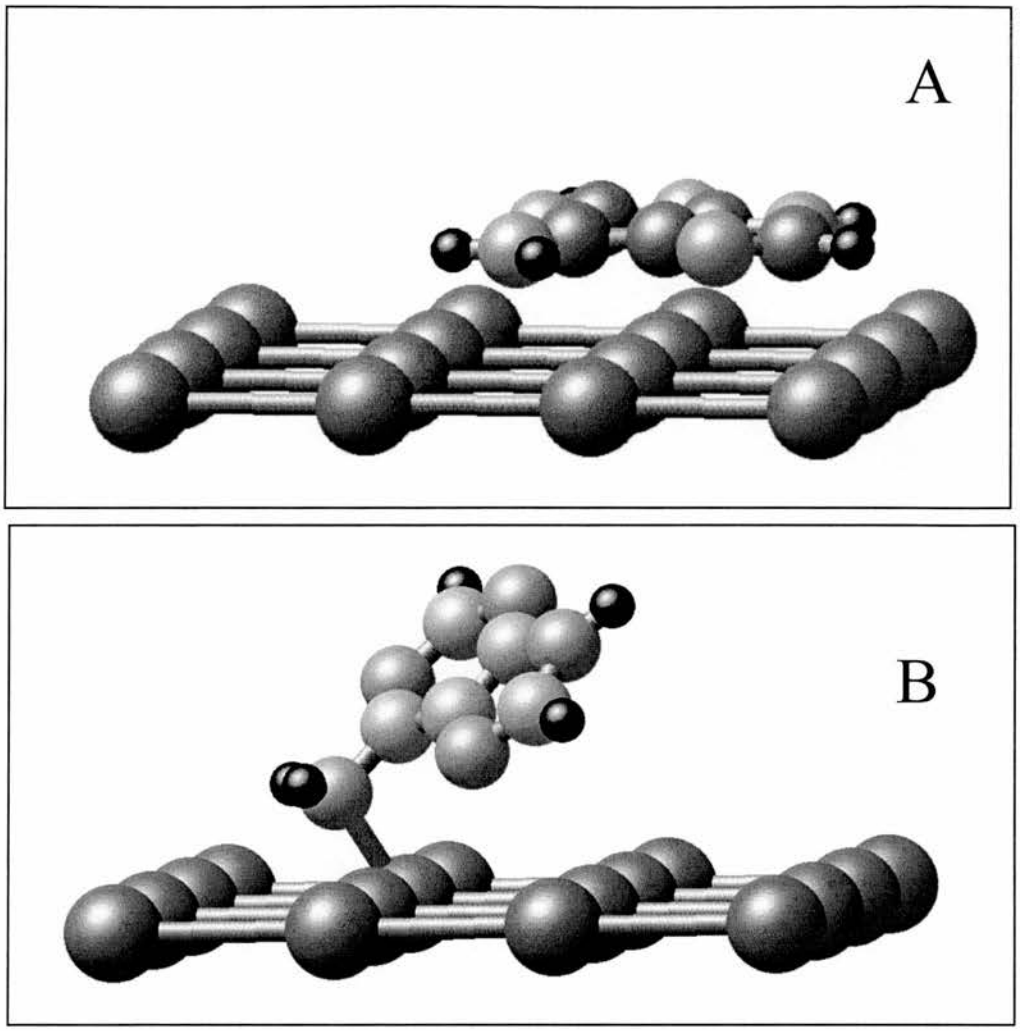

Fig 7.7 Optimised adsorption structure of adenine on Cu(110) surface

7.5 Discussion

To begin, some possible H-bonded dimer models of adenine intermolecular interactions are mentioned. This then allows consideration of the extended molecular row structure based on such dimers. Combining the information from spectroscopic,

microscopic and theoretical studies, it is possible to suggest a possible overlayer structure.

As already demonstrated, the molecular chain along (±1, 2) directions is about 7.5Å in width and 7.65Å in unit cell length. Both dimensions are larger than the maximum length of a single molecule. Thus, this already implies that there could be two molecules per unit cell, corresponding to the two features observed within the unit cell. Since each domain is chiral and the unit cell has C_2 symmetry, it can be concluded that the two molecular features within the unit cell are related by a C_2 rotation. On this basic, an evaluation of the H-bonded interactions between two adenine molecules with the same chirality has been performed. The total geometry optimisations and stabilisation energies were estimated for several possible dimers by means of a semiempirical PM3 method using Gaussian 98W [10]. Previous calculations have been done with an emphasis on the dimer stabilisation energy [1,6]. Here, the optimised dimer will be used to construct the molecular chain and compare the dimensions with those measured in STM.

Six different types of dimers all with C_2 symmetry, forming between NH_2 (model B and C), NH (model A), CH (model D, E, and F) and the N atoms in the purine ring, have been considered and they are shown in fig. 7.8. The calculated stabilisation energies are also indicated. It should be mentioned that these calculation

results are in good agreement with that presented by Furukawa and Kawai[6]. However, in their calculations, the dimers involving C-H···N bonding (D, E and F) were not included.

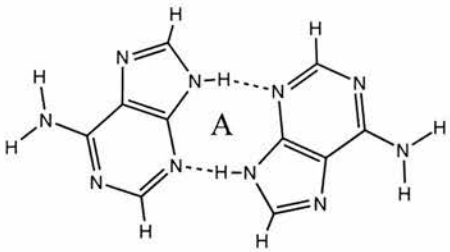

ΔE=-0.44eV/dimer

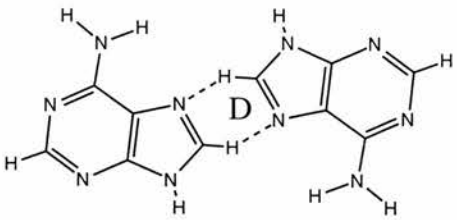

ΔE=-0.03eV/dimer

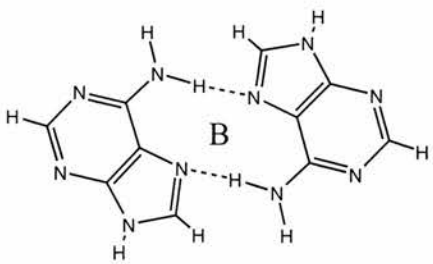

ΔE=-0.27eV/dimer

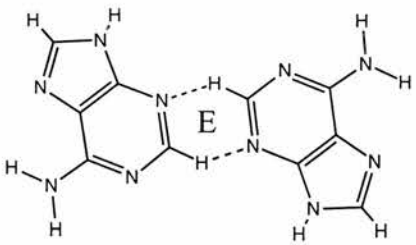

ΔE=-0.03eV/dimer

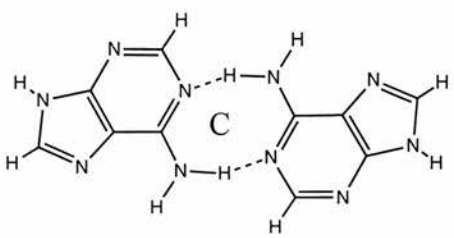

ΔE=-0.19eV/dimer

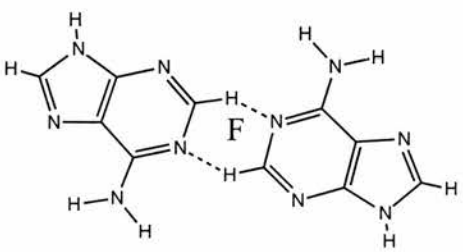

ΔE=0.02eV/dimer

Fig 7.8 Proposed hydrogen bonding between adenine dimers. The structures are optimised with semiempirical PM3 calculations. The stabilization energy is also included

From these calculations, it is clear that the most stable dimer is formed between NH and N (model A), followed by the dimers involving the NH_2 group (model B and C). Although the hydrogen bonds between the CH and N are relative weak, they still show an energy stability in models D and E, while in model F there is no energy gain. Starting with dimers based on the most stable configuration (A), we have determined the width and repeat length of various chains in which these dimers are linked to each other by H-bonding of the types B to F, hence chains AB, AC, AD, AE and AF.

It is highly likely that for a molecule, such as adenine, the hydrogen bonds play a key role in the formation of the overlayer structure. For adenine $\begin{pmatrix} 1 & 2 \\ 6 & 0 \end{pmatrix}$ structure, there are two molecules per unit cell. Thus it can be expected that two different types of hydrogen bonded interactions are present in the unit cell. This is also true of the 1D unit cell of the molecular chains found at low coverage. It can be considered that one of these interactions is the most stable dimer interaction described as A above.

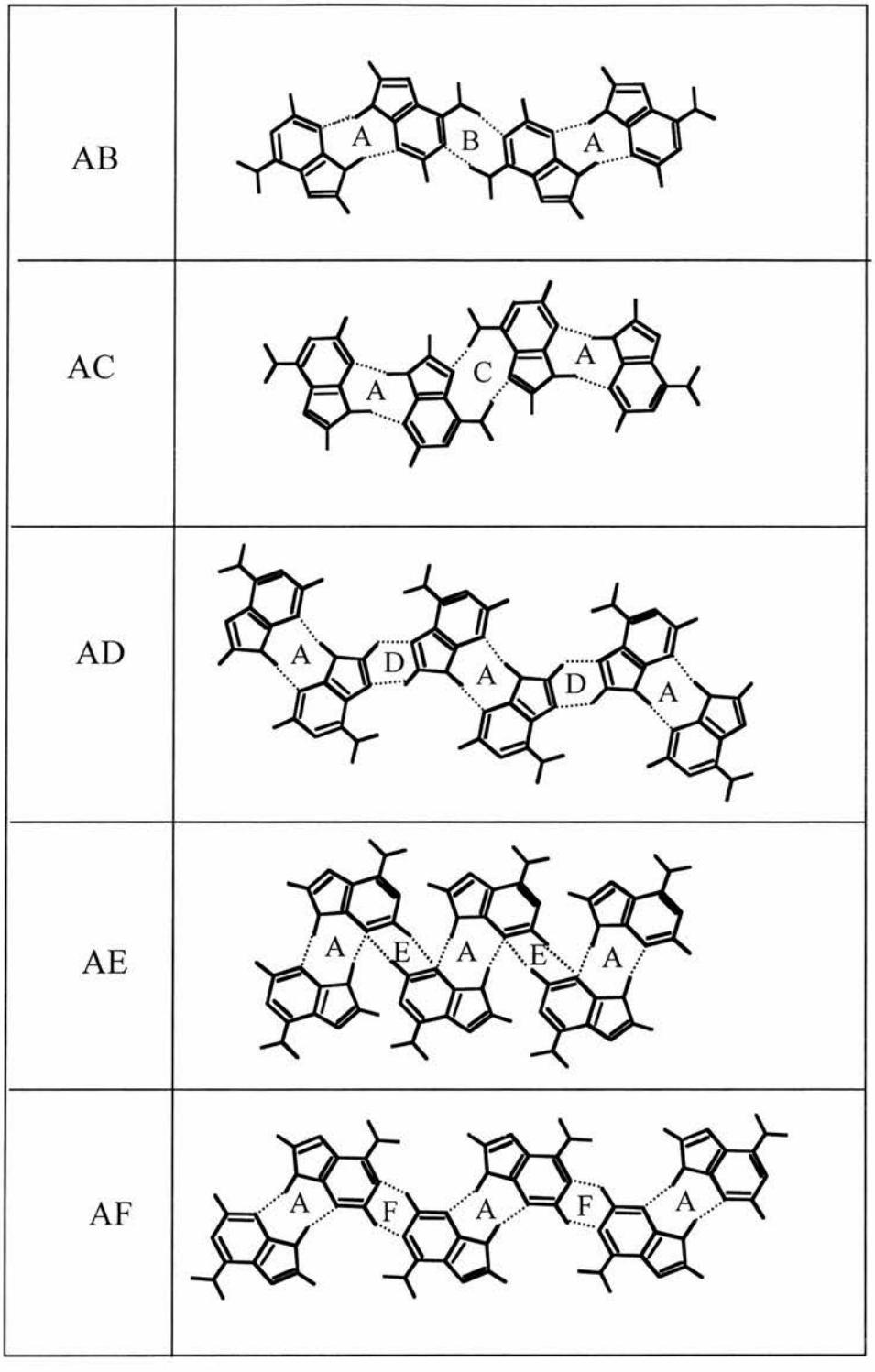

Fig 7.9 Possible molecular dimer chians linked with H-bonding. All the dimensions are propotional to the optimised dimer structures in fig. 7.8

Figure 7.9 shows the possible models of the rows which we have considered. The molecular chain can be developed with alternation of different type of hydrogen bonds along particular directions. Model AB and AC involve the hydrogen bonds from the NH_2 group, which should be energetically favourable. However, constrained by the hydrogen bonding direction, the periodicities of the molecular chains are about 12.5Å which are much larger than the 7.65Å, determined from the (1, 2) periodicity and measured from the STM images. Thus, the involvement of NH_2 in the hydrogen bond, which is responsible for the formation of molecular chain, can be excluded. This could arise from the distortion of the molecular structure at the amino N atom bonding to the copper substrate, which then inhibits an optimum orientation for the H-bonding interaction.

Models AD, AE and AF involve a hydrogen bond with a CH group. Model AE has a width of 12Å, which is also much larger than that measured from the STM image. Also, the hydrogen bond in this model would require one of the N atom of the purine ring which has already been involved in the hydrogen bonding of the original dimer A. Thus, the structure proposed in model AE is also excluded. Both AD and AF models have similar dimensions with a periodicity of 7.8Å and a width of 8Å. It is expected that the models calculated here would have a systematic error less than ±1Å. Within this tolerance, both AD and AF models can fit the observed structure very well. However, energetically, model AF is rather less favourable, compared with model AD, therefore a model AD is proposed that best fits the experimental results. To confirm this, in fig. 7.10,

an STM image of a small length of molecular chain with a superimposed model AD is presented. Not only do the dimensions of the model fit the features in the image, the angles of the molecular alignment as well as all the hydrogen bonding distances are also matched very well.

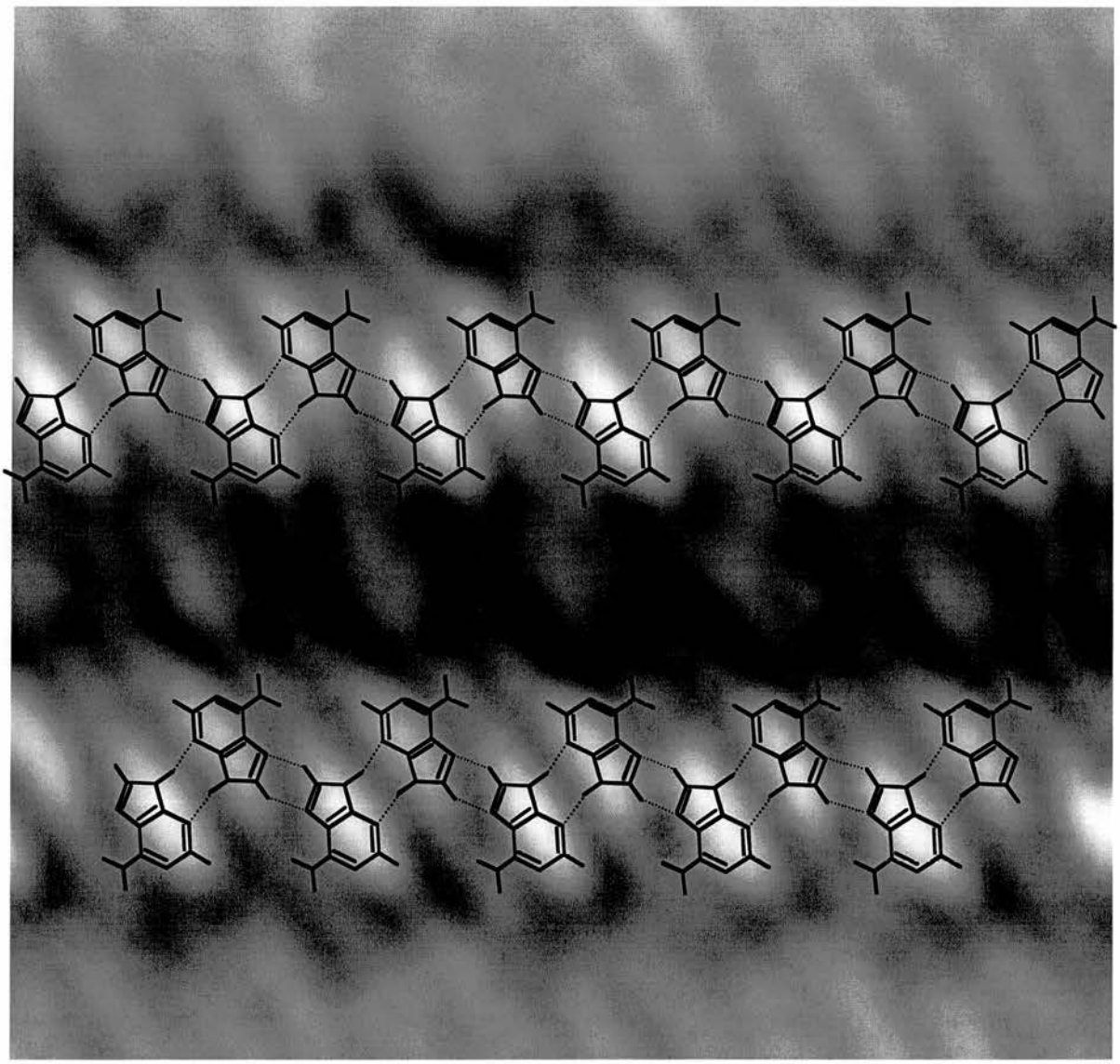

Fig 7.10 A small area of STM image (42Åx40Å) shows the adenine dimer chain structure superimposed with a suggested real space model. The intermolecular H bonding is labelled with the dashed line

As mentioned earlier, each domain is homochiral and two reflection domain have opposite chirality. The origin of this surface induced chirality relies on the adsorption geometry that breaks the only mirror plane symmetry of the free adenine molecule. Thus, the registry of the adsorbate on the Cu surface is strictly related to the chirality of each domain, i. e. molecules of one chirality are aligned in rows along (1, 2) while those of the opposite chirality adopt the (-1, 2) row direction.

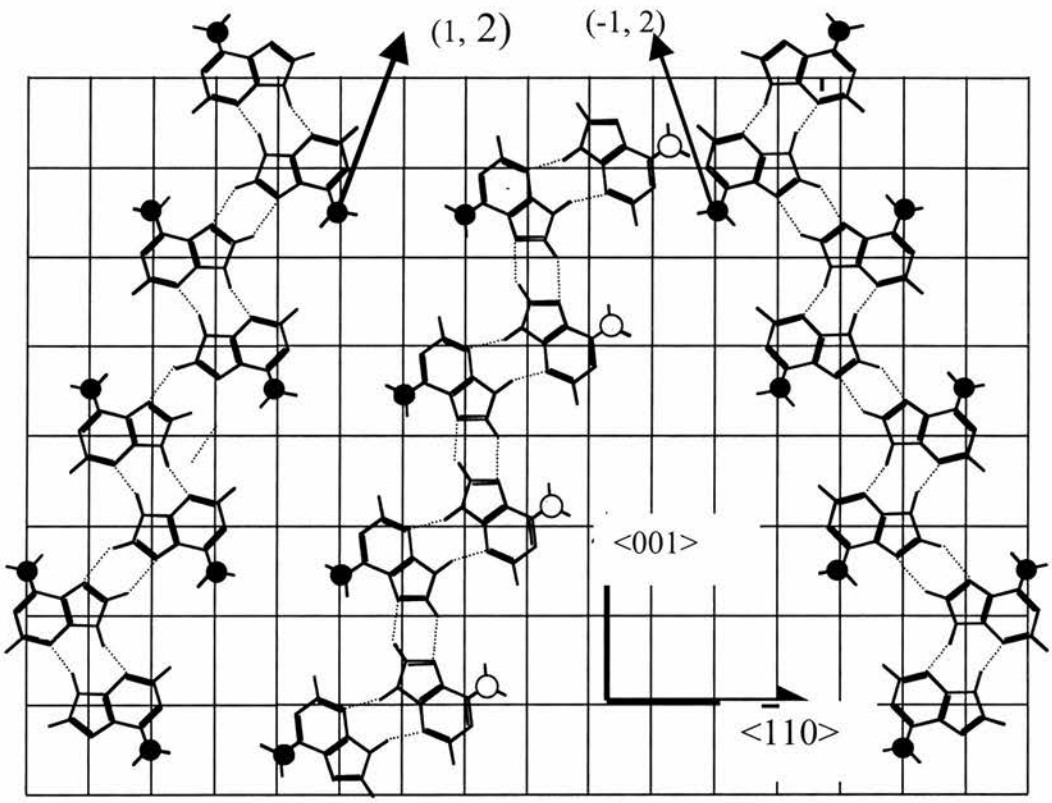

Fig 7.11 The registry of adenine dimer chains on Cu(110) mesh. Model I and III have the opposite chirality and growing along (1, 2) and (-1, 2) directions. Model II has the same chirality as model III , but growing along the (1, 2) direction. All the amino N atoms (black dots) are bonding at atop sites, except in the model II (grey dots).

In the case of structure I (fig. 7.11), the row of molecular dimers along (1, 2) shows that all N atoms (black circles) of the amino groups can be located in the preferred on-top sites. In a chain of opposite chirality aligned along the same (1, 2) direction, only half of the relevant N atom can be accommodated in on-top position (Structure II of fig.7.11) and it is necessary instead to adopt (-1, 2) as the chain direction (structure III of fig 7.11).

References:

1 S. J. Sowerby, M. Edelwirth, and W. M. Heckl, *J. Phys. Chem. B* **102,** 5914-5922 (1998).

2 S. J. Sowerby, P. A. Stockwell, W. M. Heckl, and G. B. Petersen, *Orig. Life Evol. Biosph.* **30,** 81-99 (2000).

3 N. J. Tao and Z. Shi, *J. Phys. Chem.* **98,** 1464-1471 (1994).

4 J. E. Freund, M. Edelwirth, P. Kröbel, and W. M. Heckl, *Phys. Rev. B* **55,** 5394-5397 (1997).

5 M. Furukawa, H. Tanaka, K. Sugiura, Y. Sakata, and T. Kawai, *Surf. Sci.* **445,** L58-L63 (2000).

6 M. Furukawa, H. Tanaka, and T. Kawai, *Surf. Sci.* **445,** 1-10 (2000).

7 P. Colarusso, K. Q. Zhang, B. J. Guo, and P. F. Bernath, *Chem. Phys. Lett.* **269,** 39-48 (1997).

8 S. Mohan and V. Ilangovan, *Indian J. Pure Appl. Phys.* **31,** 750-754 (1993).

9 Z. Dhaouadi, M. Ghomi, J. C. Austin, R. B. Girling, R. E. Hester, P. Mojzes, L. Chinsky, P. Y. Turpin, C. Coulombeau, H. Jobic, and J. Tomkinson, *J. Phys. Chem.* **97,** 1074-1084 (1993).

10 M. J. Frisch, G. W. Trucks, H. B. Schlegel, G. E. Scuseria, M. A. Robb, J. R. Cheeseman, V. G. Zakrzewski, J. A. Montgomery, R. E. Stratmann, J. C. Burant, S. Dapprich, J. M. Millam, A. D. Daniels, K. N. Kudin, M. C. Strain, O. Farkas, J. Tomasi, V. Barone, M. Cossi, R. Cammi, B. Mennucci, C. Pomelli, C. Adamo, S. Clifford, J. Ochterski, G. A. Petersson, P. Y. Ayala, Q. Cui, K. Morokuma, D. K. Malick, A. D. Rabuck, K. Raghavachari, J. B. Foresman, J. Cioslowski, J. V. Ortiz, B. B. Stefanov, G. Liu, A. Liashenko, P. Piskorz, I. Komaromi, R. Gomperts, R. L. Martin, D. J. Fox, T. Keith, M. A. Al-Laham, C. Y. Peng, A. Nanayakkara, C. Gonzalez, M. Challacombe, P. M. W. Gill, B. G. Johnson, W. Chen, M. W. Wong, J. L. Andres, M. Head-Gordon, E. S. Replogle, and J. A. Pople, , Revision A.7 ed. (Gaussian, Inc., Pittsburgh PA, 1998).

11 S. J. Sowerby, W. M. Heckl, and G. B. Petersen, *J. Mol. Evol.* **43,** 419-424 (1996).

12 M. Bohringer, W. D. Schneider, R. Berndt, K. Glockler, M. Sokolowski, and E. Umbach, *Phys. Rev. B* **57,** 4081-4087 (1998).

13 E. P. Go, K. Thuermer, and J. E. Reutt-Robey, *J. Phys. Chem. B* **104,** 8507-8511 (2000).

14 M. Bohringer, K. Morgenstern, W. D. Schneider, and R. Berndt, *Surf. Sci.* **457,** 37-50 (2000).

15 M. J. Nowak, H. Rostkowska, L. Lapinski, J. S. Kwiatkowski, and J. Leszczynski, *Spectroc. Acta Pt. A-Molec. Biomolec. Spectr.* **50,** 1081-1094 (1994).

16 L. Houben, K. Schoone, J. Smets, L. Adamowicz, and G. Maes, *J. Mol. Struct.* **410,** 397-401 (1997).

17 G. N. Ten, V. V. Nechaev, V. I. Berezin, and V. I. Baranov, *J. Struct. Chem.* **38,** 262-267 (1997).

18 J. Leszczynski, *Int. J. Quantum Chem.* , 43-55 (1992).

19 T. P. Balasubramanian, P. T. Muthiah, Ananthasaravanan, and S. K. Mazumdar, *J. Inorg. Biochem.* **63,** 175-181 (1996).

CHAPTER 8 . Conclusions

Phenylglycine

At saturation coverage, the molecules form well ordered chiral structures with a chiral unit cell which determines the LEED patterns of the two enantiomers are readily differentiated. The origin of enantiomeric specificity in the structure is thought to arise from the interadsorbate H-bonding which occurs in the saturated monolayer. The commensurate $\begin{pmatrix} 5 & -3 \\ 4 & 1 \end{pmatrix}$ unit cell (R phenylglycine) contains six adsorbate molecules most likely in anionic form by analogy with glycine and formally 17 Cu atoms, although reconstructions in the outermost Cu layer may well produce a structure with 18 Cu atoms , such that each O and N atom of the adsorbate is bonded to a separate Cu atom in equivalent local bonding geometries. Comparison is made with analogous structures observed for the non-chiral species glycine and R-, S-alanine adsorbed on Cu (110).Also observed for both these species, the stable structure on annealing the surface is a (3×2) periodicity with a glide line, although in a chiral adsorption system a glide line is formally forbidden.

Amino benzoic Acid

A coverage and temperature dependent studies shows a novel sequence of periodic structures linked to successive removal of hydrogen from the adsorbed species, as shown by LEED, STM, HREELS and TPD. At room temperature, flat-lying molecules with a primitive unit cell of (3x4) periodicity with glide plane along the <001> direction are observed. Annealing this surface to 464 K causes partial desorption of H_2 and a variation of the intensity in HREELS of various bands and

formation of a $\begin{pmatrix} 2 & 4 \\ 5 & -2 \end{pmatrix}$ periodicity. STM images suggest the formation of dimers, as a result of the dehydrogenation. On annealing to higher temperature (510 K), further dehydrogenation forms a $\begin{pmatrix} 1 & 2 \\ 6 & -5 \end{pmatrix}$ structure. Finally, at 540 K, a $\begin{pmatrix} 1 & 2 \\ 4 & -3 \end{pmatrix}$ periodicity is revealed in which all species correspond to dehydrogenated dimers. Through this sequence, all species retain a flat-lying orientation on the surface. It was also found that ABA exhibited coverage dependent behaviour whereby increasing surface coverage restricted molecules to adsorbing in an upright orientation. The resulting structures formed continuous nanowires at domain boundaries. HREELS allowed the distinction between flat-lying molecules flipping into an upright orientation and the correct scenario of the ABA adsorbing directly in an upright manner.

α - pyridone

Room temperature dosing allows a formation of an ordered (8×2)gg monolayer. The two perpendicular glide planes place restrictions on the relative position of molecules within the unit cell. From STM images the features within the unit cell are assigned as dimers, and thus a model of the hydrogen bonding dimers satisfying the glide plane symmetry requirements has been proposed. Indeed the STM image confirms the presence of the central dimer that would satisfy the symmetry conditions. This model is further validated with the information gained from HREELS that the molecules are oriented parallel to the surface when the ordered structure is formed.

Cytosine/Thymine

Both of these molecules form well ordered two dimensional crystals . Cytosine initially forms a (6×6) unit cell. STM images prove that twelve molecules exist per unit cell, each with the same dimensions and thus probably the same orientation. The molecules are oriented in an upright /tilted geometry.as suggested by the dominance of in-plane modes from HREELs measurements and comparison with ab-initio calculations some evidence of deprotonation Upon further annealing there is a rearrangement of molecules and a (6×2) gg overlayer is produced. Again the molecules are upright and HREELs along with the calculations suggests some evidence of deprtotonation, thus a model is suggested whereby cytosine molecules in adjacent zig zags are dimerised, one proton is lost per dimer, leading to a delocalisation of charge and subsequent bonding to the copper through the oxygen.

Thymine has similarities in behaviour to cytosine although the phase diagram is not as rich. Only a (6×2)gg unit cell forms and again the molecules are in an upright/tilted orientation. It is hypothesised based on the available data that the four molecules per unit cell are again arranged in a zig zag formation, with the line of the zig zag along the [100] exhibiting π stacking characteristics.

Adenine

An ordered $\begin{pmatrix} 1 & 2 \\ 6 & 0 \end{pmatrix}$ adenine structure on Cu(110) surfaces. The structure is achieved by annealing an adenine saturated surface at 430K. At low coverage, rather than 2D islands, one-dimensional ordered molecular chain along the (±1, 2) directions has been observed. EEL spectroscopy reveals that the purine ring is

parallel to the substrate, while the C-NH_2 bond is tilted. *Ab initio* calculations confirm the molecular orientation and shows an sp^3 hybridisation on the $N(H_2)$ atom, which is directly bonded to the substrate. Following a detailed construction of several possible models of the H-bonded chains, a model is suggested which consistently fits the experimental data. This involves both N-H···N and C-H···N hydrogen bonding.

It is evident that there are several patterns emerging from the observation of the adsorption behaviour of these small biomolecules. In terms of chirality there are some interesting comparisons to be made between the amino acid phenylglycine and the nucleic acid base adenine. The former adsorbate/ substrate complex unit cell was entirely chiral and thus the LEED pattern was representative of one orientation of domain. On the other hand adenine is only a prochiral molecule producing a non chiral LEED pattern. However under inspection with the STM, chiral domains could be seen to exist, of the 2 symmetry related orientations, information which is lost in the diffraction pattern due to averaging effects, and thus the STM was essential in revealing these structures. Although the presence of the two related domains is predictable the size of them would not have been apparent. It was attempted to increase the size by annealing treatments and thus any further strategies for increasing chiral domain size, rather than racemic separation or creation of a chiral surface per se, must be dealt with real space imaging techniques.

There are clear relationships in terms of the structures formed by the pyrimidines and the analogue α pyridone. Firstly it is apparent that the two perpendicular glide plane unit cell is present in thymine, cytosine and α pyridone. The glide planes are characteristic of zig zag arrangements of molecules in real

space and these zig zags have been postulated to form with hydrogen bonding interactions, thus it can be concluded that hydrogen bonding of these molecules causes a characteristic zig zag arrangement.

In particular cytosine and thymine have exactly the same unit cell symmetry and dimensions, both can form a (6×2)gg . Obviously in both cases the unit cell area is the same but it is interesting to note that the arrangement of molecules within this unit cell is significantly different even though the same symmetry constraints are required. This can be thought to be due to the difference in the size of the molecules, i.e the difference in the presence of either an Nh2 group as in the case of cytosine or a CH3 group as in the case of thymine.

Amino benzoic acid demonstrated conclusively the signatures of flat lying and upright molecules. This was especially helpful in terms of comparison with the nucleic acid bases, in the case of the pyrimidine being oriented predominantly in an upright manner and with the case of adenine, in a more flat-lying orientation. This flat-lying signature was also apparent in the α-pyridione case.